1970

# Digital computer calculation of corona thresholds in nonuniform fields

Mohamed Said Abou-Seada
*Iowa State University*

# DIGITAL COMPUTER CALCULATION OF CORONA THRESHOLDS IN NONUNIFORM FIELDS

by

Mohamed Said Abou-Seada

A Dissertation Submitted to the
Graduate Faculty in Partial Fulfillment of
The Requirements for the Degree of
DOCTOR OF PHILOSOPHY

Major Subject: Electrical Engineering

Approved:

Signature was redacted for privacy.

In Charge of Major Work

Signature was redacted for privacy.

Head of Major Department

Signature was redacted for privacy.

Dean of Graduate College

Iowa State University
Ames, Iowa

1970

TABLE OF CONTENTS

# LIST OF FIGURES

# LIST OF TABLES

# I. INTRODUCTION

In recent years, extra-high voltage (EHV) dc has been used for the transmission of electrical energy. The advent of dc transmission is attributed to the economical and electrical advantages it offers over ac (1), which includes the transmission of bulk amounts of electrical energy over much longer distances than possible with ac. Various projects, such as the Konti-Skan project (2), New Zealand's South- and North-Island dc transmission (3), the dc project between the Italian mainland and Sardinia (4), and the Sakuma project in Japan (5) have been put recently into testing or commercial operation. Notable dc transmission projects are under construction such as the 750-kv dc interconnection of the Pacific Northwest-Southwest in the United States (6), Vancouver Island project in Canada (7), and Kingsnorth project in England (8).

One of the drawbacks of using EHV dc, as well as ac, is the appearance of corona around the transmission line conductors. Corona may be regarded as the partial breakdown of the gas surrounding the conductor. It is caused by gas ionization caused by the extremely high electric fields adjacent to the conductor. Corona gives rise to the flow of a current and the energy losses accompanying it may become appreciable, thus endangering the economy of EHV trans-

mission. Increasing the conductor diameter has always been a good tool in suppressing high corona losses without too great a capital investment. However, it was experimentally found that increasing the conductor diameter results in increasing the radio interference from the line (9). Above a certain diameter; and even using hollow conductors, they become too bulky to be easily handled. Thus bundle conductors were introduced and are now a matter of course in EHV and future UHV (ultra-high voltage of 1000 KV and above) transmission. To increase the corona onset, that is starting, voltage, and hence reduce corona losses at a given voltage, the conductors must be designed and arranged to yield as low a surface potential gradient as possible.

Theoretical calculation of the corona starting voltages of any nonplanar conductor is not possible even if the field distribution function is known. In the case of bundle conductors calculation of corona onset voltages is even more difficult due to the lack of accurate information about the electric field distribution. Furthermore there was a great difficulty in deriving a suitable mathematical model that physically represents the actual processes of corona. Only a mathematical semi-empirical interpretation was in use for the case of breakdown in the uniform field. Because of all these difficulties, manufacturers and utilities, both in the United States and abroad, have found themselves forced to

resort to full-scale experimental techniques with all the tremendous investment and operating costs they involve, as undertaken for instance in the United States, France, Germany and the Soviet Union (10-14).

The electric field distribution is required not only to predict the corona starting voltages, but also to estimate the magnitude and possibly also the frequency spectrum of the radio interference produced by the corona discharges. This problem is becoming increasingly significant (15).

Thus, there is a great need for accurate field values of bundle conductors and a reliable theoretical method for calculating the corona onset voltages. A new approach was needed to solve this problem.

The purpose of this research work was therefore the prediction of corona onset voltage based on numerical-theoretical considerations and using generally known physical constants. This dissertation describes the work done in two steps toward accomplishing this aim. First, a numerical method based on a charge simulation technique and the method of images as applied for the computation of the potential and electric field distribution of smooth unipolar and bipolar twin-bundle conductors. Secondly, with the knowledge of the field distribution, the streamer development theory introduced by Loeb for uniform fields (16) was modified to suit the nonuniform field distribution of the twin-bundle

conductor line. Using the accurately computed values of the electric field, a digital technique solves for the minimum voltage that satisfies the streamer propagation condition. This is the corona starting voltage since streamers are the first corona mode.

# II. REVIEW OF LITERATURE

## A. The Electric Field Computation

As early as 1909, Thomas (17, 18) suggested the division of a cylindrical line conductor into two, three or more subconductors separated from one another but mounted on the same insulator, the current dividing between them. His purpose was to increase the transmission capacity and to decrease the line inductance. The bundle conductor system was patented by Whitehead (19) in 1910. His express purpose for using bundle conductors was to keep the electric field within acceptable limits so that "the point at which breakdown of insulation occurs is raised above that which it would be for a single conductor of a cross-sectional area equal to that of the said subconductors".

Many mathematical attempts have been undertaken to calculate the electric field at the surface of bundle conductors. Because of this constraint some steps in the analytical derivations were bypassed and various simplifying assumptions were made, which usually lead to a low degree of accuracy.

In 1956, Miller (15) developed equations for the maximum surface gradient of a unipolar twin-bundle conductor line based on a previous work by Grary reported by Clarke (20). To simplify the problem, he assumed that the subconductors

separation is much greater than the subconductor diameter and that the subconductor charge could be represented by one axial line charge located on each subconductor axis. He used the method of images to account for the ground plane. He, inaccurately, stated that the point at which the surface gradient is maximum is the outmost point on the subconductor surface along the line through the centers of the two subconductors. Under these conditions he derived the following equation for the maximum surface gradient per unit conductor voltage:

$$g_m = 4\left(\frac{1}{2a} + \frac{1}{2r}\right)Q \qquad 2.1$$

where $r$ = subconductor radius

$2a$ = subconductor spacing

$Q$ = axial line charge per unit length per unit voltage on each subconductor

$$= \frac{1}{2 \log_e \frac{2h}{r} + 2 \log_e \frac{h}{a}}$$

where

$h$ = height of center of bundle above ground.

In 1959, Reichman (21) used the maximum surface gradient equations developed by Miller to present the relationship between the different geometrical line parameters and the line voltage for a fixed maximum surface gradient of 16.65 kv/cm

(rms), a value representing the corona onset potential gradient as obtained from field tests conducted by the Hydro-Electric Power Commission of Ontario. King (22) suggested that a slight displacement of the one axial charge from the center of each subconductor would improve the accuracy, a principle adopted in 1960 by Sreenivasan (23), who under the assumption of small ratio of subconductor diameter to subconductor spacing and neglecting the effect of the ground plane, gave the following expression for the charge displacement, x, of a unipolar twin-bundle line:

$$x = \frac{r \times \frac{r}{2a}}{1 + \frac{r}{a} - \frac{r^2}{2a^2}}$$

where

r = subconductor radius

2a = subconductor spacing.

He defined a proximity factor M to account for shifting of the charge centers and the effect of the other subconductor on the maximum surface gradient, given by:

$$M = 1 + \frac{r}{a} - \frac{r^2}{2a^2} + \frac{r^4}{8a^4} + \ldots$$

for small values of $\frac{r}{a}$. Using this technique, he developed relations between the line geometrical parameters which would result in an optimum maximum surface gradient.

Assuming that the ground plane is at an infinitely large distance, rigorous analytical solution to the electric field of the twin unipolar bundle conductor configuration was obtained by Quilico (24), by solving the Laplace's equation in a bipolar coordinate system. His bipolar coordinates $\alpha$ and $\beta$ were expressed in terms of the Cartesian coordinates x and y, where the x-axis is through the centers of the two bundle conductors and the y-axis is the normal bisector, as

$$x^2 + (y - c \cot \alpha)^2 = \left(\frac{c}{\sin \alpha}\right)^2$$

$$(x - c \coth \beta)^2 + y^2 = \left(\frac{c}{\sinh \beta}\right)^2$$

and the solution to the electric field distribution is given in terms of the bipolar coordinates as

$$E_\alpha = \frac{Q}{\pi \varepsilon_0 c}\left[\frac{\sin \alpha}{2} + (\cosh \beta - \cos \alpha) \sum_{n=1}^{\infty} \frac{e^{-n\beta_0}}{\cosh n\beta_0} \cosh n\beta \sin n\alpha\right]$$

$$E_\beta = \frac{Q}{\pi \varepsilon_0 c}\left[\frac{\sinh \beta}{2} + (\cosh \beta - \cos \alpha) \sum_{n=1}^{\infty} \frac{e^{-n\beta_0}}{\cosh n\beta_0} \sinh n\beta \cos n\alpha\right]$$

where

Q = charge per unit length of each subconductor

$\varepsilon_0$ = permittivity of free space

$c = r \sinh \beta_0$

$a = r \cosh \beta_0$

$= \log_e (k + \sqrt{k^2 - 1})$

$k = \frac{a}{r}$

with r as the subconductor radius and 2a its spacing.

Dareskii (25) and Timascheff (26, 27) used similar conformal transformation techniques to calculate the electric field pattern near a unipolar twin-bundle conductor, neglecting the existence of the ground plane. Timascheff (26), by further assuming that the subconductor spacing is much greater than the subconductor radius and that the equipotential lines in the neighborhood of the subconductors are shaped almost exactly like nonconcentric circles, used the conformal mapping $W=Z^2$ to "fold" the whole complex W-plane into a half plane of Z, where the field pattern corresponding to one of the conductors appears. By selecting a certain radius $\alpha$ of a single "basic" circle in the W-plane, he was able to make the subconductor cross section almost coincide with the suitable equipotential curve in the Z-plane, so that the field pattern is not disturbed. $\alpha$ is obtained from the relation

$$\frac{a}{r} = \frac{\sqrt{1+\alpha} + \sqrt{1-\alpha}}{\sqrt{1+\alpha} - \sqrt{1-\alpha}}$$

where

r = subconductor radius

2a = subconductor spacing

Transforming the points of intersection of the force lines and radii of the equipotential circles in the W-plane,

Timascheff obtained the field pattern of one subconductor in the Z-plane. The field pattern of the other subconductor was obtained by mirroring the pattern of the first subconductor in the Z-plane. However, even with the simplifying assumptions mentioned before, Timascheff's technique did not yield any numerical information about the potential or electric field distribution but gave only a picture of the shape of the equigradient curves in the vicinity of the subconductors. In 1963, in a following paper (27), Timascheff, using the same simplifying assumptions, assigned numerical values to the equigradient curves in the vicinity of the subconductors. A great handicap in using this numerical information is that all calculations and numerical values associated with the equigradient curves were expressed as ratios to the maximum surface gradient, a value that is not accurately known.

Tikhodeev (28, 29) proposed a method of successive images in a cylinder of charges in a system of parallel conductors for the evaluation of their electric fields. In this method, the actual charge distribution on the conductor surfaces is replaced by a series of image line charges. To determine the magnitudes and locations of these charges, use was made of the fact that the image of an infinitely long line charge +Q placed parallel to an infinitely long cylindrical conductor of radius r, and at a distance l from its axis is a line charge -Q at a distance = $r^2/l$ away from the axis of the conductor (30). The same technique was used by Sarma and

Janischewskyj (31). However, Aleksandrov (32, 33) has shown that there is no gain in accuracy by using the method of successive images over the simplified method of representing the charge on each subconductor by one line charge along its axis.

## B. The Corona Threshold

Experimental values of corona thresholds for various gap geometries are available in standard textbooks on high voltage engineering (34, 35) and electrical breakdown of gases (36, 37). Many empirical formulae have been derived to express the corona starting field strengths and to calculate it for standard geometries. However, these empirical formulae are only valid within certain ranges and under specified conditions, and extrapolation would lead to large errors. Quantitative criteria for breakdown have been proposed based on the classical Townsend theory of the growth of ionization (38, 39, 40).

### 1. The Townsend theory (36, 37, 41, 42, 43)

Electrons and ions are always present in gases, such as air because of the natural background of radioactive and cosmic radiation. According to this theory, the primary ionizing process in the gas is ionization of a neutral gas molecule by collision with an energetic electron that has been accelerated by the applied electric field. A new

electron-ion is therefore formed. This cumulative process makes the number of electrons and positive ions grow exponentially and is therefore known as an electron avalanche.

The positive ions, however, lose more energy in each collision because of their much larger mass, and it is very unlikely that they can ionize in the gas. They can, however, produce new electrons by bombardment of the surface of the negative electrode. Such a process is called secondary emission. Other important secondary processes that are vital for producing new electrons required to maintain the current are photoelectric emission from the cathode and photoionization in the gas caused by photons originating from excited atoms or from recombination processes.

The growth of the current in a uniform field because of various primary and secondary processes can be written as

$$I = I_0\{\frac{\exp(\alpha d)}{1-\gamma[\exp(\alpha d)-1]}\} \qquad 2.1$$

where

$I_0$ = initial current due solely to external ionizing sources

$d$ = gap length

$\alpha$ = Townsend's first ionization coefficient

= number of ionizing collisions for an electron per unit length of path in the direction of the field

$\gamma$ = Townsend's second ionization coefficient, which represents all the possible secondary processes

Equation 2.1 determines the voltage level at which a uniform field gap breaks down, because breakdown must occur when the current tends towards infinity. This happens when the denominator becomes zero, i.e., breakdown takes place when

$$\gamma[\exp(\alpha d)-1] = 1 \qquad 2.2$$

which means that the current be flow indefinitely if each electron on the average produces by one or more secondary process a successor.

This is Townsend's breakdown criterion. It does not give any information about the temporal growth of the processes leading to breakdown. It is, however, inherent in the Townsend theory that many generations of electron avalanches are required to build up a breakdown.

The second Townsend coefficient $\gamma$ is very sensitive to electrode conditions and gas impurities, and it will only be well defined under carefully controlled laboratory conditions. The above equation is valid only in the uniform field where $\alpha$ is not dependent on x. Equation 2.2 is, therefore, of little use to the high voltage design engineer.

Schumann (44) has suggested that the Townsend criterion for breakdown in air at atmospheric pressure be written as

$$\int_0^d \alpha dx = K$$

where K is a constant equal to 20. Another version of

the Townsend criterion which should apply to cathode initiated types of breakdown has been suggested by Ver Plank (45), and Hutton (46) who replaced the constant K with a function of the field strength at the cathode.

2. The streamer theory (36, 38, 39, 40 43)

A Townsend type of breakdown requires a whole sequence of avalanches. For a 1-cm gap in atmospheric air, therefore, formative time lags of several microseconds should be expected. The gap may, however, break down in less than 0.1 us. Also, both branched and zig-zagged spark channels were observed at high values of pressure and gap distance products. These observations, beside others, led to the concept of the streamer type of breakdown. According to the streamer theory the space charge field from the electrons and ions in the head of an avalanche may cause an instability in the development of the avalanche resulting in the formation of fast moving anode and cathode directed streamers from the avalanche head. These streamers form a conducting plasma channel across the gap, and the voltage breaks down. The second basic mechanism active in the formation of streamers is photoionization in the gas.

Different attempts have been made to develop a quantitative criterion for streamer formation in the uniform field. Meek (36) made the assumption that cathode and anode directed

streamers would develop when the radial space charge field of the avalanche head attains the same order of magnitude of the externally applied field. This led to the criterion for onset of a streamer formation in a nonuniform gap, represented by the following two simultaneous equations:

$$E_r = K\ \alpha_x \exp\left(\int_0^x \alpha dx\right)/(x/p)^{\frac{1}{2}}$$

and

$$E_r = K_1 E$$

where,

$x$ = The critical avalanche length, i.e., the length of the avalanche at the moment when it becomes unstable and streamers are formed

$\alpha_x$ = The first Townsend ionization coefficient at the avalanche head

$P$ = Gas pressure

$E_r$ = space charge field

$E$ = external field

$K$ = constant

$K_1$ = constant of proportionality

A similar criterion was proposed by Raether (40). Both Meek and Raether assumed that the streamer formation occurs according to the above mentioned equations when $K_1=1$. However, in later work (47-51) the exact value to be assigned to $K_1$ has been discussed in some detail and values less than 0.1 have been considered as adequate. Raether and Meek, further elaborating on their criteria for streamer formation

in uniform fields in air, developed the following equations:

$$\alpha x_c = 17.7 + \log_e x_c$$

known as Raethers breakdown criterion, and

$$\alpha x + \log_e \frac{\alpha}{P} = 14.46 + \log_e \frac{K_1 V_b}{Pd} - 0.5 \log_e (Px) + \log_e x$$

known as Meek's breakdown criterion,

where

$V_b$ = breakdown voltage

$x$ = avalanche length

$x_c$ = critical avalanche length

$d$ = gap distance

The shortcomings of both Raether's and Meek's breakdown criteria resulted from the fact that they were based on the assumption that the space charge field attains the order of magnitude of the applied field, and not on the actual physical processes that lead to the development of streamers. It was not even possible to include any quantity that depends on photoionization in the gas, which was held responsible for the formation of streamers.

Pedersen (52) suggested that the equation determining breakdown or formation of streamers in air be of the following form

$$\alpha_x \exp\{\int_0^x \alpha dx\} = G\{x, \rho, f(E_x), u, 0/0\ H_2O, \ldots\}$$

where G is an unknown function of the critical avalanche length x, air density $\rho$, field distribution $f(E_x)$, photoionization in the gas u, humidity percent $H_2O$, and other possible variables. Assuming that x and $\rho$ are the dominating variables in a function of this type (53, 54) Pedersen approximated his equation to take the form

$$\alpha_x \exp\{\int_0^x \alpha dx\} = G\{x,\rho\}$$

For air at atmospheric pressure, this breakdown equation was written as

$$\log_e(\alpha_x) + \int_0^x \alpha dx = g(x)$$

where g(x) is another unknown function of x. In a uniform field, the equation takes the form

$$\log_e(\alpha) + \alpha x = g(x)$$

Using the above equations together with experimentally measured breakdown field strengths in air under uniform fields, Pederson was able to calculate the streamer thresholds for a system of two spheres, one of them earthed, with a reasonable degree of accuracy. But in spite of the close agreement between the calculated and the standard values of corona thresholds, the approximation made by Pederson resulted in neglecting the effect of photoionization in the gas, a process which is primarily responsible for streamer

formation.

Loeb (16) formulated a criterion for streamer propagation in a uniform field based on the actual physical processes - namely ionization by electron collision and photoionization that develop in a gas leading to the avalanche-streamer transition. Loeb's criterion for streamer propagation in a uniform field is given by the following equation:

$$\frac{1}{3} f_1 f_2 \left(\frac{u\bar{\alpha}'\bar{r}^3}{x_c^{\frac{1}{2}}}\right) \int_{\bar{r}}^{x_c} \bar{r}^{\frac{3}{2}} e^{-ur} e^{\int_{\bar{r}}^{r} \alpha' dr'} \, dr = 1$$

where

$\bar{r}$ = radius of assumed positive ion spherical space charge

$x_c$ = distance traveled by initiating free electron towards anode

$f_1$ = ratio of number of photons to number of ions in the positive ion spherical space charge

$f_2$ = probability of photoionization

$u$ = gas absorption coefficient

$\alpha'$ = first Townsend coefficient due to external field

$\bar{\alpha}'$ = first Townsend coefficient due to both external and space charge fields

It is noted, however, that in spite of the fact that Loeb's criterion for streamer advance in uniform fields precisely represents the physical phenomenon as leading to the avalanche-streamer formation, it was never used to predict corona onset voltages. This is attributed to the

complexity involved in its solution for the corona voltage, a value that is indirectly inherent in the criterion equation; since $\bar{r}$, $x_c$, $\alpha'$, and $\bar{\alpha}'$ are all voltage dependent.

# III. SOLUTION OF THE ELECTRIC FIELD PROBLEM USING A CHARGE SIMULATION TECHNIQUE

A cylindrical conductor parallel to an infinite plane and having its charge distributed along its surface can be regarded as if composed of a great number of line charges coinciding with its circumference. The same principle can be applied to the bundle conductor composed of several parallel cylinders. These line charges have different charges per unit length although symmetry greatly reduces the number of unknown line charges.

The potential at any point is given by the sum of the potentials due to the individual charges under the justified assumption of a constant permittivity which is true for air and most dielectrics. Obtaining the potential at various points of known potential, such as the boundary electrodes, yield a number of equations in terms of the line charges. Theoretically, it is possible to set any number of such independent equations and solve for the values of the line charges. However, the equations have coefficients with such close numerical values that their simultaneous solution with any digital computer available is not feasible. Furthermore, these line charges will yield potentials satisfying the boundary conditions only at the selected points on the electrodes where the potential is set equal to that of the electrode. At other points on the electrodes

circumference there will be a deviation of potential from that of the boundary potential resulting in an error in computing the electric field due to the presence of a tangential component of electric field.

Hence, the objective here was to find some other equations in terms of the line charges based on something other than the potentials of the boundaries. This problem was successfully solved in the calculation of the potential and its gradient of the rod-to-plane studies (55). It is explained in detail in the following discussion where it will also be shown that the assumed lumped charges need not be taken at the conductor's surface, but can be "placed" inside the conductor. The reason for this fictitious choice lies in the better and faster computation obtained with the digital computer.

This study was divided into two parts, the unipolar line against ground and the bipolar line also with ground present. In both cases ground wires were neglected. The former case applies to dc lines as operated, usually temporarily with ground return, as well as to the central phase of three phase ac lines, and the latter applies to both dc and single phase ac.

## A. The Unipolar Twin-Bundle Line

### 1. Potential and electric field

Referring to the electrode configuration shown in Figure 3.1, the method adopted for the computation of the potential and electric field is as follows: line charges of an arbitrarily chosen number, N, and of unknown magnitudes $[Q_j;\ j=1,2,\ldots,N]$ are uniformly "placed" on a fictitious coaxial cylinder of radius RC inside each subconductor of radius RS. The relative locations of these line charges as given by $(B_j,\ j=1,2,\ldots,N)$ are chosen arbitrarily beforehand and are assumed part of the input data fed into the computer. They could be varied at any computer run. Symmetry dictates the location of the corresponding charges of subconductor II as those of subconductor I. Image charges of all those line charges are "placed" on the other side of the plane representing ground to account for the assumed zero potential of ground.

The potential $\phi(r,z)$ at any point $P(r,z)$, where the origin and the coordinates r and z are as shown in Figure 3.1, is the algebraic sum of the potentials due to each of the line charges and their images, and is given by (56)

$$\phi(r,z) = -\sum_{j=1}^{N} Q_j \log_e\left[\frac{DC(1,j)\cdot DC(2,j)}{DI(1,j)\cdot DI(2,j)}\right] \qquad 3.1$$

where the distances are as shown in Figure 3.1 and are given

Figure 3.1. Charge representation of the unipolar twin-bundle conductor system

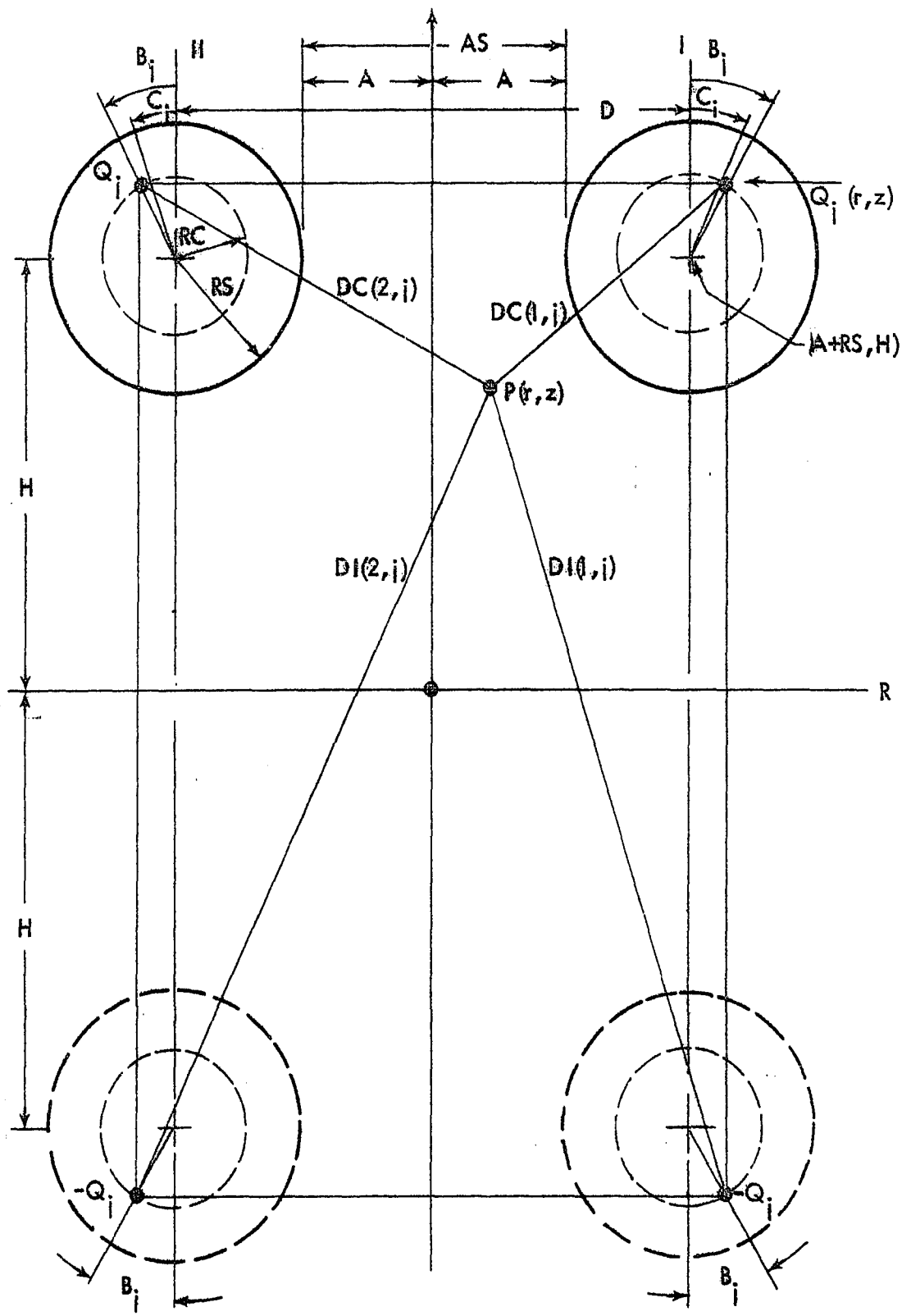
Z
AS
A
A
D
H
I
$B_i$
$C_i$
$Q_i$
$Q_i$ (r,z)
RC
RS
DC(2,i)
DC(1,i)
(A+RS,H)
P(r,z)
H
DI(2,i)
DI(1,i)
R
H
$-Q_i$
$Q_i$
$B_i$
$B_i$

by

$$DC(1,j) = \{[r(Q_j)-r]^2 + [z(Q_j)-z]^2\}^{\frac{1}{2}} \qquad 3.2$$

$$DC(2,j) = \{[r(Q_j)+r]^2 + [z(Q_j)-z]^2\}^{\frac{1}{2}} \qquad 3.3$$

$$DI(1,j) = \{[r(Q_j)-r]^2 + [z(Q_j)+z]^2\}^{\frac{1}{2}} \qquad 3.4$$

$$DI(2,j) = \{[r(Q_j)+r]^2 + [z(Q_j)+z]^2\}^{\frac{1}{2}} \qquad 3.5$$

and, $r(Q_j)$, $z(Q_j)$ are the r and z coordinates of the line charge $Q_j$ on subconductor I. They can also be expressed in terms of the subconductor spacing 2A, subconductor radius RS, height of subconductor center above ground H as:

$$r(Q_j) = A + RS + RC \cdot \sin B_j \qquad 3.6$$

$$z(Q_j) = H + RC \cdot \cos B_j \ . \qquad 3.7$$

The potential $\phi(\rho,\alpha)$ at any point P, at a radial distance $\rho$ from the center of subconductor I and at an angle $\alpha$ from the vertical through that center, is obtained from equation 3.1 by making the substitution

$$r = A + RS + \rho \cdot \sin \alpha \ ;$$

$$z = H + \rho \cdot \cos \alpha$$

in equations 3.2 through 3.5. The electric field $\underline{E}$ at P is given by

$$\underline{E}(\rho,\alpha) = - \underline{\nabla}\phi(r,z)$$

$$= - \left[\frac{\partial}{\partial r}\,\phi(r,z) \cdot \underline{r} + \frac{\partial}{\partial z}\phi(r,z) \cdot \underline{z}\right]$$

$$= - \left[E_r(\rho,\alpha) \cdot \underline{r} + E_z(\rho,\alpha) \cdot \underline{z}\right] . \qquad 3.8$$

The exact and complete expression for $\underline{E}$ is hence obtained by substituting the partial derivatives of $\phi$ as given by 3.1, thus obtaining:

$$E_r(\rho,\alpha) = \sum_{j=1}^{N} Q_j \{[-RRT(1,j) + \rho \cdot \sin\alpha]/W1$$

$$+ [RRT(2,j) + \rho \cdot \sin\alpha]/S1$$

$$+ [RRT(1,j) - \rho \cdot \sin\alpha]/U1$$

$$- [RRT(2,j) + \rho \cdot \sin\alpha]/V1\}$$

and

$$E_z(\rho,\alpha) = \sum_{j=1}^{N} Q_j \{[ZZT(2,j) + \rho \cdot \cos\alpha]/W1$$

$$+ [ZZT(2,j) + \rho \cdot \cos\alpha]/S1$$

$$+ [ZZT(1,j) - \rho \cdot \cos\alpha]/U1$$

$$+ [ZZT(1,j) - \rho \cdot \cos\alpha]/V1\}$$

where

$$RRT(1,j) = r(Q_j) - (A+RS)$$

$$RRT(2,j) = r(Q_j) + (A+RS)$$

$$ZZT(1,j) = z(Q_j) - H$$

$$ZZT(2,j) = z(Q_j) + H$$

$$U1 = [RRT(1,j) - \rho \cdot \sin \alpha]^2 + [ZZT(1,j) - \rho \cdot \cos \alpha]^2$$

$$V1 = [RRT(2,j) + \rho \cdot \sin \alpha]^2 + [ZZT(1,j) - \rho \cdot \cos \alpha]^2$$

$$W1 = [RRT(1,j) - \rho \cdot \sin \alpha]^2 + [ZZT(2,j) + \rho \cdot \cos \alpha]^2$$

$$S1 = [RRT(2,j) + \rho \cdot \sin \alpha]^2 + [ZZT(2,j) + \rho \cdot \cos \alpha]^2.$$

2. Boundary conditions

The potential of any point on the circumference of both subconductors I and II must equal to one unit which is the assumed potential above ground. To satisfy this condition, points are chosen on the conductor surface and their potential is equated to unity. In addition, the potential gradient along the surface must be equal to zero.

To fulfill this requirement, the potential at any point on the circumference of subconductor I is expressed as a function of the angle c between the line connecting the point and the center of subconductor I, and the vertical as shown in Figure 3.1. This is done using the geometrical transformation:

$$r = A + RS(1 + \sin c)$$

$$z = H + RS \cdot \cos c$$

and by applying it to 3.1, the following equation giving the potential at any point $c_i$ on subconductor I results

$$\phi(c)\Big|_{c=c_i} = -\sum_{j=1}^{N} Q_j \log_e\left[\frac{DC(1,j;\ c_i)\ \cdot\ DC(2,j;\ c_i)}{DI(1,j;\ c_i)\ \cdot\ DI(2,j;\ c_i)}\right]$$

$$= -\frac{1}{2}\sum_{j=1}^{N} Q_j \log_e\left[\frac{UU(i,j)\ \cdot\ VV(i,j)}{WW(i,j)\ \cdot\ SS(i,j)}\right] \qquad 3.9$$

where

$$UU(i,j) = [RRT(1,j) - RS \cdot \sin c_i]^2 + [ZZT(1,j) - RS \cos c_i]^2$$

$$VV(i,j) = [RRT(2,j) + RS \cdot \sin c_i]^2 + [ZZT(1,j) - RS \cdot \cos c_i]^2$$

$$WW(i,j) = [RRT(1,j) - RS \cdot \sin c_i]^2 + [ZZT(2,j) + RS \cdot \cos c_i]^2$$

$$SS(i,j) = [RRT(2,j) + RS \cdot \sin c_i]^2 + [ZZT(2,j) + RS \cdot \cos c_i]^2 .$$

To satisfy the boundary condition of unit applied potential on the circumference of subconductors I and II, selected points on subconductor I given by $c_i$ where $i=1,2,\ldots,M$ are set. At each point, $\phi(c_i)$ is set equal to unity. Then the first and even order derivatives (second, fourth,...) of $\phi(c_i)$ with respect to c are evaluated and set equal to zero. The constraints imposed on the first and even order derivatives preclude that $\phi(c_i)$ attains either a

maximum or a minimum value in the neighborhood of the points (57). Therefore, a unit equipotential surface will result having a curvature equal to RS and passing through the points $c_i$.

Thus, the equations representing the above conditions are:

$$\phi(c)\Big|_{c=c_i} = 1 \qquad 3.10$$

$$\frac{d\phi(c)}{dc}\Big|_{c=c_i} = 0 \qquad i=1,2,\ldots, M . \qquad 3.11$$

$$\frac{d^n\phi(c)}{dc^n}\Big|_{c=c_i} = 0, \; n=2,4, \ldots \qquad 3.12$$

According to 3.11 and 3.12, expressions for the first and even order derivatives of $\phi(c)$ with respect to c must be obtained. However, values of n greater than four will not be used since the resulting expressions become too cumbersome without improving the accuracy of the results. Using n=2 and n=4 leads to a unit equipotential surface adequately close to the subconductor circumference. The resulting expressions for the first, second and fourth order derivatives of $\phi(c)$ are:

$$\frac{d\phi(c)}{dc}\Big|_{c=c_i} = \sum_{j=1}^{N} Q_j[DC11(i,j) + DC21(i,j) - DI11(i,j) - DI21(i,j)]$$

where

$$DC11(i,j) = -RS[RRT(1,j) \cdot \cos c_i - ZZT(1,j) \cdot \sin c_i]/UU(i,j)$$

$$DC21(i,j) = RS[RRT(2,j) \cdot \cos c_i + ZZT(1,j) \cdot \sin c_i]/VV(i,j)$$

$$DI11(i,j) = -RS[RRT(1,j) \cdot \cos c_i + ZZT(2,j) \cdot \sin c_i]/WW(i,j)$$

$$DI21(i,j) = RS[RRT(2,j) \cdot \cos c_i - ZZT(2,j) \cdot \sin c_i]/SS(i,j)$$

$$\left.\frac{d^2\phi(c)}{dc^2}\right|_{c=c_i} = \sum_{j=1}^{N} Q_j[DC12(i,j) + DC22(i,j) - DI12(i,j) - DI22(i,j)]$$

where

$$DC12(i,j) = U(i,j) - 2[DC11(i,j)]^2$$

$$DC22(i,j) = V(i,j) - 2[DC21(i,j)]^2$$

$$DI12(i,j) = W(i,j) - 2[DI11(i,j)]^2$$

$$DI22(i,j) = S(i,j) - 2[DI21(i,j)]^2$$

$$U(i,j) = RS[RRT(1,j) \cdot \sin c_i + ZZT(1,j) \cdot \cos c_i]/UU(i,j)$$

$$V(i,j) = RS[-RRT(2,j) \cdot \sin c_i + ZZT(1,j) \cdot \cos c_i]/VV(i,j)$$

$$W(i,j) = RS[RRT(1,j) \cdot \sin c_i - ZZT(2,j) \cdot \cos c_i]/WW(i,j)$$

$$S(i,j) = RS[-RRT(2,j) \cdot \sin c_i - ZZT(2,j) \cdot \cos c_i]/SS(i,j)$$

$$\left.\frac{d^4\phi(c)}{dc^4}\right|_{c=c_i} = \sum_{j=1}^{N} Q_j [DC14(i,j) + DC24(i,j) - DI14(i,j) - DI24(i,j)]$$

where

$$DC14(i,j) = 6[DC11(i,j)]^2[1 + 2 \cdot U(i,j) + 4 \cdot DC12(i,j)] - DC12(i,j)[1 + 6 \cdot U(i,j)]$$

$$DC24(i,j) = 6[DC21(i,j)]^2[1 + 2 \cdot V(i,j) + 4 \cdot DC22(i,j)] - DC22(i,j)[1 + 6 \cdot V(i,j)]$$

$$DI14(i,j) = 6[DI11(i,j)]^2[1 + 2 \cdot W(i,j) + 4 \cdot DI12(i,j)] - DI12(i,j)[1 + 6 \cdot W(i,j)]$$

$$DI24(i,j) = 6[DI21(i,j)]^2[1 + 2 \cdot S(i,j) + 4 \cdot DI22(i,j)] - DI22(i,j)[1 + 6 \cdot S(i,j)] .$$

The other boundary condition is that the potential of ground be zero. This condition is automatically satisfied by including the image charges which are symmetrically located with respect to the ground plane.

3. Choice of parameters

To satisfy the above conditions and to obtain solvable equations that yield a unit equipotential surface coinciding with the circumferences of the two subconductors, care must be taken in choosing the parameters RC; $B_j$, j=1,2,...,N, and $c_i$, i=1,2,...,M. To set up N boundary equations in N unknowns (the line charges $Q_j$), M should be equal to N/4 since at each point $c_i$, four boundary equations are applied. Two factors are considered in choosing the values of the parameters $B_j$ and $c_i$; the distribution of these parameters with respect to each other and with respect to the subconductors surface, and the number, N, of the unknown line charges.

The potential of various points on the conductor's surface was computed using the values of line charges obtained for different choices of RC, N, $B_j$, and $c_i$ and for different practical conductor dimensions. Various results with different values for $B_j$ and $c_i$ indicated that the unit equipotential surface fits the conductor's boundary best when $RC = \frac{1}{2}$ RS, N=16, and when four values of $B_j$ lie between

each two successive values of $c_i$. The following choice of values for $B_j$ and $c_i$ has yielded the best results with the boundary surface having almost a unit potential with only a few points departing by less than 0.1%. This choice is

$B_j$ (radians)

0.3927 0.7500 1.1752 1.6000 1.9635 2.3500 2.7489

3.1000 3.5343 3.9000 4.3197 4.7000 5.1051 5.5000

5.8905 6.1000

$c_i$ (radians)

0.0 1.5708 3.1416 4.7124

Results were obtained for the case of a two bundle conductor of subconductor radius of RS = 2.235 cm and spacing D = 45.72 cm and height above ground of H = 23.622 m. This configuration was proposed for the west coast dc line (11). In Figure 3.2 the resulting line charges are reproduced from the computer output. To check the correctness and accuracy of computations, the potential around the surface of subconductor I, which is the same as that of subconductor II because of symmetry, was computed and the values obtained are reproduced in Figure 3.3.

## B. The Bipolar Twin-Bundle Line

### 1. Potential and electric field

Referring to Figure 3.4, the procedure adopted for the computation of the potential and electric field is as follows:

Figure 3.2. Equivalent axial charges, unipolar line

Q( 1) = 0.000010

Q( 2) = -0.014596

Q( 3) = -0.001503

Q( 4) = -0.005769

Q( 5) = -0.011350

Q( 6) = 0.003052

Q( 7) = -0.010651

Q( 8) = -0.005269

Q( 9) = 0.000654

Q(10) = -0.012750

Q(11) = 0.000648

Q(12) = -0.003867

Q(13) = -0.009198

Q(14) = 0.002568

Q(15) = -0.004270

Q(16) = -0.009054

Figure 3.3. Potential distribution on subconductor circumference, unipolar line

| ANGLE (DEGREES) | POTENTIAL (P.U.) |
|---|---|
| 0.0 | 1.000000 |
| 15.000 | 1.000095 |
| 30.000 | 1.000491 |
| 45.000 | 1.000730 |
| 60.000 | 1.000436 |
| 75.000 | 1.000077 |
| 90.000 | 1.000000 |
| 105.000 | 0.999922 |
| 120.000 | 0.999563 |
| 135.000 | 0.999302 |
| 150.000 | 0.999560 |
| 165.000 | 0.999921 |
| 180.000 | 1.000000 |
| 195.000 | 1.000078 |
| 210.000 | 1.000422 |
| 225.000 | 1.000644 |
| 240.000 | 1.000386 |
| 255.000 | 1.000067 |
| 270.000 | 1.000000 |
| 285.000 | 0.999933 |
| 300.000 | 0.999605 |
| 315.000 | 0.999326 |
| 330.000 | 0.999531 |
| 345.000 | 0.999906 |

Figure 3.4. Charge representation of the bipolar twin-bundle conductor system

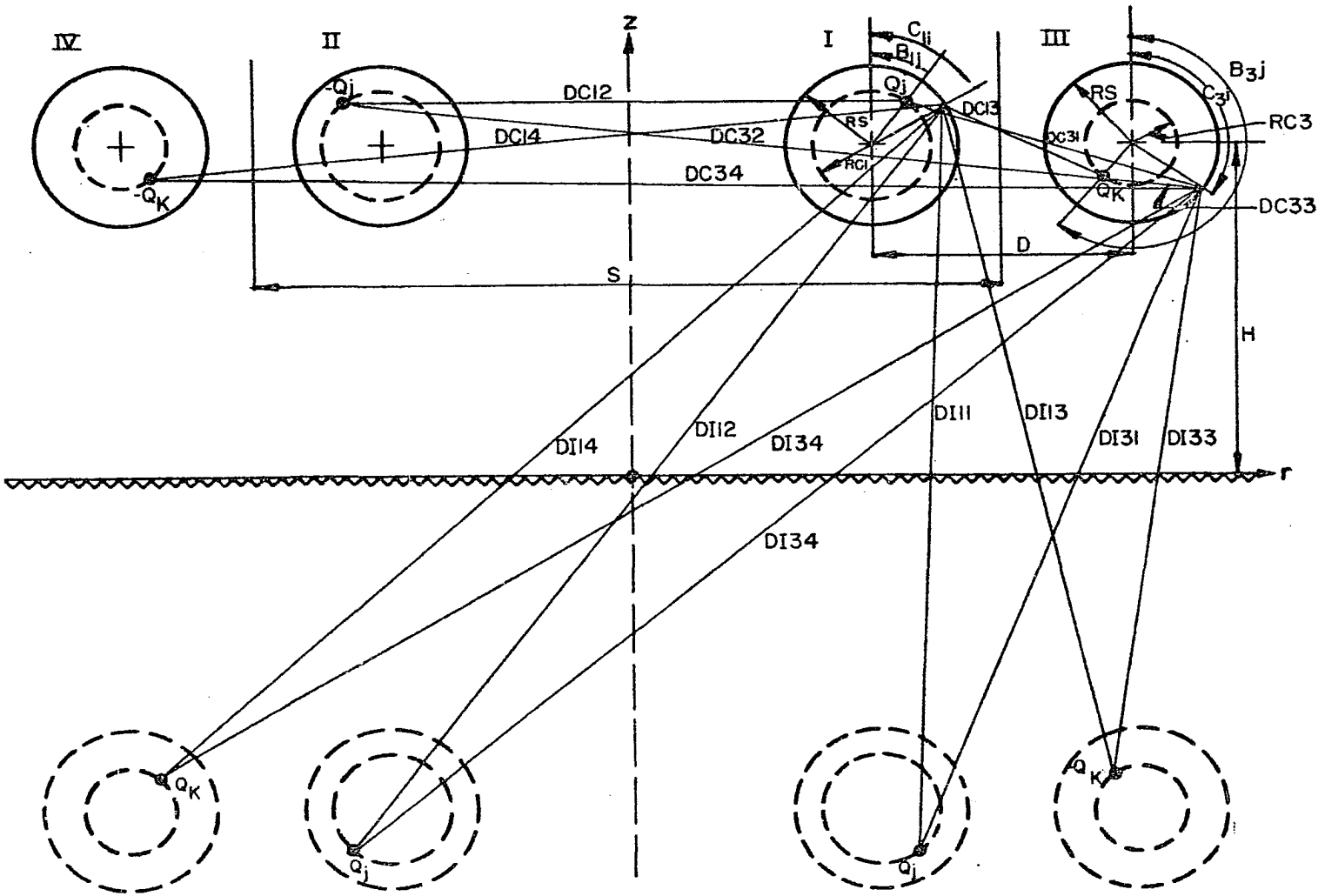
IV
II
I
III
z
r
$C_{1j}$
$B_{1j}$
$B_{3j}$
$C_{3j}$
$-Q_j$
$Q_j$
$-Q_K$
$Q_K$
RS
RC1
RC3
DC12
DC13
DC14
DC32
DC34
DC31
DC33
D
S
H
DI14
DI12
DI34
DI11
DI13
DI31
DI33
DI34

line charges of arbitrarily chosen number, M, and of unknown magnitudes ($Q_j$, j=1,2,...,M) are distributed along the subconductors parallel to their axes on fictitious coaxial cylinders. The radii of these cylinders (RC1 and RC3), where the subscript 1 and 3 refer to subconductors I and III of the same polarity, and the relative locations of these line charges ($B_{1j}$, j=1,2,...,N, and $B_{3j}$, j=N+1, N+2, ..., M) are part of the input data fed into the computer. They can be varied at any computer run during the development of this study. The relations between the location of the charges of the positive and negative subconductors are governed by symmetry of the configuration. Image charges with respect to the plane of ground of all line charges of the positive and negative subconductors are included to produce a zero potential on the ground plane as illustrated in Figure 3.4.

The potential at any point P(r,z) is the algebraic sum of the potentials due to each of the line charges and their images, and is given by:

$$\phi(r,z) = -\{\sum_{j=1}^{N} Q_j \log_e [\frac{DC1(1,j) \cdot DI1(2,j)}{DC1(2,j) \cdot DI1(1,j)}] + \sum_{j=N+1}^{M} Q_j \log_e [\frac{DC1(3,j) \cdot DI1(4,j)}{DC1(4,j) \cdot DI1(3,j)}]\} \qquad 3.13$$

where DC1(1,j), DC1(2,j), DC1(3,j), and DC1(4,j) are the distances from the point P(r,z) to the charges on subconductors I, II, III, and IV respectively, and DI1(1,j),

DI1(2,j), DI1(3,j), and DI1(4,j) are the distances to their images, respectively. These distances are given by the following equations

$$DC1(1,j) = \{[r1(Q_j)-r]^2 + [z1(Q_j)-z]^2\}^{\frac{1}{2}} \quad 3.14$$

$$DC1(2,j) = \{[r1(Q_j)+r]^2 + [z1(Q_j)-z]^2\}^{\frac{1}{2}} \quad 3.15$$

$$DC1(3,j) = \{[r3(Q_j)-r]^2 + [z3(Q_j)-z]^2\}^{\frac{1}{2}} \quad 3.16$$

$$DC1(4,j) = \{[r3(Q_j)+r]^2 + [z3(Q_j)-z]^2\}^{\frac{1}{2}} \quad 3.17$$

$$DI1(1,j) = \{[r1(Q_j)-r]^2 + [z1(Q_j)+z]^2\}^{\frac{1}{2}} \quad 3.18$$

$$DI1(2,j) = \{[r1(Q_j)+r]^2 + [z1(Q_j)+z]^2\}^{\frac{1}{2}} \quad 3.19$$

$$DI1(3,j) = \{[r3(Q_j)-r]^2 + [z3(Q_j)+z]^2\}^{\frac{1}{2}} \quad 3.20$$

$$DI1(4,j) = \{[r3(Q_j)+r]^2 + [z3(Q_j)+z]^2\}^{\frac{1}{2}} \quad 3.21$$

where the coordinates of the charges on subconductor I are

$$r1(Q_j) = \frac{1}{2}(S-D) + RC1 \cdot \sin B_{1j} \quad 3.22$$

$$z1(Q_j) = H + RC1 \cdot \cos B_{1j} \quad 3.23$$

and the coordinates of the charges on subconductor III are

$$r3(Q_j) = \frac{1}{2}(S+D) + RC3 \cdot \sin B_{3j} \quad 3.24$$

$$z3(Q_j) = H + RC3 \cdot \cos B_{3j} \; . \quad 3.25$$

The potential $\phi(\rho_1,\alpha_1)$ at any point P, at a radial

distance $\rho_1$ from the center of subconductor I and at an angle $\alpha_1$ from the vertical through that center, is obtained from equation 3.13 by applying the following substitution to equations 3.14 through 3.21

$$r = \frac{1}{2}(S-D) + \rho_1 \cdot \sin \alpha_1$$

$$z = H + \rho_1 \cdot \cos \cdot \alpha_1$$

The electric field $\underline{E}$ at P is given by

$$\underline{E}(\rho_1,\alpha_1) = -[E_r(\rho_1,\alpha_1) \cdot \underline{r} + E_z(\rho_1,\alpha_1) \cdot \underline{z}] \qquad 3.26$$

where the field components $E_r$ and $E_z$ are obtained by partial differentiation of $\phi$, as given by 3.13, with respect to r and z, respectively. The resulting expressions are as follows

$$\begin{aligned} E_r(\rho_1,\alpha_1) = \sum_{j=1}^{N} Q_j \{ & [X11-\rho_1 \cdot \sin \alpha_1]/DC1(1,j) \\ & - [X12 + \rho_1 \cdot \sin \alpha_1]/DI1(2,j) \\ & + [X12 + \rho_1 \cdot \sin \alpha_1]/DC1(2,j) \\ & - [X11 - \rho_1 \cdot \sin \alpha_1]/DI1(1,j)\} \\ + \sum_{j=N+1}^{M} Q_j \{ & [X13 - \rho_1 \cdot \sin \alpha_1]/DC1(3,j) \\ & - [X14 + \rho_1 \cdot \sin \alpha_1]/DI1(4,j) \\ & + [X14 + \rho_1 \cdot \sin \alpha_1]/DC1(4,j) \end{aligned}$$

$$- [X13 - \rho_1 \cdot \sin \alpha_1]/DI1(3,j)\}$$

and

$$E_z(\rho_1,\alpha_1) = \sum_{j=1}^{N} Q_j \{[Y11 - \rho_1 \cdot \cos \alpha_1]/DC1(1,j)$$

$$- [Y12 + \rho_1 \cdot \cos \alpha_1]/DI1(2,j)$$

$$- [Y11 - \rho_1 \cdot \cos \alpha_1]/DC1(2,j)$$

$$+ [Y12 + \rho_1 \cdot \cos \alpha_1]/DI1(1,j)\}$$

$$+ \sum_{j=N+1}^{M} Q_j \{[Y13 - \rho_1 \cdot \cos \alpha_1]/DC1(3,j)$$

$$- [Y14 + \rho_1 \cdot \cos \alpha_1]/DI1(4,j)$$

$$- [Y13 - \rho_1 \cdot \cos \alpha_1]/DC1(4,j)$$

$$+ [Y14 + \rho_1 \cdot \cos \alpha_1]/DI1(3,j)\}$$

where

$$X11 = RC1 \cdot \sin B_{1j}$$

$$X12 = S-D + RC1 \cdot \sin B_{1j}$$

$$X13 = D + RC3 \cdot \sin B_{3j}$$

$$X14 = S + RC3 \cdot \sin B_{3j}$$

$$Y11 = RC1 \cdot \cos B_{1j}$$

$$Y12 = 2H + RC1 \cdot \cos B_{1j}$$

$$Y13 = RC3 \cdot \cos B_{3j}$$

$$Y14 = 2H + RC3 \cdot \cos B_{3j}$$

Similarly, the potential $\phi(\rho_3,\alpha_3)$ at any point P, at a radial distance $\rho_3$ from the center of subconductor III and at an angle $\alpha_3$ from the vertical through that center, is obtained from equation 3.13 by applying the following substitution to equations 3.14 through 3.21

$$r = \frac{1}{2}(S+D) + \rho_3 \cdot \sin \alpha_3$$

$$z = H + \rho_3 \cdot \cos \alpha_3$$

The electric field $\underline{E}$ at P is given by

$$\underline{E}(\rho_3,\alpha_3) = -[E_r(\rho_3,\alpha_3) \cdot \underline{r} + E_z(\rho_3,\alpha_3) \cdot \underline{z}] \qquad 3.27$$

where the expressions for $E_r$ and $E_z$ are as follows

$$\begin{aligned} E_r(\rho_3,\alpha_3) = \sum_{j=1}^{N} Q_j \{ & [X31 - \rho_3 \cdot \sin \alpha_3]/DC1(1,j) \\ & - [X32 + \rho_3 \cdot \sin \alpha_3]/DI1(2,j) \\ & + [X32 + \rho_3 \cdot \sin \alpha_3]/DC1(2.j) \\ & - [X31 - \rho_3 \cdot \sin \alpha_3]/DI1(1,j)\} \\ + \sum_{j=N+1}^{M} Q_j \{ & [X33 - \rho_3 \cdot \sin \alpha_3]/DC1(3,j) \\ & - [X34 + \rho_3 \cdot \sin \alpha_3]/DI1(4,j) \\ & + [X34 + \rho_3 \cdot \sin \alpha_3]/DC1(4,j) \\ & - [X33 - \rho_3 \cdot \sin \alpha_3]/DI1(3,j)\} \end{aligned}$$

and

$$E_z(\rho_3,\alpha_3) = \sum_{j=1}^{N} Q_j \{[Y31 - \rho_3 \cdot \cos \alpha_3]/DC1(1,j)$$

$$- [Y32 + \rho_3 \cdot \cos \alpha_3]/DI1(2,j)$$

$$- [Y31 - \rho_3 \cdot \cos \alpha_3]/DC1(2,j)$$

$$+ [Y32 + \rho_3 \cdot \cos \alpha_3]/DI1(1,j)\}$$

$$+ \sum_{j=N+1}^{M} Q_j \{[Y33 - \rho_3 \cdot \cos \alpha_3]/DC1(3,j)$$

$$- [Y34 + \rho_3 \cdot \cos \alpha_3]/DI1(4,j)$$

$$- [Y33 - \rho_3 \cdot \cos \alpha_3]/DC1(4,j)$$

$$+ [Y34 + \rho_3 \cdot \cos \alpha_3]/DI1(3,j)\}$$

$$X31 = RC1 \cdot \sin B_{1j} - D$$

$$X32 = S + RC1 \cdot \sin B_{1j}$$

$$X33 = RC3 \cdot \sin B_{3j}$$

$$X34 = S + D + RC3 \cdot \sin B_{3j}$$

$$Y31 = RC1 \cdot \cos B_{1j}$$

$$Y32 = 2H + RC1 \cdot \cos B_{1j}$$

$$Y33 = RC3 \cdot \cos B_{3j}$$

$$Y34 = 2H + RC3 \cdot \cos B_{3j}$$

2. Boundary conditions

The potential of any point on the boundaries of both the positive and negative subconductors is assumed equal to one unit. In order to obtain unit equipotential surfaces on the subconductor boundaries, the potential at any point on the circumference of subconductor I and subconductor III are expressed as functions of one variable only, as in the foregoing case of the unipolar line. This variable is thus the angle of the lines passing through the point and the center of subconductors I and III from the vertical, c1 and c3, respectively. This is done by substituting (r1, z1) and (r3, z3), respectively, for (r,z) in equations 3.14 through 3.21, where

$$r1 = \frac{1}{2}(S-D) + RS \cdot \sin c1$$

$$z1 = H + RS \cdot \cos c1$$

$$r3 = \frac{1}{2}(S+D) + RS \cdot \sin c3$$

$$z3 = H + RS \cdot \cos c3.$$

Then Equation 3.13 results in the following potential equations for points on subconductors I and III, having angles $c1_i$ and $c3_i$, respectively:

$$\phi(c1_i) = -\{\sum_{j=1}^{N} Q_j \log_e [\frac{DC11(i,j;c1) \cdot DI12(i,j;c1)}{DC12(i,j;c1) \cdot DI11(i,j;c1)}]$$

$$+ \sum_{j=N+1}^{M} Q_j \log_e \left[\frac{DC13(i,j;c1) \cdot DI14(i,j;c1)}{DC14(i,j;c1) \cdot DI13(i,j;c1)}\right]\} \qquad 3.28$$

$$\phi(c3_i) = -\{\sum_{j=1}^{N} Q_j \log_e \left[\frac{DC31(i,j;c3) \cdot DI32(i,j;c3)}{DC32(i,j;c3) \cdot DI31(i,j;c3)}\right]$$

$$+ \sum_{j=N+1}^{M} Q_j \log_e \left[\frac{DC33(i,j;c3) \cdot DI32(i,j;c3)}{DC34(i,j;c3) \cdot DI33(i,j;c3)}\right]\} \qquad 3.29$$

To satisfy the boundary condition of unit potential on both the positive and negative subconductor boundaries, selected points on subconductors I and III ($cl_i$, i=1,2,...,K and $c3_i$, i=1,2,...,L) are chosen, at each of which $\phi(cl_i)$ and $\phi(c3_i)$ are set equal to unity; the first and even order derivatives (second, fourth, ...) of $\phi(cl)$ with respect to cl and $\phi(c3)$ with respect to c3 are evaluated and set equal to zero, in order to satisfy the boundary conditions as previously explained. Thus the equations representing the above conditions are:

$$\phi(cl)\Big|_{cl=cl_i} = 1 \qquad 3.30$$

$$\frac{d\phi(cl)}{dcl}\Big|_{cl=cl_i} = 0 \qquad i=1,2,...,K \qquad 3.31$$

$$\frac{d^n\phi(cl)}{dcl^n}\Big|_{cl=cl_i} = 0, \quad n=2,4,... \qquad 3.32$$

and

$$\phi(c3)\Big|_{c3=c3_i} = 1 \tag{3.33}$$

$$\frac{d\phi(c3)}{dc3}\Big|_{c3=c3_i} = 0 \qquad i=1,2,\ldots,L \tag{3.34}$$

$$\frac{d^n\phi(c3)}{dc3^n}\Big|_{c3=c3_i} = 0, \quad n=2,4,\ldots \tag{3.35}$$

According to Equations 3.31, 3.32, 3.34, and 3.35 expressions for the first and even order derivatives of $\phi(c1)$ with respect to c1, and $\phi(c3)$ with respect to c3 are obtained. However, values of n greater than four are not used since the resulting expressions for the higher order derivatives become too cumbersome and lengthy. The resulting equations for the first, second, and fourth order derivatives of $\phi(c1)$ with respect to c1, evaluated at $c1_i$, are:

$$\begin{aligned}\frac{d\phi(c1)}{dc1}\Big|_{c1=c1_i} = &\sum_{j=1}^{N} Q_j[DC111(i,j;c1)+DI121(i,j;c1) \\ &- DC121(i,j;c1) - DI111(i,j;c1)] \\ &+ \sum_{j=N+1}^{M} Q_j[DC131(i,j;c1) + DI141(i,j;c1) \\ &- DC141(i,j;c1) - DI131(i,j;c1)]\end{aligned}$$

where

$$DC111(i,j;cl) = -RS(X11\cdot\cos cl_i - Y11\cdot\sin cl_i)/DC11(i,j;cl)$$

$$DC121(i,j;cl) = -RS(-X12\cdot\cos cl_i - Y11\cdot\sin cl_i)/DC12(i,j;cl)$$

$$DI111(i,j;cl) = -RS(X11\cdot\cos cl_i + Y12\cdot\sin cl_i)/DI11(i,j;cl)$$

$$DI121(i,j;cl) = -RS(-X12\cdot\cos cl_i + Y12\cdot\sin cl_i)/DI12(i,j;cl)$$

$$DC131(i,j;cl) = -RS(X13\cdot\cos cl_i - Y13\cdot\sin cl_i)/DC13(i,j;cl)$$

$$DC141(i,j;cl) = -RS(-X14\cdot\cos cl_i - Y13\cdot\sin cl_i)/DC14(i,j;cl)$$

$$DI131(i,j;cl) = -RS(X13\cdot\cos cl_i + Y14\cdot\sin cl_i)/DI13(i,j;cl)$$

$$DI141(i,j;cl) = -RS(-X14\cdot\cos cl_i + Y14\cdot\sin cl_i)/DI14(i,j;cl)$$

$$\left.\frac{d^2\phi(cl)}{dcl^2}\right|_{cl=cl_i} = \sum_{j=1}^{N} Q_j [DC112(i,j;cl) + DI122(i,j;cl) - DC122(i,j;cl) - DI112(i,j;cl)] + \sum_{j=N+1}^{M} Q_j [DC132(i,j;cl) + DI142(i,j;cl) - DC142(i,j;cl) - DI132(i,j;cl)]$$

where

$$DC112(i,j;cl) = UC11(i,j;cl) - 2[DC11(i,j;cl)]^2$$

$$DC122(i,j;cl) = UC12(i,j;cl) - 2[DC12(i,j;cl)]^2$$

$$DI112(i,j;cl) = UI11(i,j;cl) - 2[DI11(i,j;cl)]^2$$

$$DI122(i,j;cl) = UI12(i,j;cl) - 2[DI12(i,j;cl)]^2$$

$$DC132(i,j;cl) = UC13(i,j;cl) - 2[DC13(i,j;cl)]^2$$

$$DC142(i,j;cl) = UC14(i,j;cl) - 2[DC14(i,j;cl)]^2$$

$$DI132(i,j;cl) = UI13(i,j;cl) - 2[DI13(i,j;cl)]^2$$

$$DI142(i,j;cl) = UI14(i,j;cl) - 2[DI14(i,j;cl)]^2$$

and,

$$UC11(i,j;cl) = RS(X11\cdot\sin cl_i + Y11\cdot\cos cl_i)/DC11(i,j;cl)$$

$$UC12(i,j;cl) = RS(-X12\cdot\sin cl_i + Y11\cdot\cos cl_i)/DC12(i,j;cl)$$

$$UI11(i,j;cl) = RS(X11\cdot\sin cl_i - Y12\cdot\cos cl_i)/DI11(i,j;cl)$$

$$UI12(i,j;cl) = RS(-X12\cdot\sin cl_i - Y12\cdot\cos cl_i)/DI12(i,j;cl)$$

$$UC13(i,j;cl) = RS(X13\cdot\sin cl_i + Y13\cdot\cos cl_i)/DC13(i,j;cl)$$

$$UC14(i,j;cl) = RS(-X14\cdot\sin cl_i + Y13\cdot\cos cl_i)/DC14(i,j;cl)$$

$$UI13(i,j;cl) = RS(X13\cdot\sin cl_i - Y14\cdot\cos cl_i)/DI13(i,j;cl)$$

$$UI14(i,j;cl) = RS(-X14\cdot\sin cl_i - Y14\cdot\cos cl_i)/DI14(i,j;cl)$$

$$\left.\frac{d^4\phi(cl)}{dcl^4}\right|_{cl=cl_i} = \sum_{j=1}^{N} Q_j [DC114(i,j;cl) + DI124(i,j;cl) - DC124(i,j;cl) - DI114(i,j;cl)]$$

$$+ \sum_{j=1+N}^{M} Q_j [DC134(i,j;c1) + DI144(i,j;c1)$$

$$-DC144(i,j;c1) - DI134(i,j;c1)]$$

where

$$DC114(i,j;c1) = 6[DC111(i,j;c1)]^2 \{1+2[UC11(i,j;c1)] + 4[DC112(i,j;c1)]\} - DC112(i,j;c1) \{1 + 6[UC11(i,j;c1)]\}$$

$$DC124(i,j;c1) = 6[DC121(i,j;c1]^2 \{1+2[UC12(i,j;c1)] + 4[DC122(i,j;c1)]\} - DC122(i,j;c1) \{1 + 6[UC12(i,j;c1)]\}$$

$$DI114(i,j;c1) = 6[DI111(i,j;c1)]^2 \{1+2[UI11(i,j;c1)] + 4[DI112(i,j;c1)]\} - DI112(i,j;c1) \{1 + 6[UI11(i,j;c1)]\}$$

$$DI124(i,j;c1) = 6[DI121(i,j;c1)]^2 \{1+2[UI12(i,j;c1)] + 4[DI122(i,j;c1)]\} - DI122(i,j;c1) \{1 + 6[UI12(i,j;c1)]\}$$

$$DC134(i,j;c1) = 6[DC131(i,j;c1)]^2 \{1+2[UC13(i,j;c1)] + 4[DC132(i,j;c1)]\} - DC132(i,j;c1) \{1 + 6[UC13(i,j;c1)]\}$$

$$DC144(i,j;c1) = 6[DC141(i,j;c1)]^2 \{1+2[UC14(i,j;c1)] + 4[DC142(i,j;c1)]\} - DC142(i,j;c1) \{1 + 6[UC14(i,j;c1)]\}$$

$$DI134(i,j;c1) = 6[DI131(i,j;c1)]^2 \{1+2[UI13(i,j;c1)] + 4[DI132(i,j;c1)]\} - DI132(i,j;c1) \{1 + 6[UI13(i,j;c1)]\}$$

$$DI144(i,j;c1) = 6[DI141(i,j;c1)]^2 \{1+2[UI14(i,j;c1)] + 4[DI142(i,j;c1)]\} - DI142(i,j;c1) \{1 + 6[UI14(i,j;c1)]\}$$

The corresponding equations for the first, second and fourth order derivatives of $\phi(c3)$ with respect to c3, evaluated at $c3_i$ are:

$$\left.\frac{d\phi(c3)}{dc3}\right|_{c3=c3_i} = \sum_{j=1}^{N} Q_j [DC311(i,j;c3) + DI321(i,j;c3) - DC321(i,j;c3) - DI311(i,j;c3)] + \sum_{j=N+1}^{M} Q_j [DC311(i,j;c3) + DI341(i,j;c3)$$

$$- DC341(i,j;c3) - DI331(i,j;c3)]$$

where

$$DC311(i,j;c3) = -RS(X31\cdot\cos c3_i - Y31\cdot\sin c3_i)/DC31(i,j;c3)$$

$$DC321(i,j;c3) = -RS(-X32\cdot\cos c3_i - Y31\cdot\sin c3_i)/DC32(i,j;c3)$$

$$DI311(i,j;c3) = -RS(X31\cdot\cos c3_i + Y32\cdot\sin c3_i)/DI31(i,j;c3)$$

$$DI321(i,j;c3) = -RS(-X32\cdot\cos c3_i + Y32\cdot\sin c3_i)/DI32(i,j;c3)$$

$$DC331(i,j;c3) = -RS(X33\cdot\cos c3_i - Y33\cdot\sin c3_i)/DC33(i,j;c3)$$

$$DC341(i,j;c3) = -RS(-X34\cdot\cos c3_i - Y33\cdot\sin c3_i)/DC34(i,j;c3)$$

$$DI331(i,j;c3) = -RS(X33\cdot\cos c3_i + Y34\cdot\sin c3_i)/DI33(i,j;c3)$$

$$DI341(i,j;c3) = -RS(-X34\cdot\cos c3_i + Y34\cdot\sin c3_i)/DI34(i,j;c3)$$

$$\left.\frac{d^2\phi(c3)}{dc3^2}\right|_{c3=c3_i} = \sum_{j=1}^{N} Q_j [DC312(i,j;c3) + DI322(i,j;c3)$$

$$- DC322(i,j;c3) - DI312(i,j;c3)]$$

$$+ \sum_{j=N+1}^{M} Q_j [DC332(i,j;c3) + DI342(i,j;c3)$$

$$- DC342(i,j;c1) - DI332(i,j;c3)]$$

where

$$DC312(i,j;c3) = UC31(i,j;c3) - 2[DC31(i,j;c3)]^2$$

$$DC322(i,j;c3) = UC32(i,j;c3) - 2[DC32(i,j;c3)]^2$$

$$DI312(i,j;c3) = UI31(i,j;c3) - 2[DI31(i,j;c3)]^2$$

$$DI322(i,j;c3) = UI32(i,j;c3) - 2[DI32(i,j;c3)]^2$$

$$DC332(i,j;c3) = UC33(i,j;c3) - 2[DC33(i,j;c3)]^2$$

$$DC342(i,j;c3) = UC34(i,j;c3) - 2[DC34(i,j;c3)]^2$$

$$DI332(i,j;c3) = UI33(i.j;c3) - 2[DI33(i,j;c3)]^2$$

$$DI342(i,j;c3) = UI34(i,j;c3) - 2[DI34(i,j;c3)]^2$$

and,

$$UC31(i,j;c3) = RS(X31\cdot\sin c3_i + Y31\cdot\cos c3_i)/DC31(i,j;c3)$$

$$UC32(i,j;c3) = RS(-X32\cdot\sin c3_i + Y31\cdot\cos c3_i)/DC32(i,j;c3)$$

$$UI31(i,j;c3) = RS(X31\cdot\sin c3_i - Y32\cdot\cos c3_i)/DI31(i,j;c3)$$

$$UI32(i,j;c3) = RS(-X32\cdot\sin c3_i - Y32\cdot\cos c3_i)/DI32(i,j;c3)$$

$$UC33(i,j;c3) = RS(X33\cdot\sin c3_i + Y33\cdot\cos c3_i)/DC33(i,j;c3)$$

$$UC34(i,j;c3) = RS(-X34\cdot\sin c3_i + Y33\cdot\cos c3_i)/DC34(i,j;c3)$$

$$UI33(i,j;c3) = RS(X33\cdot\sin c3_i - Y34\cdot\cos c3_i)/DI33(i,j;c3)$$

$$UI34(i,j;c3) = RS(-X34\cdot\sin c3_i - Y34\cdot\cos c3_i)/DI34(i,j;c3)$$

$$\left.\frac{d^4\phi(c3)}{dc3^4}\right|_{c3=c3_i} = \sum_{j=1}^{N} Q_j[DC314(i,j;c3) + DI324(i,j;c3) - DC324(i,j;c3) - DI314(i,j;c3)] + \sum_{j=1+N}^{M} Q_j[DC334(i,j;c3) + DI344(i,j;c3)$$

$$- DC344(i.k;c3) - DI334(i,j;c3)]$$

where

$$DC314(i,j;c3) = 6[DC311(i,j;c3)]^2 \{1+2[UC31(i,j;c3)] + 4[DC312(i,j;c3)]\} - DC312(i,j;c3) \{1 + 6[UC31(i,j;c3)]\}$$

$$DC324(i,j;c3) = 6[DC321(i,j;c3)]^2 \{1+2[UC32(i,j;c3)] + 4[DC322(i,j;c3)]\} - DC322(i,j;c3) \{1 + 6[UC32(i,j;c3)]\}$$

$$DI314(i,j;c3) = 6[DI311(i,j;c3)]^2 \{1+2[UI31(i,j;c3)] + 4[DI312(i,j;c3)]\} - DI312(i,j;c3) \{1 + 6[UI31(i,j;c3)]\}$$

$$DI324(i,j;c3) = 6[DI321(i,j;c3)]^2\{1+2[UI32(i,j;c3)] + 4[DI322(i,j;c3)]\} - DI322(i,j;c3) \{1 + 6[UI32(i,j;c3)]\}$$

$$DC334(i,j;c3) = 6[DC331(i,j;c3)]^2 \{1+2[UC33(i,j;c3)] + 4[DC332(i,j;c3)]\} - DC332(i,j;c3) \{1 + 6[UC33(i,j;c3)]\}$$

$$DC344(i,j;c3) = 6[DC341(i,j;c3)]^2 \{1+2[UC34(i,j;c3)] + 4[DC342(i,j;c3)]\} - DC342(i,j;c3) \{1 + 6[UC34(i,j;c3)]\}$$

$$DI334(i,j;c3) = 6[DI331(i,j;c3)]^2 \{1+2[UI33(i,j;c3)] + 4[DI332(i,j;c3)]\} - DI332(i,j;c3) \{1 + 6[UI33(i,j;c3)]\}$$

$$DI344(i,j;c3) = 6[DI341(i,j;c3)]^2 \{1+2[UI34(i,j;c3)] + 4[DI342(i,j;c3)]\} - DI342(i,j;c3) \{1 + 6[UI34(i,j;c3)]\}$$

The other boundary condition is that the potential of ground be zero, which is again automatically satisfied by including the image charges which are symmetrically located with respect to the ground plane.

## 3. Choice of parameters

To satisfy the boundary conditions of unit equipotential surfaces on both the positive and negative subconductors, care is taken in choosing the parameters RC1; RC3, $B_{1j}$, j=1,2,...,N; $B_{3j}$, j=N+1, N+2, ..., M; $c1_i$, i=1,2,...,K; $c3_i$, i=1,2,...,L. However, a restriction that K+L=M/4 should exist in order to get M boundary equations in M un-

knowns (the line charges $Q_j$) so that a solution of the equations is possible.

The values of the parameters that yielded unit equipotential surfaces adequately close to the subconductors boundaries are

RC1 = 0.3 RS

RC3 = 0.4 RS

Number of line charges in each subconductor = 16

$B_{1j}$ or $B_{3j}$ (radians)

0.3927 0.7500 1.1752 1.6000 1.9635 2.3500 2.7489 3.1000
3.5343 3.9000 4.3197 4.7000 5.1051 5.5000 5.8905 6.1000

$c1_i$ or $c3_i$ (radians)

0.0 1.5708 3.1416 4.7124.

Results were obtained for the 1100 kV test bipolar line (9) of subconductor radius RS = 2.25 cm, D = 45.70 cm, S = 1070.00 cm, and H = 1220.00 cm. In Figure 3.5, the resulting line charges are shown. To check the correctness and accuracy of computations, the potentials around the surfaces of the two positive subconductors were computed and the values obtained are reproduced in Figure 3.6.

Figure 3.5. Equivalent axial charges, bipolar line

| SUBCONDUCTOR "1" | | SUBCONDUCTOR "2" | |
|---|---|---|---|
| Q( 1) = | -0.005483 | Q(17) = | -0.004692 |
| Q( 2) = | -0.007598 | Q(18) = | -0.012562 |
| Q( 3) = | -0.003367 | Q(19) = | -0.005965 |
| Q( 4) = | -0.003856 | Q(20) = | -0.007982 |
| Q( 5) = | -0.006363 | Q(21) = | -0.011059 |
| Q( 6) = | -0.002522 | Q(22) = | -0.002984 |
| Q( 7) = | -0.007578 | Q(23) = | -0.010216 |
| Q( 8) = | -0.007743 | Q(24) = | -0.007271 |
| Q( 9) = | -0.005656 | Q(25) = | -0.002815 |
| Q(10) = | -0.011742 | Q(26) = | -0.010755 |
| Q(11) = | -0.007017 | Q(27) = | -0.002084 |
| Q(12) = | -0.009101 | Q(28) = | -0.004980 |
| Q(13) = | -0.010590 | Q(29) = | -0.008128 |
| Q(14) = | -0.007321 | Q(30) = | -0.002421 |
| Q(15) = | -0.003438 | Q(31) = | -0.002804 |
| Q(16) = | -0.011352 | Q(32) = | -0.011405 |

Figure 3.6. Potential distribution on subconductor circumference, bipolar line

| SUBCONDUCTOR "1" | | SUBCONDUCTOR "2" | |
|---|---|---|---|
| ANGLE (DEGREES) | POTENTIAL (P.U.) | ANGLE (DEGREES) | POTENTIAL (P.U.) |
| 0.0 | 1.000000 | 0.0 | 1.000000 |
| 15.000 | 1.000002 | 15.000 | 1.000017 |
| 30.000 | 1.000009 | 30.000 | 1.000084 |
| 45.000 | 1.000013 | 45.000 | 1.000122 |
| 60.000 | 1.000008 | 60.000 | 1.000074 |
| 75.000 | 1.000001 | 75.000 | 1.000014 |
| 90.000 | 1.000000 | 90.000 | 1.000000 |
| 105.000 | 0.999999 | 105.000 | 0.999986 |
| 120.000 | 0.999992 | 120.000 | 0.999927 |
| 135.000 | 0.999988 | 135.000 | 0.999886 |
| 150.000 | 0.999992 | 150.000 | 0.999926 |
| 165.000 | 0.999998 | 165.000 | 0.999986 |
| 180.000 | 1.000000 | 180.000 | 1.000000 |
| 195.000 | 1.000002 | 195.000 | 1.000014 |
| 210.000 | 1.000008 | 210.000 | 1.000073 |
| 225.000 | 1.000012 | 225.000 | 1.000109 |
| 240.000 | 1.000007 | 240.000 | 1.000067 |
| 255.000 | 1.000001 | 255.000 | 1.000012 |
| 270.000 | 1.000000 | 270.000 | 1.000000 |
| 285.000 | 0.999999 | 285.000 | 0.999988 |
| 300.000 | 0.999992 | 300.000 | 0.999932 |
| 315.000 | 0.999987 | 315.000 | 0.999885 |
| 330.000 | 0.999991 | 330.000 | 0.999918 |
| 345.000 | 0.999998 | 345.000 | 0.999983 |

# IV. CALCULATION OF THE CORONA THRESHOLD IN NONUNIFORM FIELDS

## A. Mathematical Model

Referring to Figure 4.1 and assuming that one free electron at a distance $x_1$ is accelerated towards the positive subconductor by the external electric field, an electron avalanche and an associated positive ion space charge will be developed due to ionization by electron collision. The number of electrons created in a slab at a distance x and thickness dx is

$$dn = n\alpha(x)\, dx \tag{4.1}$$

where

n = number of electrons entering the slab

$\alpha(x)$ = number of electrons produced per unit length in field direction by electron collision known as Townsend's first ionization coefficient corresponding to the external electric field at x

Integrating equation 4.1, we get

$$n = \exp\left(\int_{x_1}^{x} \alpha(x')dx'\right) \tag{4.2}$$

and substituting for n from 4.2 into 4.1, we get

$$dn = \alpha(x)\, \exp\left(\int_{x_1}^{x} \alpha(x')\, dx'\right) dx \tag{4.3}$$

At x'=x the electron cloud will be confined to a roughly cylindrical volume of radius r (16), due to radial diffusion caused by the high random velocity of the electrons. The radius r is obtained from the diffusion equation (42)

$$r = \sqrt{6\ D_e t} \qquad 4.4$$

where

$D_e$ = diffusion coefficient for electrons

$t$ = avalanche transit time

$= \int_{x_1}^{x} \frac{1}{V_e(x')} dx'$, where $V_e(x')$ is the electron drift velocity in the field direction at the point x'

The avalanche electrons will be absorbed by the positive subconductor leaving behind the space charge of positive ions. The density of the positive ion space charge $\sigma$ at x'=x is given by

$$\sigma = \frac{dn}{\pi r^2 dx} = \frac{\alpha(x)\exp\left(\int_{x_1}^{x} \alpha(x')dx'\right)}{\pi r^2} \qquad 4.5$$

To estimate the electric field caused by the positive ion space charge, the space charge is assumed to be contained in a sphere of radius r. According to Loeb (16) this spherical approximation will yield space charge fields differing slightly from those resulting from the actual, much complicated space charge distribution. The total

number of positive ions N in the spherical volume at x'=x is the product of the density of ions at x given by Equation 4.5 and the spherical volume of radius r, thus

$$N = \frac{4}{3} r\alpha(x) \exp\left(\int_{x_1}^{x} \alpha(x')\, dx'\right) \qquad 4.6$$

The spherical positive space charge will result in an electric field, referred to as the space charge field, given by

$$\vec{E}_y = \frac{eN}{4\pi\varepsilon_0 y^2} \cdot \vec{y} \qquad 4.7$$

where

$\vec{E}_y$ = space charge field vector at a point distance y from the center of the spherical space charge

$\varepsilon_0$ = permittivity of free space

e = electron charge (positive ion charge)

$\vec{y}$ = unit radial vector

Therefore, the resultant field at any point in the gap will be the vectorial sum of the external and space charge fields at that point.

Accompanying the creation of the N positive ions in the spherical space charge, there will be a corresponding number of excited states resulting from electric collisions during the formation of the first electron avalanche. The ratio of the number of excited states to the number of ionized states, denoted by f, can be considered relatively constant

(16). These excited states, upon returning back to their stable conditions, will emit an equivalent number of photons. Thus the number of photons $I_0$ created in the spherical volume of the positive ion space charge will be given by

$$I_0 = fN = \frac{4}{3} fr\alpha(x) \exp\left(\int_{x_1}^{x} \alpha(x')\, dx'\right) \qquad 4.8$$

Due to the absorption of the gas (air), the number of photons I reaching a distance $\rho$ from the center of the space charge sphere will be

$$I = I_0 e^{-u\rho} \qquad 4.9$$

where u = absorption coefficient of the gas (air). The number of photons absorbed in the semi-spherical shell of inner radius $\rho$ and outer radius $\rho+d\rho$ is given by $-\frac{1}{2} dI$, where

$$-\frac{1}{2} dI = \frac{1}{2} I_0\, ue^{-u\rho}\, d\rho \qquad 4.10$$

Assuming that a fraction P of the absorbed photons succeed in liberating photoelectrons, the number of photoelectrons created in the spherical shell between $\rho$ and $\rho+d\rho$

$$\begin{aligned} &= \frac{1}{2} PI_0\, ue^{-u\rho}\, d\rho \\ &= \frac{1}{2} PfN\, ue^{-u\rho}\, d\rho \end{aligned} \qquad 4.11$$

where

P = probability of photoionization

These photoelectrons will be accelerated by the resultant electric field, and therefore each photoelectron will start an auxiliary avalanche, the tip of which reaches the surface of the spherical positive ion space charge, and hence causes the streamer to advance. The density of positive ions $\sigma'$ will be given by an equation similar to 4.4,

$$\sigma' = \frac{\alpha'(x)\ \exp\left(\int_{1-\rho}^{1-r} \alpha'(x')\ dx'\right)}{\pi r'^2} \qquad 4.12$$

where

$\alpha'(x')$ = Townsend's first ionization coefficient corresponding to the resultant electric field at x'

$r'$ = radius of the new spherical positive ion space charge

The number of positive ions in the tip of each auxiliary avalanche is

$$= \sigma' \cdot \frac{4}{3} \pi r'^3 \qquad 4.13$$

and from 4.11 the number of positive ions, dN', in the tips of the auxiliary avalanches starting between $\rho$ and $\rho+d\rho$ will be given by

$$dN' = \sigma' \cdot \frac{4}{3} \pi r'^3 \cdot \frac{1}{2} Pf N\ u e^{-u\rho} d\rho$$

$$= \frac{2}{3} Pf N r'\ u e^{-u\rho}\ \alpha'(x)\ \exp\left(\int_{1-\rho}^{1-r} \alpha'(x')dx'\right)d\rho \qquad 4.14$$

Since the radius of the space charge varies with $\sqrt{D_e t}$, and

the electron drift velocity increases only with the square root of the electric field, assuming that the electron drift velocities of the main and auxiliary avalanches to be approximately equal will not be far from reality. This approximation will simplify the derivation of the equation representing the criterion for streamer propagation, since it enables the replacement of r' in terms of r by the approximate relation following directly from the diffusion equation

$$r' = r\left(\frac{\rho-r}{1-x_1}\right)^{\frac{1}{2}} \qquad 4.15$$

and

$$dN' = \frac{2}{3} PfNr\left(\frac{\rho-r}{1-x_1}\right)^{\frac{1}{2}} ue^{-u\rho}\alpha'(x)\ \exp\left(\int_{1-\rho}^{1-r}\alpha'(x')dx'\right)d\rho \qquad 4.16$$

Integrating Equation 4.16 yields the total number of new positive ions, N', produced by the secondary action of photoionization in the gas,

$$N' = \int_R^r \frac{2}{3} PfNr\left(\frac{\rho-r}{1-x_1}\right)^{\frac{1}{2}} ue^{-u\rho}\ \alpha'(x)\ \exp\left(\int_{1-\rho}^{1-r}\alpha'(x')dx'\right)d\rho \qquad 4.17$$

where the lower limit of integration, R, represents the distance from the center of the first spherical space charge at which a photoelectron will just be capable of ionizing by collision.

The condition for streamer advance is that N=N' thus yielding the following equation representing the criterion

for streamer propagation

$$\int_R^r \frac{2}{3} \text{Pfr}\left(\frac{\rho-r}{1-x_1}\right)^{\frac{1}{2}} u e^{-u\rho}\, \alpha'(x)\, \exp\left(\int_{1-\rho}^{1-r} \alpha'(x')dx'\right)d\rho = 1 \qquad 4.18$$

The onset voltage for the avalanche-streamer transition, which is the corona threshold, does not appear explicitly in Equation 4.18. However, it directly determines most of the terms in the equation. Thus, the corona threshold is the positive conductor to ground potential that would make Equation 4.18 hold.

## B. Physical Parameters

In order to evaluate the integral of Equation 4.18 reliable values of the physical constants must be known. Most important is $\alpha(E)$.

Experimental data on $\alpha$ given as $\alpha/P = f(E/P)$, the ratio of Townsend's first ionization coefficient to pressure, as a function of E/P: the ratio of electric field to pressure in air is available in the literature for a wide range of E/P. However, most, if not all, empirical equations available in the literature that express $\alpha/P$ as a function of E/P for air were obtained a long time ago based on measurements that were not adequately accurate. Therefore, it is thought to be advantageous to use more recent measurements of $\alpha/P$ for different values of E/P in air and develop a new set of equations that would accurately represent those measurements

Figure 4.1. Streamer development

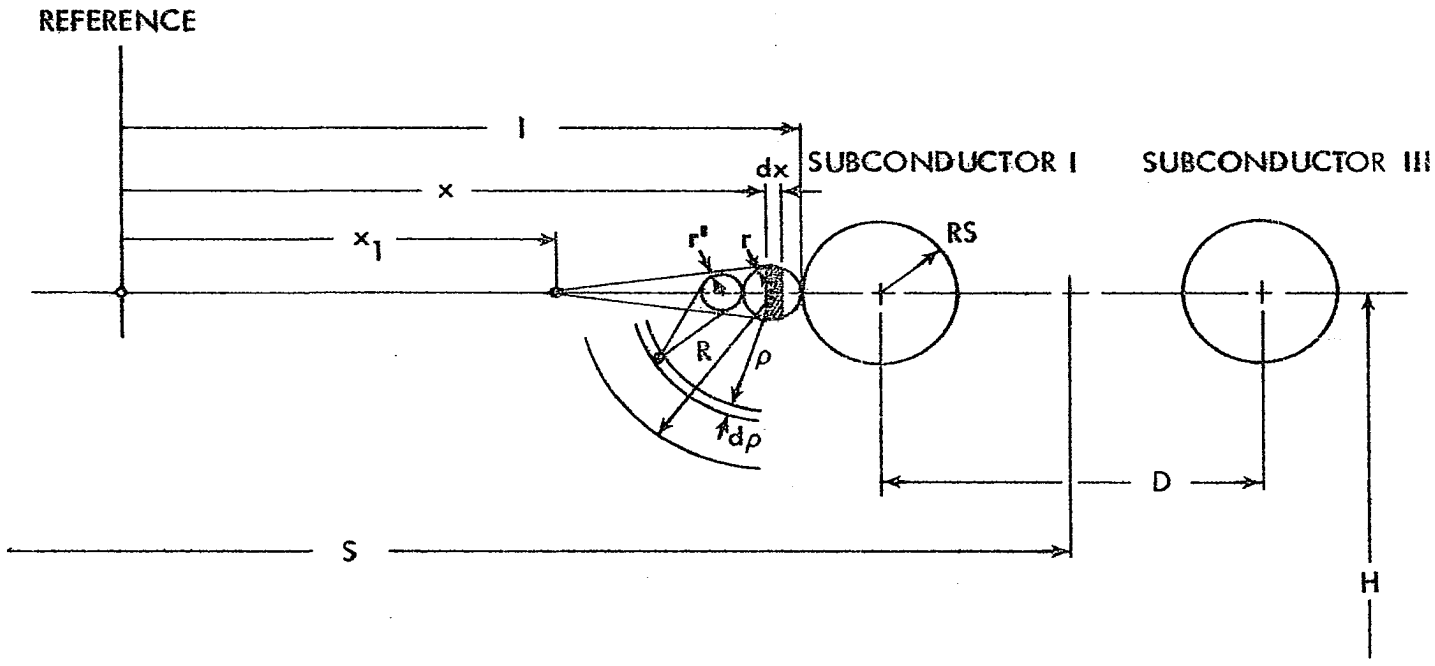
REFERENCE
l
x
$x_1$
dx
SUBCONDUCTOR I
SUBCONDUCTOR III
RS
r'
r
R
ρ
dρ
D
S
H

for different ranges of E/P.

Recent measurements by Dutton, Harris, and Jones, as reported by Brown (58), cover the range of E/P between 30 and 40 (volts/cm·torr). Loeb (59) reported measurements by Sanders in Hg-contaminated air which are expected to be a little higher than those in pure air, and by himself in pure air for values of E/P above 40 (volts/cm·torr). Table 4.1 is a listing of the values of E/P and the corresponding values of $\alpha/P$, together with the natural logarithm of $\alpha/P$.

In Figure 4.2 the natural logarithm of $\alpha/P$ is plotted against E/P. The resulting curve is very closely approximated by four straight line portions, making it possible to accurately express $\alpha/P$ as an exponential function of E/P over each of the four ranges of E/P. The resulting formulas are as follows:

(i) $30.0 < \frac{E}{P} \leq 32.5$

$$\frac{\alpha}{P} = 9.36 \times 10^{-6} \exp(0.805 \frac{E}{P} - 20)$$

(ii) $32.5 < \frac{E}{P} \leq 42.5$

$$\frac{\alpha}{P} = 6.09 \times 10^{-6} \exp(0.2 \frac{E}{P})$$

(iii) $42.5 < \frac{E}{P} < 64.0$

$$\frac{\alpha}{P} = 1.59 \times 10^{-3} \exp(0.07 \frac{E}{P})$$

(iv) $64.0 \leq \frac{E}{P} \leq 100.0$

$$\frac{\alpha}{P} = 12.83 \times 10^{-3} \exp(0.039 \frac{E}{P})$$

Table 4.1. Measurements of $\frac{\alpha}{P}$

| $\frac{E}{P}$ Volts/Cm·Torr | $\frac{\alpha}{P} \times 10^3$ $Cm^{-1} \cdot Torr^{-1}$ | $\log_e \frac{\alpha}{P}$ |
|---|---|---|
| 30[a] | 0.6 | -7.42 |
| 32[a] | 3.0 | -5.81 |
| 34[a] | 5.8 | -5.15 |
| 36[a] | 9.0 | -4.71 |
| 38[a] | 13.4 | -4.31 |
| 40[a] | 18.5 | -3.99 |
| 50[b] | 55.4 | -2.89 |
| 55[c] | 74.0 | -2.60 |
| 60[b] | 127.0 | -2.06 |
| 70[b] | 224.0 | -1.50 |
| 75[c] | 240.0 | -1.43 |
| 80[b] | 340.0 | -1.08 |
| 90[b] | 491.0 | -0.71 |
| 100[c] | 530.0 | -0.63 |
| 100[b] | 637.0 | -0.45 |

[a]Dutton, Harris, and Jones (58).

[b]Sanders (59).

[c]Loeb (59).

Figure 4.2. $\frac{\alpha}{P}$ as a function of $\frac{E}{P}$ for air

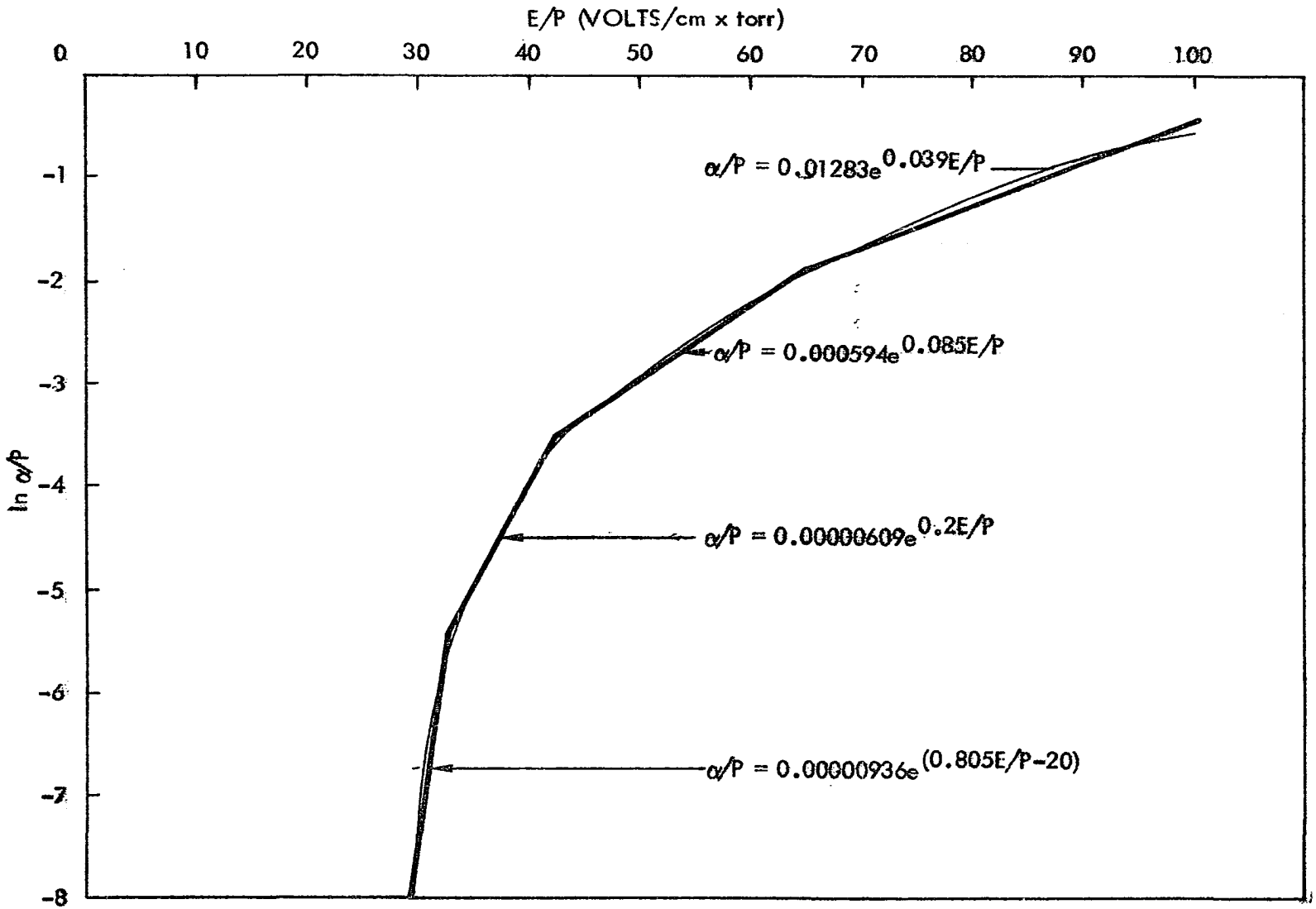
E/P (VOLTS/cm x torr)
0
10
20
30
40
50
60
70
80
90
100
-1
-2
-3
-4
-5
-6
-7
-8
ln α/P
α/P = 0.01283e^0.039E/P
α/P = 0.000594e^0.085E/P
α/P = 0.00000609e^0.2E/P
α/P = 0.00000936e^(0.805E/P-20)

To calculate the radius of the positive ion space charge, Equation 4.4, the electron transit time, t, is needed. Again, to calculate t, the distribution of electron drift velocities must be known.

Recent experimental data on electron drift velocities in air for different values of $\frac{E}{P}$ are reported by Brown (58). These data are plotted in Figure 4.3. For the range of $\frac{E}{P}$ between 30 and 100 volts/cm·torr which is the range relevant to this work, the graph is accurately that of a straight line whose equation is given by

$$V_e = [2.74(\frac{E}{P}) + 39.1] \times 10^5 \quad \text{cm/sec}$$

where

$V_e$ = electron drift velocity corresponding to $\frac{E}{P}$ volts/cm·torr

The value of the diffusion coefficient of electrons in dry air at normal temperature and pressure is taken as $D_e = 430$ cm$^2$/sec (16). The absorption coefficient in air is taken as u=5 cm$^{-1}$ (16). The value of the product of the ratio of excited to ionized states, f, and the probability of photoionization, P, is estimated by Loeb (16) to be in the order of $2 \times 10^{-3}$.

Figure 4.3. Electron drift velocity in dry air

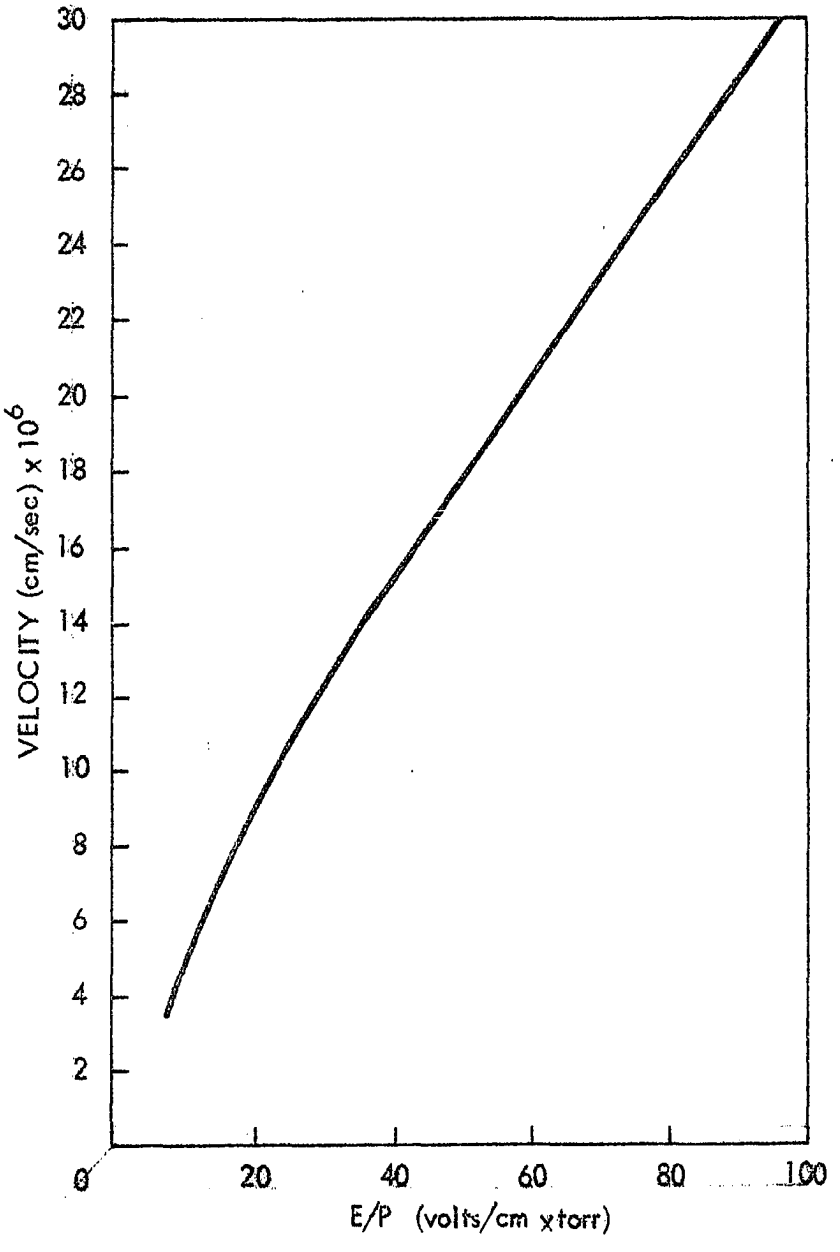
30
28
26
24
22
20
18
16
14
12
10
8
6
4
2
0
VELOCITY (cm/sec) x 10^6
20
40
60
80
100
E/P (volts/cm xtorr)

# V. PROGRAMMING

## A. Data Format

The input data consists of the title, date, study number, study type, subconductor radius RS, subconductor spacing D, subconductor height above ground H, subconductors separation S (for the bipolar case), air pressure PRES, electron diffusion coefficient EDIFC, and air absorption coefficient UEW. The study type is either 1, 2, or 3. The number 1 calls for the computation of only the potential, magnitude and direction of electric field in a vicinity of radial distance = 28 RS from the center of each subconductor. The potential and electric field throughout this portion of the gap is computed for radial increments of $\frac{1}{2}$ RS and angular increments of 15 degrees. The number 2 indicates the computation and output of only the corona starting voltage. The number 3 calls for the output of the external, space charge, and resultant field distributions, $\alpha$-distribution, $\alpha'$-distribution, electron drift velocity-distribution, total number of positive ion space charge N, electrons transit time t, radius of positive ion space charge r, corona starting voltage, and all other computational details.

The preparation of data cards is according to the following instructions:

| Item | Card Columns | Format[1] | Description |
|---|---|---|---|
| 1 | 1-60 | A | Title |
| 2 | 1-20 | A | Date |
| 3 | 1-20 | A | Study number |
| 4 | 10 | I | Study type |
| 5 | 1-8 | F | Subconductor radius |
| 6 | 1-8 | F | Subconductor spacing |
| 7 | 1-8 | F | Subconductor height |
| 8 | 1-8 | F | Subconductors separation |
| 9 | 1-8 | F | Air pressure |
| 10 | 1-8 | F | Electron diffusion coefficient |
| 11 | 1-8 | F | Air absorption coefficient |

## B. Procedure

The Fortran program is written for the IBM 360 computer available at the Iowa State University Computation Center. Double precision arithmetic is used throughout the main program and the subroutines.

Considering the block diagram, Figure 5.1, outlining the

[1]For definition of these formats see Organick (60).

Figure 5.1. Block diagram

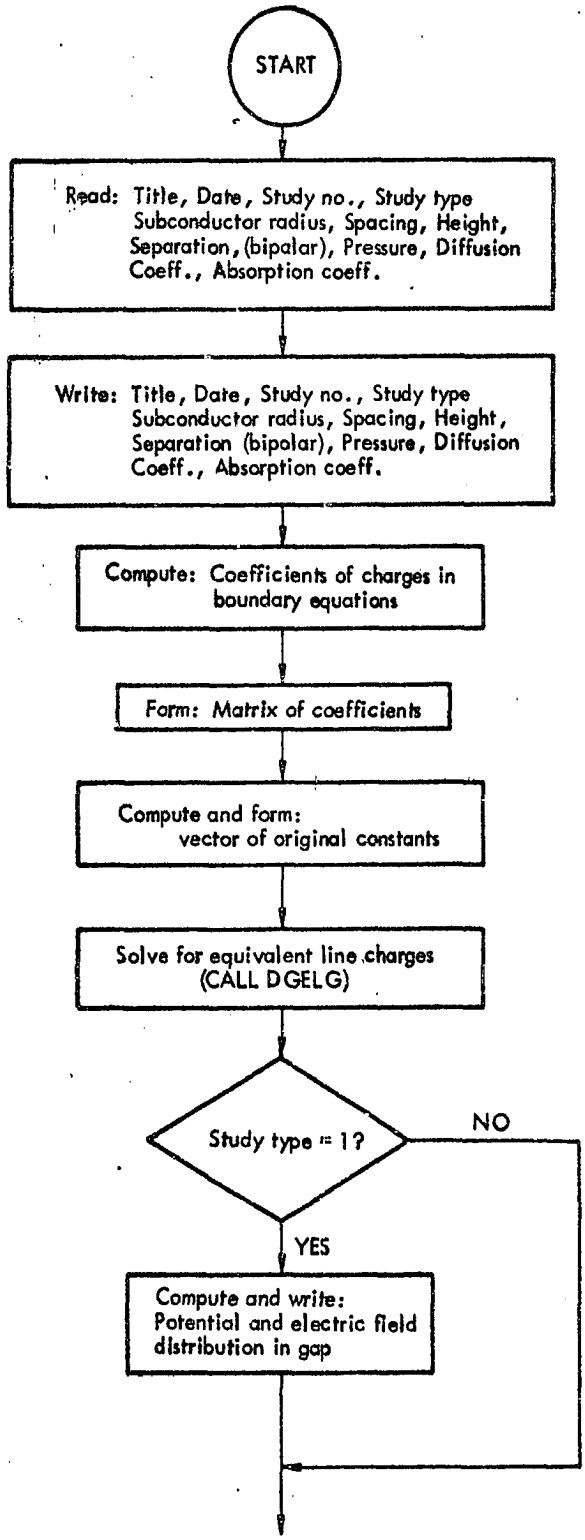
START
Read: Title, Date, Study no., Study type
Subconductor radius, Spacing, Height,
Separation, (bipalar), Pressure, Diffusion
Coeff., Absorption coeff.
Write: Title, Date, Study no., Study type
Subconductor radius, Spacing, Height,
Separation (bipolar), Pressure, Diffusion
Coeff., Absorption coeff.
Compute: Coefficients of charges in
boundary equations
Form: Matrix of coefficients
Compute and form:
vector of original constants
Solve for equivalent line charges
(CALL DGELG)
Study type = 1?
NO
YES
Compute and write:
Potential and electric field
distribution in gap

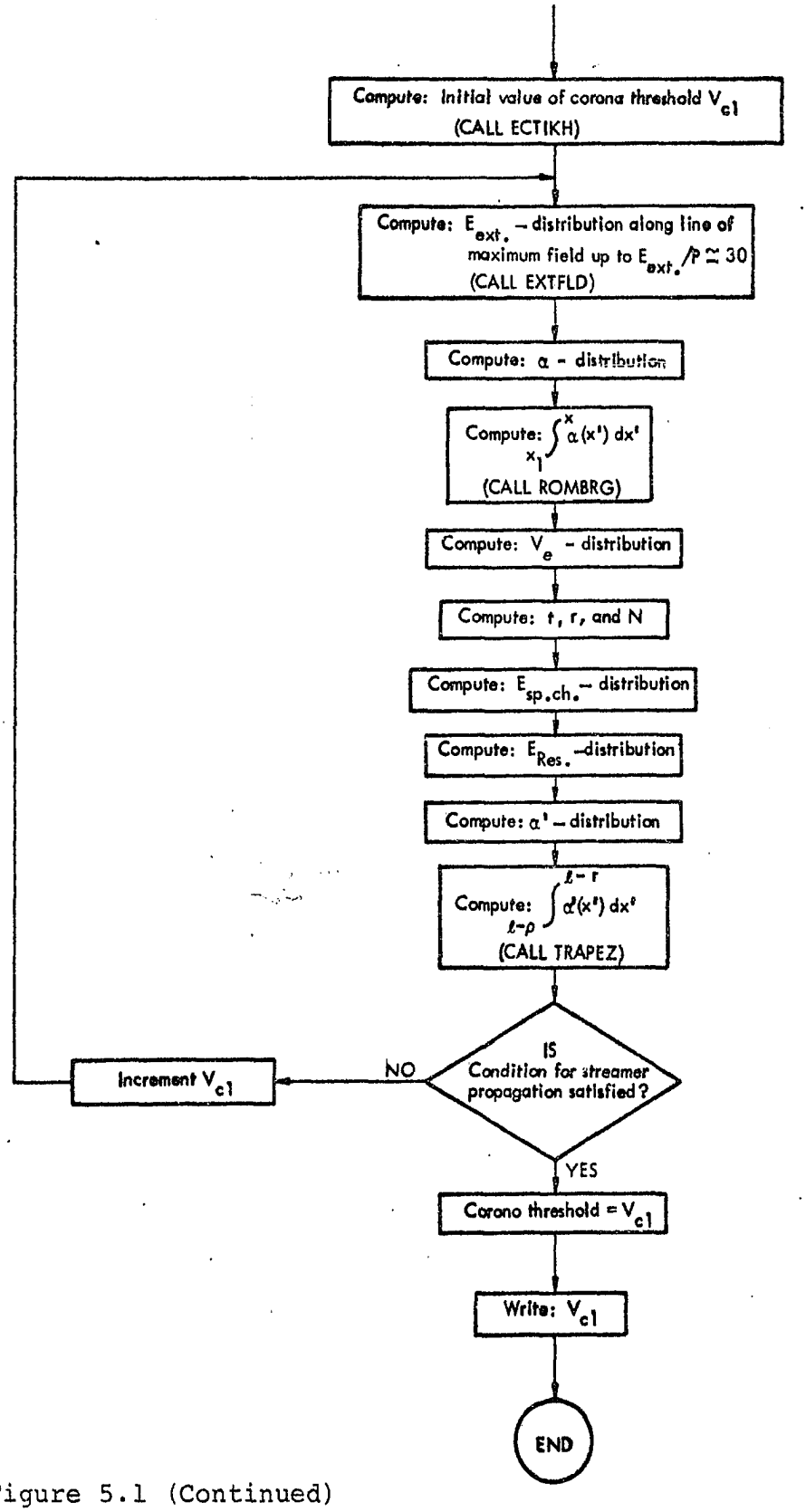


Figure 5.1 (Continued)

computational steps, the procedure for computing the corona threshold is as follows:

1. The input data are read in according to the format given in the previous section.
2. The coefficients of charges in the equations representing the boundary conditions (Equations 3.10 through 3.12 for the unipolar case and Equations 3.30 through 3.35 for the bipolar case) are computed and the boundary equations are formed and arranged in the matrix form shown in Figure 5.2.
3. Subroutine DGELG is called, and the simultaneous solution of the equations representing the boundary conditions (for the equivalent line charges Q (1) through Q(N)) is obtained. This subroutine uses a Gaussian algorithm (61). The method of solution is by elimination using the largest pivotal divisor. Each stage of elimination consists of interchanging rows when necessary to avoid division by zero or small elements. The forward solution to obtain Q(N) is done in N stages. The back solution for the other line charges is calculated by successive substitutions.
4. For study type 1, the potential, magnitude and direction of the electric field in the vicinity of the subconductors are computed and printed out. For

Figure 5.2. Boundary equations arranged in matrix form

$$
\begin{bmatrix}
F0(1,1,c_1) & \cdots & F0(1,2;c_1) & \cdots & F0(1,N;c_1) \\
\cdots & & \cdots & & \cdots \\
F0(N/4,1;c_{N/4}) & \cdots & F0(N/4,2;c_{N/4}) & \cdots & F0(N/4,N;c_{N/4}) \\
F1(N/4+1,1;c_1) & \cdots & F1(N/4+1,2;c_1) & \cdots & F1(N/4+1,N;c_1) \\
\cdots & & \cdots & & \cdots \\
F1(N/2,1;c_{N/4}) & \cdots & F1(N/2,2;c_{N/4}) & \cdots & F1(N/2,N;c_{N/4}) \\
F2(N/2+1,1;c_1) & \cdots & F2(N/2+1,2;c_1) & \cdots & F2(N/2+1,N;c_1) \\
\cdots & & \cdots & & \cdots \\
F2(3N/4,1;c_{N/4}) & \cdots & F2(3N/4,2;c_{N/4}) & \cdots & F2(3N/4,N;c_{N/4}) \\
F4(3N/4+1,1;c_1) & \cdots & F4(3N/4+1,2;c_1) & \cdots & F4(3N/4+1,N;c_1) \\
\cdots & & \cdots & & \cdots \\
F4(N,1;c_{N/4}) & \cdots & F4(N,2;c_{N/4}) & \cdots & F4(N,N;c_{N/4})
\end{bmatrix}
\begin{bmatrix}
Q(1) \\ \cdot \\ Q(\frac{N}{4}) \\ \cdot \\ \cdot \\ \cdot \\ \cdot \\ \cdot \\ \cdot \\ \cdot \\ \cdot \\ Q(N)
\end{bmatrix}
=
\begin{bmatrix}
1 \\ \cdot \\ 1 \\ 0 \\ 0 \\ 0 \\ 0 \\ 0 \\ 0 \\ 0 \\ 0 \\ 0
\end{bmatrix}
$$

study type 2 or 3 this step is skipped.

5. An approximate value of the corona threshold $V_{cl}$ is computed using the empirical equations developed by Tikhodeev (1,29). This requires first the solution of the following implicit equation for the corona field $E_c$ of a single conductor of the same radius as that of the subconductor:

$$\varepsilon_c^2 - 2\varepsilon_c \log_e \varepsilon_c = 1+0.00014 \frac{PRES}{RS} \qquad 5.1$$

where

$$\varepsilon_c = \frac{E_c}{22.8}$$

PRES = atmospheric pressure (torr)

RS= subconductor radius (cm)

The solution of Equation 5.1 is obtained using subroutine ECTIKH which starts with the method of false position (61) and then switches to an iterative technique using the secant method (61).

For the unipolar twin-bundle line, an approximate value of the corona starting voltage is given by

$$V_{cl} = K_2 \cdot E_c \cdot RS \cdot \log_e \left(\frac{2H}{RS}\right) \qquad 5.2$$

where

H = conductor height above ground (cm)

$$K_2 = \frac{\log_e[\frac{(2H)^2}{RS \cdot D}]}{(1+\frac{2RS}{D})\ \log_e(\frac{2H}{RS})} \times \frac{E_{c2}}{E_c}$$

D = subconductor spacing (cm)

$$E_{c2} = E_c - \frac{22.8\ RS \cdot \varepsilon_c[2+\frac{1}{2\varepsilon_c} - \frac{5\varepsilon_c}{2} + (\varepsilon_c+2)\ \log_e\ \varepsilon_c]}{D(\varepsilon_c - \log_e\ \varepsilon_c - 1)}$$

For the bipolar twin-bundle line, the approximate value of the corona starting voltage is given by

$$V_{c1}' = 2K_2' \cdot E_c \cdot RS \cdot \log_e\{\frac{S}{RS[1+(\frac{S}{2H})^2]^{1/2}}\} \qquad 5.3$$

where

S = subconductor separation (cm)

$$K_2' = \frac{\log_e\{\frac{S^2}{RS \cdot D[1+(\frac{S}{2H})^2]}\}}{(1+\frac{2RS}{D})\ \log_e\{\frac{S}{RS[1+(\frac{S}{2H})^2]^{1/2}}\}} \times \frac{E_{c2}}{E_c}$$

6. The external field distribution, along the line through the center of the subconductor and the point of maximum field on the surface of the subconductor, is computed using the corona voltage $V_{c1}$. This is done by the subroutine EXTFLD.
7. The corresponding α-distribution is computed, and the integral of α is evaluated between the limits

x=r and the value of x corresponding to a value of E/P of about 30 volt/cm·torr, since below this value of E/P the number of electrons lost due to electron attachment exceeds the number of electrons produced due to ionization by electron collision (16). The technique of integration adapted is a combination of the trapezoidal rule with a step = the range of of integration/100, and the Romberg method (61) to improve on the accuracy of integration.

8. The electron drift velocity distribution $V_e(x)$ corresponding to the external field distribution is computed, from which the avalanche transit time t is calculated by integrating the reciprocal of the velocity distribution. The same limits and method of integration applied in step 7 are used.
9. The radius of the positive ion space charge r is computed using Equation 4.4.
10. The total number of positive ions N is computed using Equation 4.6.
11. The space charge field distribution is computed and added vectorially to the external field. The distribution of the resultant field is obtained.
12. The $\alpha'$-distribution is computed corresponding to the resultant field values.

13. The integral of Equation 4.18 is evaluated. The limit of integration is from $\rho=r$ to $\rho=R$, where R is the point at which the resultant field/pressure is approximately 30 volt/cm · torr. This range of $\rho$ is divided into 40 increments of equal length and the value of the integrand at each increment is calculated by evaluating the integral of $\alpha'$ from $x'=r$ to $x'=$the value of $\rho$ at that increment. The integral of $\alpha'$ is computed by dividing the range of x' into 20 increments of equal length. The trapezoidal method of integration is used in this step.
14. The integral I of Equation 4.18 is compared to 1. If the difference is within $\pm$ 20%, then $V_{cl}$ is the corona threshold. If the integral I is greater than 1.2, a new value $V_c=V_{cl}[1-0.005\ (I-1)]$ is computed, if the integral I is less than 0.8, a new value $V_c=V_{cl}[1+0.2(1-I)]$ is computed.
15. The new value of $V_c$ replaces the initial value $V_{cl}$, and steps 6 through 15 are repeated.

# VI. DISCUSSION OF RESULTS

## A. Electric Field Calculations

An example of the computer output for the unipolar twin-bundle line proposed for the west coast (11), with subconductor radius RS=2.235 cm, subconductor spacing D=45.72 cm, and height above ground H=23.622 m, is shown in Figures 6.1, 6.2, and 6.3. These line dimensions are the same as those used in connection with Figures 3.2 and 3.3.

From Figures 6.1 and 6.2 it is possible to find out the effect of ground on the potential and its gradient. At $\rho$=17.8816 cm, $\phi$ on top ($\alpha$=0) is 0.825695 per unit potential (p.u.p.) compared with 0.824484 (p.u.p.) at the bottom ($\alpha$=180°) toward ground. The magnitude of the field, $|E|$, at $\alpha$=0 and 180° and $\rho$=8-1/2 RS, is 0.005334 and 0.005401 p.u.p./cm which shows that the effect of ground is not great but appreciable.

For corona breakdown studies, the highest field anywhere in this geometry is important. For this sample problem, this occurs at $\rho$=RS (conductor's surface) and $\alpha$=100.5°. Examining the outputs of different line dimensions, it is observed that the angle $\alpha$ corresponding to the point of maximum field on the conductor's surface increases with increasing D and decreasing H. Its value lies between 96° and 102° for the range of D from 5 cm to 70 cm and H from 40 m

Figure 6.1. Potential distribution in gap, unipolar line RS=2.235 cm, D=45.72 cm, H=2362.2 cm

| RADIAL / ANGLE DIST. / DEGREES | 0.0 | 15.0 | 30.0 | 45.0 | 60.0 | 75.0 | 90.0 | 105.0 | 120.0 | 135.0 | 150.0 | 165.0 |
|---|---|---|---|---|---|---|---|---|---|---|---|---|
| 2.2352 | 1.000000 | 1.000095 | 1.000491 | 1.000730 | 1.000438 | 1.000077 | 1.000000 | 0.999922 | 0.999563 | 0.999302 | 0.999560 | 0.999921 |
| 3.3528 | 0.966913 | 0.966190 | 0.965556 | 0.964990 | 0.964480 | 0.964059 | 0.963880 | 0.963857 | 0.964014 | 0.964398 | 0.965034 | 0.965856 |
| 4.4704 | 0.943376 | 0.941962 | 0.940705 | 0.939647 | 0.938820 | 0.938263 | 0.938010 | 0.938078 | 0.938477 | 0.939213 | 0.940273 | 0.941606 |
| 5.5880 | 0.925047 | 0.923038 | 0.921271 | 0.919810 | 0.918702 | 0.917984 | 0.917683 | 0.917817 | 0.918394 | 0.919409 | 0.920841 | 0.922638 |
| 6.7056 | 0.909993 | 0.907667 | 0.905228 | 0.903614 | 0.902057 | 0.901192 | 0.900844 | 0.901028 | 0.901750 | 0.903005 | 0.904768 | 0.906988 |
| 7.8232 | 0.897186 | 0.894142 | 0.891512 | 0.889381 | 0.887800 | 0.886801 | 0.886405 | 0.886630 | 0.887477 | 0.888944 | 0.891007 | 0.893617 |
| 8.9408 | 0.886012 | 0.882500 | 0.879492 | 0.877072 | 0.875287 | 0.874166 | 0.873728 | 0.873984 | 0.874941 | 0.876596 | 0.878933 | 0.881904 |
| 10.0584 | 0.876076 | 0.872121 | 0.868762 | 0.866077 | 0.864107 | 0.862875 | 0.862395 | 0.862678 | 0.863732 | 0.865558 | 0.868145 | 0.871456 |
| 11.1760 | 0.867108 | 0.862734 | 0.859048 | 0.856120 | 0.854000 | 0.852646 | 0.852127 | 0.852433 | 0.853574 | 0.855554 | 0.858371 | 0.861997 |
| 12.2936 | 0.858918 | 0.854146 | 0.850156 | 0.847002 | 0.844707 | 0.843279 | 0.842724 | 0.843049 | 0.844267 | 0.846388 | 0.849416 | 0.853336 |
| 13.4112 | 0.851363 | 0.846215 | 0.841940 | 0.838579 | 0.836141 | 0.834627 | 0.834037 | 0.834380 | 0.835667 | 0.837915 | 0.841137 | 0.845332 |
| 14.5288 | 0.844338 | 0.838833 | 0.834294 | 0.830741 | 0.828171 | 0.826577 | 0.825956 | 0.826312 | 0.827661 | 0.830025 | 0.833426 | 0.837877 |
| 15.6464 | 0.837759 | 0.831918 | 0.827132 | 0.823402 | 0.820712 | 0.819044 | 0.818392 | 0.818760 | 0.820165 | 0.822634 | 0.826199 | 0.830888 |
| 16.7640 | 0.831562 | 0.825404 | 0.820388 | 0.816495 | 0.813693 | 0.811958 | 0.811277 | 0.811655 | 0.813110 | 0.815675 | 0.819390 | 0.824300 |
| 17.8816 | 0.825695 | 0.819239 | 0.814010 | 0.809765 | 0.807061 | 0.805263 | 0.804555 | 0.804941 | 0.806461 | 0.809092 | 0.812946 | 0.818061 |
| 18.9992 | 0.820115 | 0.813380 | 0.807952 | 0.803768 | 0.800769 | 0.798914 | 0.798181 | 0.798573 | 0.800112 | 0.802842 | 0.806823 | 0.812128 |

| RADIAL / ANGLE DIST. / DEGREES | 180.0 | 195.0 | 210.0 | 225.0 | 240.0 | 255.0 | 270.0 | 285.0 | 300.0 | 315.0 | 330.0 | 345.0 |
|---|---|---|---|---|---|---|---|---|---|---|---|---|
| 2.2352 | 1.000000 | 1.000078 | 1.000422 | 1.000644 | 1.000386 | 1.000067 | 1.000000 | 0.999933 | 0.999605 | 0.999326 | 0.999531 | 0.999906 |
| 3.3528 | 0.966776 | 0.967744 | 0.968701 | 0.969526 | 0.970114 | 0.970440 | 0.970506 | 0.970293 | 0.969812 | 0.969156 | 0.968432 | 0.967679 |
| 4.4704 | 0.943137 | 0.944770 | 0.946387 | 0.947843 | 0.948993 | 0.949721 | 0.949954 | 0.949667 | 0.948901 | 0.947759 | 0.946377 | 0.944879 |
| 5.5880 | 0.924716 | 0.926959 | 0.929210 | 0.931278 | 0.932955 | 0.934053 | 0.934437 | 0.934061 | 0.932984 | 0.931351 | 0.929357 | 0.927199 |
| 6.7056 | 0.909577 | 0.912400 | 0.915272 | 0.917952 | 0.920162 | 0.921634 | 0.922167 | 0.921687 | 0.920275 | 0.918135 | 0.915536 | 0.912747 |
| 7.8232 | 0.898686 | 0.900071 | 0.903559 | 0.906861 | 0.909625 | 0.911490 | 0.912177 | 0.911579 | 0.909804 | 0.907132 | 0.903921 | 0.900513 |
| 8.9408 | 0.885431 | 0.889361 | 0.893463 | 0.897403 | 0.900749 | 0.903036 | 0.903887 | 0.903155 | 0.900925 | 0.897751 | 0.893912 | 0.889891 |
| 10.0584 | 0.875414 | 0.879075 | 0.884591 | 0.889188 | 0.893149 | 0.895891 | 0.896920 | 0.896038 | 0.893437 | 0.889605 | 0.885121 | 0.880488 |
| 11.1760 | 0.866367 | 0.871343 | 0.876674 | 0.881946 | 0.886561 | 0.889798 | 0.891021 | 0.889969 | 0.886896 | 0.882429 | 0.877280 | 0.872039 |
| 12.2936 | 0.858098 | 0.863574 | 0.869517 | 0.875484 | 0.880793 | 0.884570 | 0.886008 | 0.884765 | 0.881173 | 0.876030 | 0.870198 | 0.864350 |
| 13.4112 | 0.850464 | 0.856426 | 0.862978 | 0.869660 | 0.875705 | 0.880072 | 0.881747 | 0.880290 | 0.876129 | 0.870266 | 0.863732 | 0.857280 |
| 14.5288 | 0.843361 | 0.849792 | 0.856548 | 0.864360 | 0.871187 | 0.876201 | 0.878142 | 0.876441 | 0.871654 | 0.865026 | 0.857773 | 0.850723 |
| 15.6464 | 0.836704 | 0.843587 | 0.851341 | 0.859500 | 0.867155 | 0.872879 | 0.875115 | 0.873140 | 0.867663 | 0.860226 | 0.852236 | 0.844596 |
| 16.7640 | 0.830429 | 0.837747 | 0.846089 | 0.855008 | 0.863538 | 0.870041 | 0.872610 | 0.870324 | 0.864087 | 0.855789 | 0.847054 | 0.838832 |
| 17.8816 | 0.824484 | 0.832218 | 0.841138 | 0.850926 | 0.860280 | 0.867639 | 0.870583 | 0.867943 | 0.860869 | 0.851666 | 0.842171 | 0.833379 |
| 18.9992 | 0.818827 | 0.826957 | 0.836441 | 0.846906 | 0.857332 | 0.865633 | 0.869000 | 0.865957 | 0.857960 | 0.847801 | 0.837544 | 0.828194 |

Figure 6.2. Magnitude of electric field distribution in gap, unipolar line RS=2.235 cm, D=45.72 cm, H=2362.2 cm

| RADIAL / ANGLE DIST. / DEGREES | 0.0 | 15.0 | 30.0 | 45.0 | 60.0 | 75.0 | 90.0 | 105.0 | 120.0 | 135.0 | 150.0 | 165.0 |
|---|---|---|---|---|---|---|---|---|---|---|---|---|
| 2.2352 | 0.036488 | 0.037139 | 0.038658 | 0.039847 | 0.039686 | 0.039411 | 0.039773 | 0.039937 | 0.039050 | 0.037977 | 0.037935 | 0.037767 |
| 3.3528 | 0.024380 | 0.025060 | 0.025705 | 0.026211 | 0.026502 | 0.026637 | 0.026678 | 0.026583 | 0.026313 | 0.025945 | 0.025551 | 0.025081 |
| 4.4704 | 0.018379 | 0.018937 | 0.019422 | 0.019804 | 0.020064 | 0.020208 | 0.020246 | 0.020178 | 0.020004 | 0.019738 | 0.019396 | 0.018973 |
| 5.5980 | 0.014806 | 0.015294 | 0.015704 | 0.016024 | 0.016248 | 0.016378 | 0.016417 | 0.016368 | 0.016234 | 0.016017 | 0.015721 | 0.015364 |
| 6.7056 | 0.012444 | 0.012885 | 0.013246 | 0.013525 | 0.013720 | 0.013835 | 0.013873 | 0.013836 | 0.013725 | 0.013540 | 0.013280 | 0.012942 |
| 7.8232 | 0.010772 | 0.011176 | 0.011500 | 0.011747 | 0.011919 | 0.012021 | 0.012057 | 0.012027 | 0.011934 | 0.011773 | 0.011543 | 0.011236 |
| 8.9408 | 0.009531 | 0.009903 | 0.010196 | 0.010416 | 0.010569 | 0.010660 | 0.010693 | 0.010669 | 0.010589 | 0.010449 | 0.010243 | 0.009965 |
| 10.0584 | 0.008575 | 0.008919 | 0.009183 | 0.009381 | 0.009517 | 0.009599 | 0.009629 | 0.009610 | 0.009541 | 0.009417 | 0.009234 | 0.008981 |
| 11.1760 | 0.007818 | 0.008136 | 0.008377 | 0.008553 | 0.008675 | 0.008748 | 0.008776 | 0.008760 | 0.008700 | 0.008591 | 0.008427 | 0.008198 |
| 12.2936 | 0.007205 | 0.007498 | 0.007716 | 0.007874 | 0.007983 | 0.008048 | 0.008074 | 0.008062 | 0.008009 | 0.007914 | 0.007768 | 0.007560 |
| 13.4112 | 0.006699 | 0.006968 | 0.007165 | 0.007308 | 0.007405 | 0.007463 | 0.007487 | 0.007477 | 0.007432 | 0.007348 | 0.007217 | 0.007030 |
| 14.5288 | 0.006275 | 0.006521 | 0.006699 | 0.006826 | 0.006913 | 0.006966 | 0.006988 | 0.006980 | 0.006941 | 0.006867 | 0.006751 | 0.006582 |
| 15.6464 | 0.005914 | 0.006138 | 0.006299 | 0.006413 | 0.006490 | 0.006538 | 0.006558 | 0.006552 | 0.006518 | 0.006453 | 0.006351 | 0.006200 |
| 16.7640 | 0.005604 | 0.005807 | 0.005951 | 0.006052 | 0.006122 | 0.006164 | 0.006183 | 0.006179 | 0.006150 | 0.006093 | 0.006003 | 0.005868 |
| 17.8816 | 0.005334 | 0.005517 | 0.005645 | 0.005736 | 0.005797 | 0.005836 | 0.005853 | 0.005850 | 0.005826 | 0.005777 | 0.005697 | 0.005578 |
| 18.9992 | 0.005097 | 0.005260 | 0.005375 | 0.005455 | 0.005510 | 0.005544 | 0.005560 | 0.005559 | 0.005538 | 0.005496 | 0.005427 | 0.005321 |

| RADIAL / ANGLE DIST. / DEGREES | 180.0 | 195.0 | 210.0 | 225.0 | 240.0 | 255.0 | 270.0 | 285.0 | 300.0 | 315.0 | 330.0 | 345.0 |
|---|---|---|---|---|---|---|---|---|---|---|---|---|
| 2.2352 | 0.036640 | 0.035477 | 0.035168 | 0.034832 | 0.033575 | 0.032607 | 0.032664 | 0.033025 | 0.032912 | 0.032923 | 0.034191 | 0.035789 |
| 3.3528 | 0.024491 | 0.023853 | 0.023247 | 0.022659 | 0.022100 | 0.021692 | 0.021532 | 0.021599 | 0.021842 | 0.022276 | 0.022918 | 0.023662 |
| 4.4704 | 0.018471 | 0.017913 | 0.017332 | 0.016766 | 0.016271 | 0.015920 | 0.015774 | 0.015853 | 0.016137 | 0.016587 | 0.017155 | 0.017772 |
| 5.5980 | 0.014890 | 0.014369 | 0.013806 | 0.013243 | 0.012745 | 0.012389 | 0.012246 | 0.012342 | 0.012656 | 0.013127 | 0.013683 | 0.014259 |
| 6.7056 | 0.012523 | 0.012028 | 0.011476 | 0.010905 | 0.010383 | 0.010003 | 0.009851 | 0.009966 | 0.010314 | 0.010813 | 0.011376 | 0.011934 |
| 7.8232 | 0.010848 | 0.010376 | 0.009831 | 0.009247 | 0.008693 | 0.008277 | 0.008110 | 0.008245 | 0.008633 | 0.009168 | 0.009744 | 0.010290 |
| 8.9408 | 0.009604 | 0.009154 | 0.008617 | 0.008019 | 0.007428 | 0.006967 | 0.006781 | 0.006937 | 0.007372 | 0.007946 | 0.008536 | 0.009073 |
| 10.0584 | 0.008647 | 0.008219 | 0.007691 | 0.007080 | 0.006449 | 0.005937 | 0.005724 | 0.005907 | 0.006396 | 0.007010 | 0.007614 | 0.008141 |
| 11.1760 | 0.007889 | 0.007483 | 0.006967 | 0.006346 | 0.005675 | 0.005103 | 0.004859 | 0.005073 | 0.005622 | 0.006278 | 0.006892 | 0.007407 |
| 12.2936 | 0.007275 | 0.006892 | 0.006391 | 0.005764 | 0.005054 | 0.004415 | 0.004132 | 0.004384 | 0.005000 | 0.005697 | 0.006318 | 0.006818 |
| 13.4112 | 0.006768 | 0.006409 | 0.005926 | 0.005298 | 0.004550 | 0.003838 | 0.003507 | 0.003804 | 0.004496 | 0.005231 | 0.005854 | 0.006336 |
| 14.5288 | 0.006343 | 0.006009 | 0.005546 | 0.004923 | 0.004142 | 0.003349 | 0.002958 | 0.003313 | 0.004086 | 0.004856 | 0.005475 | 0.005937 |
| 15.6464 | 0.005982 | 0.005673 | 0.005234 | 0.004620 | 0.003813 | 0.002933 | 0.002468 | 0.002894 | 0.003755 | 0.004553 | 0.005162 | 0.005601 |
| 16.7640 | 0.005672 | 0.005387 | 0.004974 | 0.004376 | 0.003550 | 0.002583 | 0.002022 | 0.002539 | 0.003490 | 0.004308 | 0.004903 | 0.005316 |
| 17.8816 | 0.005401 | 0.005162 | 0.004756 | 0.004180 | 0.003346 | 0.002292 | 0.001611 | 0.002244 | 0.003284 | 0.004113 | 0.004685 | 0.005071 |
| 18.9992 | 0.005164 | 0.004929 | 0.004573 | 0.004025 | 0.003194 | 0.002062 | 0.001225 | 0.002008 | 0.003130 | 0.003957 | 0.004502 | 0.004859 |

Figure 6.3. Angle of electric field distribution in gap, unipolar line RS=2.235 cm, D=45.72 cm, H=2362.2 cm

| RADIAL / ANGLE DIST. / DEGREES | 0.0 | 15.0 | 30.0 | 45.0 | 60.0 | 75.0 | 90.0 | 105.0 | 120.0 | 135.0 | 150.0 | 165.0 |
|---|---|---|---|---|---|---|---|---|---|---|---|---|
| 2.2352 | 90.0000 | 75.6810 | 61.1125 | 44.8869 | 28.9238 | 14.4653 | 0.0001 | -15.5315 | -31.0681 | -45.0054 | -58.9027 | -74.4294 |
| 3.3528 | 87.9731 | 73.2294 | 58.4943 | 43.6474 | 28.8540 | 14.2528 | -0.2750 | -14.8443 | -29.3530 | -43.7091 | -58.0938 | -72.7020 |
| 4.4704 | 86.0733 | 71.5216 | 57.0685 | 42.6554 | 28.2947 | 14.0077 | -0.2275 | -14.4363 | -28.6114 | -42.7600 | -56.9499 | -71.2652 |
| 5.5880 | 84.4373 | 70.1244 | 55.9486 | 41.8430 | 27.7856 | 13.7729 | -0.2030 | -14.1508 | -28.0748 | -41.9918 | -55.9468 | -70.0057 |
| 6.7056 | 82.9701 | 68.9130 | 54.9998 | 41.1540 | 27.3439 | 13.5607 | -0.1976 | -13.9314 | -27.6428 | -41.3447 | -55.0710 | -68.8798 |
| 7.8232 | 81.6272 | 67.8369 | 54.1738 | 40.5588 | 26.9600 | 13.3716 | -0.2023 | -13.7549 | -27.2819 | -40.7891 | -54.3001 | -67.8646 |
| 8.9408 | 80.3885 | 66.8709 | 53.4459 | 40.0390 | 26.6247 | 13.2037 | -0.2124 | -13.6093 | -26.9753 | -40.3072 | -53.6180 | -66.9465 |
| 10.0584 | 79.2440 | 66.0002 | 52.8008 | 39.5824 | 26.3304 | 13.0546 | -0.2256 | -13.4878 | -26.7124 | -39.8871 | -53.0130 | -66.1160 |
| 11.1760 | 78.1884 | 65.2150 | 52.2275 | 39.1799 | 26.0713 | 12.9218 | -0.2404 | -13.3856 | -26.4860 | -39.5198 | -52.4763 | -65.3659 |
| 12.2936 | 77.2180 | 64.5074 | 51.7176 | 38.8245 | 25.8427 | 12.8035 | -0.2563 | -13.2994 | -26.2905 | -39.1984 | -52.0006 | -64.6901 |
| 13.4112 | 76.3300 | 63.8712 | 51.2644 | 38.5103 | 25.6406 | 12.6979 | -0.2728 | -13.2268 | -26.1216 | -38.9174 | -51.5792 | -64.0833 |
| 14.5288 | 75.5212 | 63.3009 | 50.8619 | 38.2326 | 25.4618 | 12.6034 | -0.2896 | -13.1658 | -25.9760 | -38.6719 | -51.2071 | -63.5403 |
| 15.6464 | 74.7888 | 62.7914 | 50.5052 | 37.9872 | 25.3035 | 12.5187 | -0.3065 | -13.1148 | -25.8506 | -38.4580 | -50.8795 | -63.0566 |
| 16.7640 | 74.1293 | 62.3379 | 50.1898 | 37.7707 | 25.1634 | 12.4428 | -0.3235 | -13.0725 | -25.7431 | -38.2723 | -50.5921 | -62.6275 |
| 17.8816 | 73.5393 | 61.9361 | 49.9116 | 37.5799 | 25.0394 | 12.3746 | -0.3405 | -13.0379 | -25.6514 | -38.1116 | -50.3411 | -62.2491 |
| 18.9992 | 73.0149 | 61.5819 | 49.6673 | 37.4121 | 24.9297 | 12.3133 | -0.3574 | -13.0100 | -25.5737 | -37.9733 | -50.1229 | -61.9171 |

| RADIAL / ANGLE DIST. / DEGREES | 180.0 | 195.0 | 210.0 | 225.0 | 240.0 | 255.0 | 270.0 | 285.0 | 300.0 | 315.0 | 330.0 | 345.0 |
|---|---|---|---|---|---|---|---|---|---|---|---|---|
| 2.2352 | -89.9997 | -104.4027 | -118.9065 | -135.0847 | -151.1378 | -165.5654 | -179.9996 | 164.4354 | 148.7936 | 134.8322 | 121.1439 | 105.6943 |
| 3.3528 | -87.4673 | -102.3224 | -117.4325 | -132.9327 | -148.6548 | -164.4040 | 179.7891 | 163.9253 | 148.2394 | 132.9392 | 117.8941 | 102.8985 |
| 4.4704 | -85.7581 | -100.4930 | -115.5831 | -131.1259 | -147.1246 | -163.4948 | 179.9140 | 163.3348 | 147.0399 | 131.2057 | 115.8319 | 100.8178 |
| 5.5880 | -84.2478 | -98.7836 | -113.7644 | -129.3509 | -145.6646 | -162.6063 | -179.9889 | 162.6366 | 145.7093 | 129.4802 | 113.9572 | 98.9998 |
| 6.7056 | -82.8602 | -97.1508 | -111.9533 | -127.5190 | -144.0714 | -161.6472 | -179.9129 | 161.8172 | 144.2370 | 127.6887 | 112.1262 | 97.3071 |
| 7.8232 | -81.5728 | -95.5798 | -110.1358 | -125.5951 | -142.3451 | -160.5641 | -179.8468 | 160.8518 | 142.5913 | 125.7989 | 110.3002 | 95.6976 |
| 8.9408 | -80.3764 | -94.0688 | -108.3117 | -123.5656 | -140.4261 | -159.3107 | -179.7840 | 159.7066 | 140.7416 | 123.7970 | 108.4711 | 94.1582 |
| 10.0584 | -79.2667 | -92.6209 | -106.4889 | -121.4289 | -138.2827 | -157.8373 | -179.7202 | 158.3383 | 138.6590 | 121.6835 | 106.6433 | 92.6869 |
| 11.1760 | -78.2412 | -91.2415 | -104.6801 | -119.1923 | -135.8881 | -156.0850 | -179.6520 | 156.6913 | 136.3173 | 119.4630 | 104.8281 | 91.2866 |
| 12.2936 | -77.2979 | -89.9363 | -102.9007 | -116.8710 | -133.2211 | -153.9804 | -179.5761 | 154.6938 | 133.6943 | 117.1508 | 103.0401 | 89.9618 |
| 13.4112 | -76.4346 | -88.7106 | -101.1670 | -114.4867 | -130.2691 | -151.4311 | -179.4884 | 152.2531 | 130.7753 | 114.7687 | 101.2958 | 88.7173 |
| 14.5288 | -75.6490 | -87.5681 | -99.4954 | -112.0672 | -127.0314 | -148.3210 | -179.3833 | 149.2503 | 127.5573 | 112.3445 | 99.6114 | 87.5568 |
| 15.6464 | -74.9383 | -86.5124 | -97.9010 | -109.6449 | -123.5240 | -144.5069 | -179.2518 | 145.5364 | 124.0539 | 109.9109 | 98.0027 | 86.4835 |
| 16.7640 | -74.2993 | -85.5448 | -96.3975 | -107.2549 | -119.7838 | -139.8223 | -179.0790 | 140.9323 | 120.3000 | 107.5038 | 96.4836 | 85.4989 |
| 17.8816 | -73.7286 | -84.6658 | -94.9960 | -104.9331 | -115.8707 | -134.0947 | -178.8364 | 135.2454 | 116.3549 | 105.1602 | 95.0659 | 84.6035 |
| 18.9992 | -73.2226 | -83.8745 | -93.7052 | -102.7140 | -111.8666 | -127.1935 | -178.4833 | 128.3150 | 112.3018 | 102.9159 | 93.7586 | 83.7966 |

to 7 m. The effect of ground is responsible for the shifting of this point from $\alpha=90°$ in case of the absence of the ground plane.

The angle of the field vector is given in Figure 6.3 and shows the dissymmetry caused by considering the effect of ground.

Another example of the output for the bipolar twin-bundle line is shown in Figures 6.4, 6.5 and 6.6. This sample problem was for RS=2.25 cm, D=45.70 cm, S=1070.00 cm, and H=1220.00 cm which are the same dimensions used in connection with Figures 3.5 and 3.6.

Note from these figures that the effect of ground on the potential and its gradient is much less appreciable than in the unipolar line. This, however, is expected since only a proportion of the field lines emanating from the positive conductor terminate on ground due to the existence of the negative conductor.

Note also that the highest field occurs at $\rho=RS$ (conductor's surface) and $\alpha=270°$ for subconductor I, and $\alpha=90°$ for subconductor III. This location was shown to be unchanged with varying the conductor geometrical parameters. This is another proof of the negligible effect of ground on the electric field values for the bipolar line.

It is certainly not expedient to present more computations of $\phi$ and E for other practical conductor sizes. It

Figure 6.4. Potential distribution in gap, bipolar line RS=2.25 cm, D=45.70 cm, S=1070.0 cm, H=1220.0 cm

POTENTIAL DISTRIBUTION IN GAP (AROUND SUBCONDUCTOR #1)

| RADIAL / ANGLE DIST. / DEGREES | 0.0 | 15.0 | 30.0 | 45.0 | 60.0 | 75.0 | 90.0 | 105.0 | 120.0 | 135.0 | 150.0 | 165.0 |
|---|---|---|---|---|---|---|---|---|---|---|---|---|
| 2.2500 | 1.000000 | 1.000002 | 1.000009 | 1.000013 | 1.000008 | 1.000001 | 1.000000 | 0.999999 | 0.999992 | 0.999988 | 0.999992 | 0.999998 |
| 3.3750 | 0.954896 | 0.956149 | 0.957377 | 0.958479 | 0.959356 | 0.959919 | 0.960108 | 0.959902 | 0.959322 | 0.958433 | 0.957324 | 0.956095 |
| 4.5000 | 0.922811 | 0.925067 | 0.927294 | 0.929311 | 0.930931 | 0.931978 | 0.932333 | 0.931952 | 0.930879 | 0.929240 | 0.927208 | 0.924973 |
| 5.6250 | 0.897820 | 0.900978 | 0.904126 | 0.907010 | 0.909346 | 0.910871 | 0.911390 | 0.910835 | 0.909277 | 0.906913 | 0.904009 | 0.900849 |
| 6.7500 | 0.877293 | 0.881298 | 0.885337 | 0.889079 | 0.892145 | 0.894164 | 0.894856 | 0.894119 | 0.892059 | 0.888958 | 0.885190 | 0.881136 |
| 7.8750 | 0.859825 | 0.864644 | 0.869560 | 0.874172 | 0.877997 | 0.880561 | 0.881420 | 0.880488 | 0.877894 | 0.874027 | 0.869384 | 0.864449 |
| 9.0000 | 0.844582 | 0.850189 | 0.855976 | 0.861477 | 0.866101 | 0.869210 | 0.870292 | 0.869148 | 0.865981 | 0.861309 | 0.855771 | 0.849962 |
| 10.1250 | 0.831026 | 0.837398 | 0.844053 | 0.850467 | 0.855935 | 0.859657 | 0.860963 | 0.859586 | 0.855799 | 0.850275 | 0.843819 | 0.837138 |
| 11.2500 | 0.818789 | 0.825905 | 0.833426 | 0.840779 | 0.847141 | 0.851531 | 0.853084 | 0.851451 | 0.846988 | 0.840563 | 0.833163 | 0.825613 |
| 12.3750 | 0.807611 | 0.815449 | 0.823833 | 0.832150 | 0.839462 | 0.844580 | 0.846410 | 0.844492 | 0.839292 | 0.831911 | 0.823542 | 0.815126 |
| 13.5000 | 0.797300 | 0.805838 | 0.815080 | 0.824385 | 0.832705 | 0.838621 | 0.840759 | 0.838525 | 0.832519 | 0.824123 | 0.814761 | 0.805484 |
| 14.6250 | 0.787711 | 0.796926 | 0.807019 | 0.817335 | 0.826723 | 0.833514 | 0.835997 | 0.833409 | 0.826520 | 0.817050 | 0.806672 | 0.796540 |
| 15.7500 | 0.778730 | 0.788600 | 0.799534 | 0.810880 | 0.821399 | 0.829151 | 0.832023 | 0.829038 | 0.821180 | 0.810572 | 0.799158 | 0.788183 |
| 16.8750 | 0.770271 | 0.780769 | 0.792531 | 0.804926 | 0.816639 | 0.825447 | 0.828758 | 0.825325 | 0.816404 | 0.804595 | 0.792127 | 0.780322 |
| 18.0000 | 0.762261 | 0.773364 | 0.785938 | 0.799394 | 0.812367 | 0.822335 | 0.826142 | 0.822205 | 0.812115 | 0.799039 | 0.785506 | 0.772885 |

POTENTIAL DISTRIBUTION IN GAP (AROUND SUBCONDUCTOR #1)

| RADIAL / ANGLE DIST. / DEGREES | 180.0 | 195.0 | 210.0 | 225.0 | 240.0 | 255.0 | 270.0 | 285.0 | 300.0 | 315.0 | 330.0 | 345.0 |
|---|---|---|---|---|---|---|---|---|---|---|---|---|
| 2.2500 | 1.000000 | 1.000002 | 1.000008 | 1.000012 | 1.000007 | 1.000001 | 1.000000 | 0.999999 | 0.999992 | 0.999987 | 0.999991 | 0.999998 |
| 3.3750 | 0.954843 | 0.953656 | 0.952602 | 0.951735 | 0.951092 | 0.950699 | 0.950570 | 0.950709 | 0.951111 | 0.951763 | 0.952640 | 0.953702 |
| 4.5000 | 0.922717 | 0.920992 | 0.919719 | 0.917186 | 0.916056 | 0.915368 | 0.915144 | 0.915390 | 0.916099 | 0.917247 | 0.918795 | 0.920680 |
| 5.6250 | 0.897689 | 0.894740 | 0.892160 | 0.890062 | 0.888523 | 0.887589 | 0.887286 | 0.887621 | 0.888585 | 0.890151 | 0.892270 | 0.894865 |
| 6.7500 | 0.877126 | 0.873419 | 0.870202 | 0.867603 | 0.865704 | 0.864556 | 0.864185 | 0.864598 | 0.865785 | 0.867718 | 0.870344 | 0.873579 |
| 7.8750 | 0.859624 | 0.855207 | 0.851405 | 0.848350 | 0.846129 | 0.844790 | 0.844358 | 0.844840 | 0.846227 | 0.848489 | 0.851576 | 0.855400 |
| 9.0000 | 0.844348 | 0.839259 | 0.834912 | 0.831440 | 0.828926 | 0.827415 | 0.826929 | 0.827474 | 0.829040 | 0.831603 | 0.835112 | 0.839484 |
| 10.1250 | 0.830759 | 0.825031 | 0.820174 | 0.816318 | 0.813536 | 0.811868 | 0.811333 | 0.811935 | 0.813667 | 0.816504 | 0.820403 | 0.825288 |
| 11.2500 | 0.818489 | 0.812154 | 0.806820 | 0.802607 | 0.799578 | 0.797767 | 0.797187 | 0.797842 | 0.799725 | 0.802815 | 0.807077 | 0.812442 |
| 12.3750 | 0.807279 | 0.800365 | 0.794583 | 0.790038 | 0.786782 | 0.784839 | 0.784219 | 0.784923 | 0.786944 | 0.790269 | 0.794867 | 0.800684 |
| 13.5000 | 0.796936 | 0.789471 | 0.783268 | 0.778415 | 0.774948 | 0.772884 | 0.772227 | 0.772976 | 0.775126 | 0.778668 | 0.783580 | 0.789820 |
| 14.6250 | 0.787314 | 0.779325 | 0.772728 | 0.767587 | 0.763926 | 0.761750 | 0.761059 | 0.761850 | 0.764119 | 0.767862 | 0.773067 | 0.779705 |
| 15.7500 | 0.778302 | 0.769816 | 0.762840 | 0.757439 | 0.753597 | 0.751317 | 0.750595 | 0.751425 | 0.753806 | 0.757736 | 0.763214 | 0.770226 |
| 16.8750 | 0.769810 | 0.760853 | 0.753537 | 0.747878 | 0.743868 | 0.741493 | 0.740742 | 0.741609 | 0.744092 | 0.748197 | 0.753930 | 0.761294 |
| 18.0000 | 0.761768 | 0.752365 | 0.744723 | 0.738832 | 0.734665 | 0.732201 | 0.731423 | 0.732324 | 0.734904 | 0.739172 | 0.745143 | 0.752837 |

POTENTIAL DISTRIBUTION IN GAP (AROUND SUBCONDUCTOR #2#)

| RADIAL / ANGLE DIST. / DEGREES | 0.0 | 15.0 | 30.0 | 45.0 | 60.0 | 75.0 | 90.0 | 105.0 | 120.0 | 135.0 | 150.0 | 165.0 |
|---|---|---|---|---|---|---|---|---|---|---|---|---|
| 2.2500 | 1.000000 | 1.000017 | 1.000084 | 1.000122 | 1.000074 | 1.000014 | 1.000000 | 0.999986 | 0.999927 | 0.999886 | 0.999926 | 0.999986 |
| 3.3750 | 0.955945 | 0.954912 | 0.954001 | 0.953246 | 0.952673 | 0.952307 | 0.952167 | 0.952259 | 0.952577 | 0.953123 | 0.953883 | 0.954823 |
| 4.5000 | 0.924603 | 0.922737 | 0.921101 | 0.919763 | 0.918769 | 0.918150 | 0.917926 | 0.918103 | 0.918680 | 0.919645 | 0.920974 | 0.922618 |
| 5.6250 | 0.900186 | 0.897594 | 0.895340 | 0.893513 | 0.892168 | 0.891338 | 0.891042 | 0.891287 | 0.892072 | 0.893383 | 0.895192 | 0.897442 |
| 6.7500 | 0.880124 | 0.876868 | 0.874064 | 0.871809 | 0.870159 | 0.869147 | 0.868788 | 0.869090 | 0.870051 | 0.871661 | 0.873890 | 0.876684 |
| 7.8750 | 0.863048 | 0.859174 | 0.855668 | 0.853230 | 0.851311 | 0.850139 | 0.849725 | 0.850075 | 0.851189 | 0.853061 | 0.855667 | 0.858956 |
| 9.0000 | 0.848142 | 0.843686 | 0.839920 | 0.836936 | 0.834777 | 0.833462 | 0.832998 | 0.833390 | 0.834639 | 0.836744 | 0.839690 | 0.843435 |
| 10.1250 | 0.834880 | 0.829875 | 0.825684 | 0.822385 | 0.820011 | 0.818569 | 0.818061 | 0.818489 | 0.819857 | 0.822171 | 0.825425 | 0.829591 |
| 11.2500 | 0.822904 | 0.817381 | 0.812796 | 0.809211 | 0.806642 | 0.805087 | 0.804539 | 0.804998 | 0.806472 | 0.808973 | 0.812507 | 0.817064 |
| 12.3750 | 0.811959 | 0.805947 | 0.800998 | 0.797152 | 0.794408 | 0.792751 | 0.792166 | 0.792653 | 0.794221 | 0.796890 | 0.800680 | 0.805596 |
| 13.5000 | 0.801858 | 0.795385 | 0.790099 | 0.786016 | 0.783114 | 0.781365 | 0.780748 | 0.781259 | 0.782910 | 0.785729 | 0.789751 | 0.795001 |
| 14.6250 | 0.792460 | 0.785553 | 0.779956 | 0.775656 | 0.772612 | 0.770781 | 0.770134 | 0.770666 | 0.772391 | 0.775345 | 0.779578 | 0.785136 |
| 15.7500 | 0.783654 | 0.776340 | 0.770457 | 0.765961 | 0.762788 | 0.760883 | 0.760209 | 0.760739 | 0.762549 | 0.765625 | 0.770049 | 0.775890 |
| 16.8750 | 0.775355 | 0.767660 | 0.761514 | 0.756839 | 0.753551 | 0.751579 | 0.750882 | 0.751446 | 0.753295 | 0.756479 | 0.761076 | 0.767177 |
| 18.0000 | 0.767492 | 0.759443 | 0.753055 | 0.748219 | 0.744828 | 0.742797 | 0.742077 | 0.742655 | 0.744554 | 0.747834 | 0.752587 | 0.758926 |

POTENTIAL DISTRIBUTION IN GAP (AROUND SUBCONDUCTOR #2#)

| RADIAL / ANGLE DIST. / DEGREES | 180.0 | 195.0 | 210.0 | 225.0 | 240.0 | 255.0 | 270.0 | 285.0 | 300.0 | 315.0 | 330.0 | 345.0 |
|---|---|---|---|---|---|---|---|---|---|---|---|---|
| 2.2500 | 1.000000 | 1.000014 | 1.000073 | 1.000109 | 1.000067 | 1.000012 | 1.000000 | 0.999988 | 0.999932 | 0.999885 | 0.999918 | 0.999983 |
| 3.3750 | 0.955988 | 0.957019 | 0.958138 | 0.959146 | 0.959944 | 0.960455 | 0.960627 | 0.960438 | 0.959909 | 0.959106 | 0.958121 | 0.957040 |
| 4.5000 | 0.924501 | 0.926519 | 0.928532 | 0.930373 | 0.931862 | 0.932834 | 0.933174 | 0.932840 | 0.931876 | 0.930402 | 0.928583 | 0.926596 |
| 5.6250 | 0.900044 | 0.902861 | 0.905706 | 0.908342 | 0.910499 | 0.911925 | 0.912431 | 0.911948 | 0.910546 | 0.908414 | 0.905805 | 0.902985 |
| 6.7500 | 0.879944 | 0.883515 | 0.887167 | 0.890594 | 0.893437 | 0.895334 | 0.896013 | 0.895371 | 0.893510 | 0.890702 | 0.887305 | 0.883679 |
| 7.8750 | 0.862831 | 0.867124 | 0.871573 | 0.875808 | 0.879368 | 0.881770 | 0.882635 | 0.881818 | 0.879463 | 0.875946 | 0.871748 | 0.867326 |
| 9.0000 | 0.847889 | 0.852881 | 0.858124 | 0.863188 | 0.867505 | 0.870453 | 0.871522 | 0.870512 | 0.867621 | 0.863354 | 0.858332 | 0.853119 |
| 10.1250 | 0.834591 | 0.840260 | 0.846296 | 0.852214 | 0.857338 | 0.860880 | 0.862174 | 0.860949 | 0.857472 | 0.852408 | 0.846536 | 0.840533 |
| 11.2500 | 0.822580 | 0.828965 | 0.835732 | 0.842533 | 0.848514 | 0.852707 | 0.854250 | 0.852786 | 0.848667 | 0.842752 | 0.836004 | 0.829213 |
| 12.3750 | 0.811601 | 0.818581 | 0.826177 | 0.833886 | 0.840782 | 0.845689 | 0.847509 | 0.845277 | 0.840953 | 0.834130 | 0.826480 | 0.818903 |
| 13.5000 | 0.801466 | 0.809040 | 0.817440 | 0.826082 | 0.833953 | 0.839645 | 0.841776 | 0.839742 | 0.834142 | 0.826351 | 0.817773 | 0.809415 |
| 14.6250 | 0.792033 | 0.800198 | 0.809376 | 0.818979 | 0.827883 | 0.834439 | 0.836918 | 0.834545 | 0.828089 | 0.819269 | 0.809739 | 0.800606 |
| 15.7500 | 0.783193 | 0.791925 | 0.801871 | 0.812448 | 0.822457 | 0.829964 | 0.832836 | 0.830079 | 0.822690 | 0.812786 | 0.802263 | 0.792366 |
| 16.8750 | 0.774859 | 0.784134 | 0.794835 | 0.806408 | 0.817583 | 0.826139 | 0.829455 | 0.826263 | 0.817823 | 0.806749 | 0.795256 | 0.784608 |
| 18.0000 | 0.766962 | 0.776754 | 0.788195 | 0.800777 | 0.813185 | 0.822897 | 0.826717 | 0.823030 | 0.813441 | 0.801142 | 0.788645 | 0.777261 |

Figure 6.4 (Continued)

Figure 6.5. Magnitude of electric field distribution in gap, bipolar line RS=2.25 cm, D=45.70 cm, S=1070.0 cm, H=1220.0 cm

FIELD DISTRIBUTION IN GAP (AROUND SUBCONDUCTOR "1")

| RADIAL / ANGLE DIST. / DEGREES | 0.0 | 15.0 | 30.0 | 45.0 | 60.0 | 75.0 | 90.0 | 105.0 | 120.0 | 135.0 | 150.0 | 165.0 |
|---|---|---|---|---|---|---|---|---|---|---|---|---|
| 2.2500 | 0.049415 | 0.048076 | 0.046788 | 0.045632 | 0.044697 | 0.044093 | 0.043897 | 0.044115 | 0.044711 | 0.045637 | 0.046820 | 0.048139 |
| 3.3750 | 0.033025 | 0.032062 | 0.031108 | 0.030239 | 0.029536 | 0.029078 | 0.028922 | 0.029087 | 0.029552 | 0.030262 | 0.031139 | 0.032099 |
| 4.5000 | 0.024903 | 0.024074 | 0.023226 | 0.022427 | 0.021762 | 0.021318 | 0.021165 | 0.021327 | 0.021779 | 0.022450 | 0.023255 | 0.024107 |
| 5.6250 | 0.020071 | 0.019309 | 0.018503 | 0.017716 | 0.017037 | 0.016570 | 0.016406 | 0.016579 | 0.017053 | 0.017739 | 0.018531 | 0.019340 |
| 6.7500 | 0.016877 | 0.016160 | 0.015375 | 0.014578 | 0.013864 | 0.013357 | 0.013175 | 0.013366 | 0.013881 | 0.014602 | 0.015403 | 0.016191 |
| 7.8750 | 0.014617 | 0.013937 | 0.013165 | 0.012351 | 0.011591 | 0.011031 | 0.010826 | 0.011041 | 0.011608 | 0.012375 | 0.013193 | 0.013966 |
| 9.0000 | 0.012940 | 0.012291 | 0.011532 | 0.010699 | 0.009887 | 0.009266 | 0.009031 | 0.009276 | 0.009906 | 0.010723 | 0.011560 | 0.012320 |
| 10.1250 | 0.011648 | 0.011032 | 0.010287 | 0.009437 | 0.008570 | 0.007876 | 0.007605 | 0.007886 | 0.008589 | 0.009461 | 0.010314 | 0.011061 |
| 11.2500 | 0.010626 | 0.010041 | 0.009314 | 0.008451 | 0.007528 | 0.006751 | 0.006437 | 0.006763 | 0.007548 | 0.008476 | 0.009342 | 0.010070 |
| 12.3750 | 0.009798 | 0.009246 | 0.008540 | 0.007669 | 0.006692 | 0.005822 | 0.005455 | 0.005835 | 0.006713 | 0.007695 | 0.008568 | 0.009275 |
| 13.5000 | 0.009115 | 0.008597 | 0.007915 | 0.007044 | 0.006016 | 0.005043 | 0.004611 | 0.005057 | 0.006038 | 0.007070 | 0.007943 | 0.008625 |
| 14.6250 | 0.008543 | 0.008058 | 0.007405 | 0.006541 | 0.005469 | 0.004384 | 0.003870 | 0.004399 | 0.005492 | 0.006568 | 0.007436 | 0.008086 |
| 15.7500 | 0.008056 | 0.007606 | 0.006986 | 0.006136 | 0.005028 | 0.003825 | 0.003208 | 0.003842 | 0.005052 | 0.006163 | 0.007014 | 0.007634 |
| 16.8750 | 0.007637 | 0.007221 | 0.006637 | 0.005811 | 0.004680 | 0.003355 | 0.002606 | 0.003373 | 0.004705 | 0.005838 | 0.006666 | 0.007249 |
| 18.0000 | 0.007273 | 0.006891 | 0.006346 | 0.005551 | 0.004410 | 0.002967 | 0.002050 | 0.002988 | 0.004436 | 0.005578 | 0.006374 | 0.006919 |

FIELD DISTRIBUTION IN GAP (AROUND SUBCONDUCTOR "1")

| RADIAL / ANGLE DIST. / DEGREES | 180.0 | 195.0 | 210.0 | 225.0 | 240.0 | 255.0 | 270.0 | 285.0 | 300.0 | 315.0 | 330.0 | 345.0 |
|---|---|---|---|---|---|---|---|---|---|---|---|---|
| 2.2500 | 0.049471 | 0.050740 | 0.051885 | 0.052828 | 0.053511 | 0.053924 | 0.054066 | 0.053918 | 0.053471 | 0.052756 | 0.051821 | 0.050695 |
| 3.3750 | 0.033065 | 0.033970 | 0.034767 | 0.035418 | 0.035895 | 0.036184 | 0.036278 | 0.036173 | 0.035871 | 0.035386 | 0.034729 | 0.033931 |
| 4.5000 | 0.024938 | 0.025697 | 0.026349 | 0.026871 | 0.027251 | 0.027479 | 0.027553 | 0.027470 | 0.027232 | 0.026846 | 0.026318 | 0.025663 |
| 5.6250 | 0.020103 | 0.020778 | 0.021345 | 0.021792 | 0.022111 | 0.022302 | 0.022363 | 0.022294 | 0.022095 | 0.021769 | 0.021318 | 0.020748 |
| 6.7500 | 0.016907 | 0.017525 | 0.018031 | 0.018423 | 0.018700 | 0.018864 | 0.018916 | 0.018857 | 0.018686 | 0.018402 | 0.018006 | 0.017496 |
| 7.8750 | 0.014647 | 0.015217 | 0.015675 | 0.016024 | 0.016268 | 0.016412 | 0.016457 | 0.016405 | 0.016255 | 0.016004 | 0.015651 | 0.015190 |
| 9.0000 | 0.012968 | 0.013498 | 0.013915 | 0.014227 | 0.014444 | 0.014571 | 0.014610 | 0.014564 | 0.014431 | 0.014208 | 0.013891 | 0.013471 |
| 10.1250 | 0.011677 | 0.012168 | 0.012548 | 0.012830 | 0.013024 | 0.013136 | 0.013171 | 0.013130 | 0.013011 | 0.012812 | 0.012525 | 0.012142 |
| 11.2500 | 0.010654 | 0.011110 | 0.011457 | 0.011711 | 0.011885 | 0.011985 | 0.012016 | 0.011979 | 0.011873 | 0.011693 | 0.011434 | 0.011084 |
| 12.3750 | 0.009826 | 0.010247 | 0.010564 | 0.010796 | 0.010951 | 0.011040 | 0.011068 | 0.011034 | 0.010938 | 0.010777 | 0.010542 | 0.010222 |
| 13.5000 | 0.009143 | 0.009531 | 0.009820 | 0.010028 | 0.010169 | 0.010249 | 0.010274 | 0.010243 | 0.010157 | 0.010011 | 0.009798 | 0.009506 |
| 14.6250 | 0.008570 | 0.008927 | 0.009190 | 0.009378 | 0.009505 | 0.009577 | 0.009599 | 0.009571 | 0.009493 | 0.009361 | 0.009166 | 0.008902 |
| 15.7500 | 0.008083 | 0.008410 | 0.008649 | 0.008819 | 0.008933 | 0.008998 | 0.009017 | 0.008992 | 0.008921 | 0.008802 | 0.008627 | 0.008386 |
| 16.8750 | 0.007664 | 0.007962 | 0.008178 | 0.008332 | 0.008435 | 0.008493 | 0.008511 | 0.008488 | 0.008424 | 0.008316 | 0.008157 | 0.007938 |
| 18.0000 | 0.007300 | 0.007570 | 0.007766 | 0.007904 | 0.007997 | 0.008050 | 0.008065 | 0.008044 | 0.007986 | 0.007888 | 0.007745 | 0.007546 |

FIELD DISTRIBUTION IN GAP (AROUND SUBCONDUCTOR "2")

| RADIAL / ANGLE DIST. / DEGREES | 0.0 | 15.0 | 30.0 | 45.0 | 60.0 | 75.0 | 90.0 | 105.0 | 120.0 | 135.0 | 150.0 | 165.0 |
|---|---|---|---|---|---|---|---|---|---|---|---|---|
| 2.2500 | 0.048264 | 0.049350 | 0.050471 | 0.051373 | 0.051880 | 0.052150 | 0.052330 | 0.052253 | 0.051788 | 0.051099 | 0.050375 | 0.049487 |
| 3.3750 | 0.032252 | 0.033059 | 0.033772 | 0.034349 | 0.034760 | 0.035005 | 0.035088 | 0.035002 | 0.034762 | 0.034324 | 0.033769 | 0.033058 |
| 4.5000 | 0.024316 | 0.024989 | 0.025563 | 0.026019 | 0.026347 | 0.026545 | 0.026611 | 0.026546 | 0.026349 | 0.026024 | 0.025578 | 0.025017 |
| 5.6250 | 0.019593 | 0.020188 | 0.020682 | 0.021067 | 0.021342 | 0.021506 | 0.021562 | 0.021510 | 0.021350 | 0.021081 | 0.020723 | 0.020217 |
| 6.7500 | 0.016470 | 0.017011 | 0.017448 | 0.017782 | 0.018017 | 0.018157 | 0.018205 | 0.018162 | 0.018028 | 0.017799 | 0.017471 | 0.017040 |
| 7.8750 | 0.014260 | 0.014757 | 0.015148 | 0.015442 | 0.015645 | 0.015766 | 0.015808 | 0.015772 | 0.015658 | 0.015460 | 0.015172 | 0.014786 |
| 9.0000 | 0.012619 | 0.013076 | 0.013428 | 0.013688 | 0.013866 | 0.013971 | 0.014007 | 0.013977 | 0.013879 | 0.013707 | 0.013453 | 0.013105 |
| 10.1250 | 0.011355 | 0.011776 | 0.012094 | 0.012323 | 0.012479 | 0.012571 | 0.012603 | 0.012577 | 0.012493 | 0.012343 | 0.012118 | 0.011805 |
| 11.2500 | 0.010354 | 0.010741 | 0.011027 | 0.011231 | 0.011367 | 0.011447 | 0.011475 | 0.011454 | 0.011381 | 0.011250 | 0.011051 | 0.010770 |
| 12.3750 | 0.009544 | 0.009898 | 0.010154 | 0.010335 | 0.010454 | 0.010524 | 0.010549 | 0.010531 | 0.010468 | 0.010354 | 0.010179 | 0.009926 |
| 13.5000 | 0.008875 | 0.009198 | 0.009427 | 0.009586 | 0.009690 | 0.009751 | 0.009773 | 0.009758 | 0.009704 | 0.009605 | 0.009451 | 0.009226 |
| 14.6250 | 0.008314 | 0.008606 | 0.008810 | 0.008950 | 0.009041 | 0.009094 | 0.009113 | 0.009101 | 0.009055 | 0.008969 | 0.008835 | 0.008634 |
| 15.7500 | 0.007837 | 0.008100 | 0.008281 | 0.008403 | 0.008482 | 0.008527 | 0.008544 | 0.008534 | 0.008495 | 0.008422 | 0.008305 | 0.008128 |
| 16.8750 | 0.007426 | 0.007662 | 0.007821 | 0.007927 | 0.007995 | 0.008034 | 0.008049 | 0.008041 | 0.008008 | 0.007946 | 0.007845 | 0.007690 |
| 18.0000 | 0.007069 | 0.007278 | 0.007417 | 0.007508 | 0.007566 | 0.007599 | 0.007613 | 0.007606 | 0.007580 | 0.007527 | 0.007441 | 0.007306 |

FIELD DISTRIBUTION IN GAP (AROUND SUBCONDUCTOR "2")

| RADIAL / ANGLE DIST. / DEGREES | 180.0 | 195.0 | 210.0 | 225.0 | 240.0 | 255.0 | 270.0 | 285.0 | 300.0 | 315.0 | 330.0 | 345.0 |
|---|---|---|---|---|---|---|---|---|---|---|---|---|
| 2.2500 | 0.049325 | 0.047100 | 0.046035 | 0.045056 | 0.044115 | 0.043472 | 0.043313 | 0.043532 | 0.043980 | 0.044713 | 0.045831 | 0.047116 |
| 3.3750 | 0.032297 | 0.031446 | 0.030598 | 0.029812 | 0.029159 | 0.028721 | 0.028563 | 0.028698 | 0.029101 | 0.029729 | 0.030519 | 0.031388 |
| 4.5000 | 0.024355 | 0.023621 | 0.022859 | 0.022130 | 0.021514 | 0.021095 | 0.020941 | 0.021077 | 0.021479 | 0.022083 | 0.022809 | 0.023575 |
| 5.6250 | 0.019628 | 0.018953 | 0.018226 | 0.017505 | 0.016874 | 0.016433 | 0.016270 | 0.016419 | 0.016847 | 0.017470 | 0.018187 | 0.018914 |
| 6.7500 | 0.016504 | 0.015869 | 0.015159 | 0.014427 | 0.013760 | 0.013280 | 0.013100 | 0.013268 | 0.013737 | 0.014396 | 0.015124 | 0.015833 |
| 7.8750 | 0.014293 | 0.013690 | 0.012992 | 0.012241 | 0.011530 | 0.010998 | 0.010795 | 0.010987 | 0.011508 | 0.012213 | 0.012959 | 0.013656 |
| 9.0000 | 0.012650 | 0.012078 | 0.011391 | 0.010621 | 0.009858 | 0.009266 | 0.009034 | 0.009254 | 0.009837 | 0.010593 | 0.011359 | 0.012046 |
| 10.1250 | 0.011386 | 0.010844 | 0.010169 | 0.009381 | 0.008564 | 0.007901 | 0.007635 | 0.007889 | 0.008543 | 0.009354 | 0.010138 | 0.010812 |
| 11.2500 | 0.010385 | 0.009873 | 0.009214 | 0.008412 | 0.007540 | 0.006796 | 0.006487 | 0.006784 | 0.007519 | 0.008385 | 0.009184 | 0.009841 |
| 12.3750 | 0.009574 | 0.009093 | 0.008454 | 0.007644 | 0.006717 | 0.005883 | 0.005522 | 0.005870 | 0.006696 | 0.007617 | 0.008424 | 0.009062 |
| 13.5000 | 0.008905 | 0.008456 | 0.007840 | 0.007028 | 0.006051 | 0.005116 | 0.004691 | 0.005102 | 0.006028 | 0.007001 | 0.007810 | 0.008425 |
| 14.6250 | 0.008344 | 0.007928 | 0.007339 | 0.006533 | 0.005510 | 0.004466 | 0.003980 | 0.004451 | 0.005487 | 0.006505 | 0.007309 | 0.007897 |
| 15.7500 | 0.007867 | 0.007484 | 0.006927 | 0.006133 | 0.005074 | 0.003912 | 0.003307 | 0.003896 | 0.005050 | 0.006105 | 0.006897 | 0.007453 |
| 16.8750 | 0.007456 | 0.007106 | 0.006584 | 0.005811 | 0.004727 | 0.003444 | 0.002712 | 0.003426 | 0.004702 | 0.005783 | 0.006554 | 0.007076 |
| 18.0000 | 0.007099 | 0.006783 | 0.006297 | 0.005554 | 0.004457 | 0.003056 | 0.002162 | 0.003038 | 0.004431 | 0.005525 | 0.006267 | 0.006752 |

Figure 6.5 (Continued)

Figure 6.6. Angle of electric field distribution in gap, bipolar line RS=2.25 cm, D=45.70 cm, S=1070.0 cm, H=1220.0 cm

ANGLE OF FIELD IN GAP (AROUND SUBCONDUCTOR #1)

| RADIAL / ANGLE DIST. / DEGREES | 0.0 | 15.0 | 30.0 | 45.0 | 60.0 | 75.0 | 90.0 | 105.0 | 120.0 | 135.0 | 150.0 | 165.0 |
|---|---|---|---|---|---|---|---|---|---|---|---|---|
| 2.2500 | 90.0000 | 75.0098 | 60.0159 | 44.9985 | 29.9834 | 14.9911 | 0.0001 | -15.0089 | -30.0158 | -45.0003 | -59.9845 | -74.9910 |
| 3.3750 | 92.4292 | 77.5420 | 62.4650 | 47.1572 | 31.6085 | 15.8547 | -0.0192 | -15.8922 | -31.6402 | -47.1762 | -62.4700 | -77.5379 |
| 4.5000 | 94.3324 | 79.5899 | 64.5153 | 49.0147 | 33.0388 | 16.6335 | -0.0310 | -16.6920 | -33.0471 | -49.0480 | -64.5320 | -79.5915 |
| 5.6250 | 95.9955 | 81.4457 | 66.4521 | 50.8460 | 34.5050 | 17.4552 | -0.0428 | -17.5355 | -34.5707 | -50.8916 | -66.4761 | -81.4497 |
| 6.7500 | 97.5073 | 83.1964 | 68.3609 | 52.7393 | 36.0916 | 18.3755 | -0.0555 | -18.4786 | -36.1744 | -52.7956 | -68.3902 | -83.2008 |
| 7.8750 | 98.9025 | 84.8709 | 70.2692 | 54.7300 | 37.8474 | 19.4362 | -0.0692 | -19.5634 | -37.9469 | -54.7955 | -70.3019 | -84.8745 |
| 9.0000 | 100.1963 | 86.4773 | 72.1812 | 56.8322 | 39.8097 | 20.6798 | -0.0844 | -20.8327 | -39.9251 | -56.9053 | -72.2157 | -86.4789 |
| 10.1250 | 101.3962 | 88.0149 | 74.0902 | 59.0474 | 42.0103 | 22.1560 | -0.1015 | -22.3363 | -42.1407 | -59.1263 | -74.1251 | -88.0135 |
| 11.2500 | 102.5066 | 89.4794 | 75.9836 | 61.3677 | 44.4771 | 23.9264 | -0.1210 | -24.1358 | -44.6209 | -61.4503 | -76.0176 | -89.4744 |
| 12.3750 | 103.5303 | 90.8657 | 77.8458 | 63.7769 | 47.2322 | 26.0690 | -0.1439 | -26.3092 | -47.3870 | -63.8611 | -77.8776 | -90.8565 |
| 13.5000 | 104.4703 | 92.1689 | 79.6597 | 66.2517 | 50.2891 | 28.6841 | -0.1712 | -28.9563 | -50.4517 | -66.3352 | -79.6882 | -92.1549 |
| 14.6250 | 105.3295 | 93.3848 | 81.4083 | 68.7622 | 53.6478 | 31.8994 | -0.2050 | -32.2035 | -53.8141 | -68.8429 | -81.4326 | -93.3659 |
| 15.7500 | 106.1108 | 94.5106 | 83.0758 | 71.2740 | 57.2902 | 35.8737 | -0.2483 | -36.2072 | -57.4551 | -71.3497 | -83.0951 | -94.4865 |
| 16.8750 | 106.8179 | 95.5449 | 84.6480 | 73.7495 | 61.1747 | 40.7929 | -0.3067 | -41.1486 | -61.3325 | -73.8185 | -84.6619 | -95.5154 |
| 18.0000 | 107.4544 | 96.4874 | 86.1135 | 76.1509 | 65.2345 | 46.8485 | -0.3909 | -47.2119 | -65.3795 | -76.2116 | -86.1217 | -96.4527 |

ANGLE OF FIELD IN GAP (AROUND SUBCONDUCTOR #1)

| RADIAL / ANGLE DIST. / DEGREES | 180.0 | 195.0 | 210.0 | 225.0 | 240.0 | 255.0 | 270.0 | 285.0 | 300.0 | 315.0 | 330.0 | 345.0 |
|---|---|---|---|---|---|---|---|---|---|---|---|---|
| 2.2500 | -89.9997 | -104.9914 | -119.9863 | -135.0007 | -150.0126 | -165.0065 | -179.9996 | 164.9936 | 149.9870 | 134.9986 | 120.0143 | 105.0098 |
| 3.3750 | -92.4187 | -107.1591 | -121.8047 | -136.3914 | -150.9417 | -165.4705 | -179.9905 | 165.4884 | 150.9588 | 136.4108 | 121.9259 | 107.1767 |
| 4.5000 | -94.3212 | -108.8191 | -123.1670 | -137.4246 | -151.6310 | -165.8109 | -179.9801 | 165.8499 | 151.6682 | 137.4591 | 123.1970 | 108.8414 |
| 5.6250 | -95.9820 | -110.2256 | -124.2948 | -138.2661 | -152.1866 | -166.0832 | -179.9713 | 166.1395 | 152.2396 | 138.3137 | 124.3344 | 110.2540 |
| 6.7500 | -97.4904 | -111.4658 | -125.2670 | -138.9799 | -152.6527 | -166.3101 | -179.9636 | 166.3815 | 152.7198 | 139.0397 | 125.3162 | 111.5009 |
| 7.8750 | -98.8813 | -112.5730 | -126.1212 | -139.5979 | -153.0523 | -166.5034 | -179.9565 | 166.5886 | 153.1324 | 139.6691 | 126.1798 | 112.6203 |
| 9.0000 | -100.1702 | -113.5829 | -126.8788 | -140.1390 | -153.3992 | -166.6700 | -179.9498 | 166.7683 | 153.4915 | 140.2212 | 126.9467 | 113.6324 |
| 10.1250 | -101.3648 | -114.4931 | -127.5540 | -140.6160 | -153.7027 | -166.8151 | -179.9436 | 166.9257 | 153.8067 | 140.7088 | 127.6311 | 114.5500 |
| 11.2500 | -102.4695 | -115.3179 | -128.1574 | -141.0383 | -153.9698 | -166.9421 | -179.9376 | 167.0645 | 154.0849 | 141.1413 | 128.2434 | 115.3821 |
| 12.3750 | -103.4874 | -116.0645 | -128.6971 | -141.4131 | -154.2056 | -167.0537 | -179.9318 | 167.1875 | 154.3315 | 141.5260 | 128.7919 | 116.1361 |
| 13.5000 | -104.4214 | -116.7390 | -129.1800 | -141.7464 | -154.4144 | -167.1522 | -179.9262 | 167.2970 | 154.5508 | 141.8689 | 129.2833 | 116.8179 |
| 14.6250 | -105.2745 | -117.3471 | -129.6119 | -142.0431 | -154.5998 | -167.2392 | -179.9208 | 167.3946 | 154.7463 | 142.1750 | 129.7236 | 117.4332 |
| 15.7500 | -106.0498 | -117.8939 | -129.9980 | -142.3074 | -154.7645 | -167.3164 | -179.9156 | 167.4821 | 154.9209 | 142.4485 | 130.1178 | 117.9871 |
| 16.8750 | -106.7510 | -118.3842 | -130.3426 | -142.5429 | -154.9111 | -167.3848 | -179.9105 | 167.5606 | 155.0772 | 142.6929 | 130.4705 | 118.4843 |
| 18.0000 | -107.3816 | -118.8224 | -130.6499 | -142.75_8 | -155.0417 | -167.4455 | -179.9055 | 167.6312 | 155.2172 | 142.9115 | 130.7856 | 118.9294 |

ANGLE OF FIELD IN GAP (AROUND SUBCONDUCTOR #2#)

| RADIAL / ANGLE DIST. / DEGREES | 0.0 | 15.0 | 30.0 | 45.0 | 60.0 | 75.0 | 90.0 | 105.0 | 120.0 | 135.0 | 150.0 | 165.0 |
|---|---|---|---|---|---|---|---|---|---|---|---|---|
| 2.2500 | 90.0000 | 75.0896 | 60.1382 | 44.9850 | 29.8657 | 14.9302 | 0.0001 | -15.0694 | -30.1278 | -45.0021 | -59.8684 | -74.9238 |
| 3.3750 | 87.8361 | 73.0778 | 58.3929 | 43.7382 | 29.1151 | 14.5285 | -0.0433 | -14.6197 | -29.1927 | -43.7589 | -58.3523 | -73.0162 |
| 4.5000 | 86.0988 | 71.5629 | 57.1514 | 42.8083 | 28.5041 | 14.2240 | -0.0438 | -14.3074 | -28.5708 | -42.8442 | -57.1536 | -71.5407 |
| 5.6250 | 84.5870 | 70.2901 | 56.1369 | 42.0564 | 28.0095 | 13.9778 | -0.0465 | -14.0661 | -28.0832 | -42.1068 | -56.1609 | -70.2901 |
| 6.7500 | 83.2189 | 69.1758 | 55.2711 | 41.4250 | 27.5974 | 13.7727 | -0.0512 | -13.8706 | -27.6820 | -41.4890 | -55.3108 | -69.1911 |
| 7.8750 | 81.9618 | 68.1834 | 54.5181 | 40.8849 | 27.2482 | 13.5991 | -0.0569 | -13.7085 | -27.3448 | -40.9618 | -54.5711 | -68.2109 |
| 9.0000 | 80.8013 | 67.2937 | 53.8577 | 40.4184 | 26.9494 | 13.4508 | -0.0631 | -13.5725 | -27.0584 | -40.5078 | -53.9226 | -67.3317 |
| 10.1250 | 79.7306 | 66.4948 | 53.2766 | 40.0137 | 26.6923 | 13.3233 | -0.0695 | -13.4578 | -26.8137 | -40.1150 | -53.3525 | -66.5422 |
| 11.2500 | 78.7459 | 65.7782 | 52.7649 | 39.6620 | 26.4705 | 13.2134 | -0.0760 | -13.3607 | -26.6043 | -39.7749 | -52.9512 | -65.8343 |
| 12.3750 | 77.8444 | 65.1371 | 52.3150 | 39.3563 | 26.2791 | 13.1185 | -0.0825 | -13.2786 | -26.4251 | -39.4805 | -52.4111 | -65.2014 |
| 13.5000 | 77.0236 | 64.5658 | 51.9202 | 39.0911 | 26.1140 | 13.0365 | -0.0890 | -13.2095 | -26.2721 | -39.2262 | -52.0258 | -64.6378 |
| 14.6250 | 76.2810 | 64.0589 | 51.5751 | 38.8615 | 25.9718 | 12.9658 | -0.0955 | -13.1515 | -26.1420 | -39.0073 | -51.6898 | -64.1382 |
| 15.7500 | 75.6137 | 63.6117 | 51.2747 | 38.6637 | 25.8499 | 12.9049 | -0.1020 | -13.1033 | -26.0318 | -38.8199 | -51.3983 | -63.6981 |
| 16.8750 | 75.0184 | 63.2196 | 51.0148 | 38.4940 | 25.7458 | 12.8527 | -0.1084 | -13.0636 | -25.9394 | -38.6605 | -51.1469 | -63.3127 |
| 18.0000 | 74.4917 | 62.8783 | 50.7914 | 38.3496 | 25.6576 | 12.8080 | -0.1148 | -13.0314 | -25.8626 | -38.5261 | -50.9318 | -62.9778 |

ANGLE OF FIELD IN GAP (AROUND SUBCONDUCTOR #2#)

| RADIAL / ANGLE DIST. / DEGREES | 180.0 | 195.0 | 210.0 | 225.0 | 240.0 | 255.0 | 270.0 | 285.0 | 300.0 | 315.0 | 330.0 | 345.0 |
|---|---|---|---|---|---|---|---|---|---|---|---|---|
| 2.2500 | -89.9997 | -104.9204 | -119.8622 | -135.0102 | -150.1429 | -165.0747 | -179.9996 | 164.9250 | 149.8507 | 134.9768 | 120.1433 | 105.0935 |
| 3.3750 | -87.7721 | -102.6487 | -117.7080 | -133.0015 | -148.5204 | -164.2144 | 179.9830 | 164.1724 | 148.4845 | 133.0154 | 117.7756 | 102.7256 |
| 4.5000 | -86.0613 | -100.7923 | -115.8317 | -131.2731 | -147.1622 | -163.4544 | -179.9924 | 163.4694 | 147.1818 | 131.3064 | 115.8781 | 100.8399 |
| 5.6250 | -84.5675 | -99.1036 | -114.0475 | -129.5646 | -145.7755 | -162.6589 | -179.9718 | 162.7133 | 145.8263 | 129.6127 | 114.0915 | 99.1384 |
| 6.7500 | -83.2117 | -97.5085 | -112.2839 | -127.7940 | -144.2740 | -161.7705 | -179.9538 | 161.8579 | 144.3493 | 127.8548 | 112.3291 | 97.5363 |
| 7.8750 | -81.9640 | -95.9826 | -110.5177 | -125.9283 | -142.6103 | -160.7479 | -179.9366 | 160.8659 | 142.7071 | 126.0000 | 110.5647 | 96.0055 |
| 9.0000 | -80.8114 | -94.5199 | -108.7458 | -123.9545 | -140.7490 | -159.5505 | -179.9192 | 159.6985 | 140.8653 | 124.0355 | 108.7943 | 94.5387 |
| 10.1250 | -79.7478 | -93.1219 | -106.9753 | -121.8713 | -138.6599 | -158.1311 | -179.9007 | 158.3095 | 138.7939 | 121.9598 | 107.0245 | 93.1369 |
| 11.2500 | -78.7696 | -91.7930 | -105.2183 | -119.6862 | -136.3167 | -156.4321 | -179.8802 | 156.6418 | 136.4664 | 119.7802 | 105.2673 | 91.8041 |
| 12.3750 | -77.8742 | -90.5386 | -103.4901 | -117.4144 | -133.6981 | -154.3807 | -179.8571 | 154.6228 | 133.8610 | 117.5117 | 103.5380 | 90.5458 |
| 13.5000 | -77.0593 | -89.3637 | -101.8071 | -115.0777 | -130.7910 | -151.8842 | -179.8300 | 152.1595 | 130.9639 | 115.1762 | 101.8529 | 89.3669 |
| 14.6250 | -76.3223 | -88.2724 | -100.1856 | -112.7041 | -127.5941 | -148.8252 | -179.7972 | 149.1337 | 127.7730 | 112.8016 | 100.2287 | 88.2716 |
| 15.7500 | -75.6603 | -87.2677 | -98.6411 | -110.3262 | -124.1231 | -145.0583 | -179.7559 | 145.3977 | 124.3030 | 110.4206 | 98.6808 | 87.2628 |
| 16.8750 | -75.0701 | -86.3511 | -97.1872 | -107.9794 | -120.4144 | -140.4123 | -179.7014 | 140.7765 | 120.5898 | 108.0690 | 97.2230 | 86.3423 |
| 18.0000 | -74.5482 | -85.5231 | -95.8352 | -105.7002 | -116.5283 | -134.7078 | -179.6246 | 135.0841 | 116.6935 | 105.7834 | 95.8670 | 85.5105 |

Figure 6.6 (Continued)

was preferred, however, to investigate the effect of the spacing between subconductors, the separation between the positive and negative conductors for the bipolar case, and the height above ground given a certain subconductor radius. The conductor radius of RS=2.235 cm was used throughout. Figures 6.7 through 6.12 are obtained from several computer outputs representing different geometrical unipolar twin-bundle line parameters.

Figure 6.7 depicts the potential distribution along the lateral axis ($\alpha$=90°) starting at the subconductor's surface for four different spacings. The curves drop faster at smaller spacings which means higher gradients at small values of AS. This is seen in Figure 6.8 in which the electric field along the lateral axis is plotted against the distance from the center of the subconductor in multiples of RS. The potential gradient is higher at small AS and tends to be less different farther away from the conductor.

For corona breakdown studies, the maximum field occurring anywhere on the surface is of vital concern. Here the effect of AS and H on this value was examined and the results are summarized in Figure 6.9 for the 2.235 cm subconductor. Here $E_{max}$ is plotted against AS at various values of H from 7.62 to 38.10 m. Note that $E_{max}$ drops rapidly as AS is increased, reaches a minimum value and then starts to increase again. It was found that $E_{max}$ reaches a minimum at AS=35

Figure 6.7. Potential distribution along lateral axis of subconductor for different subconductor spacings, unipolar line

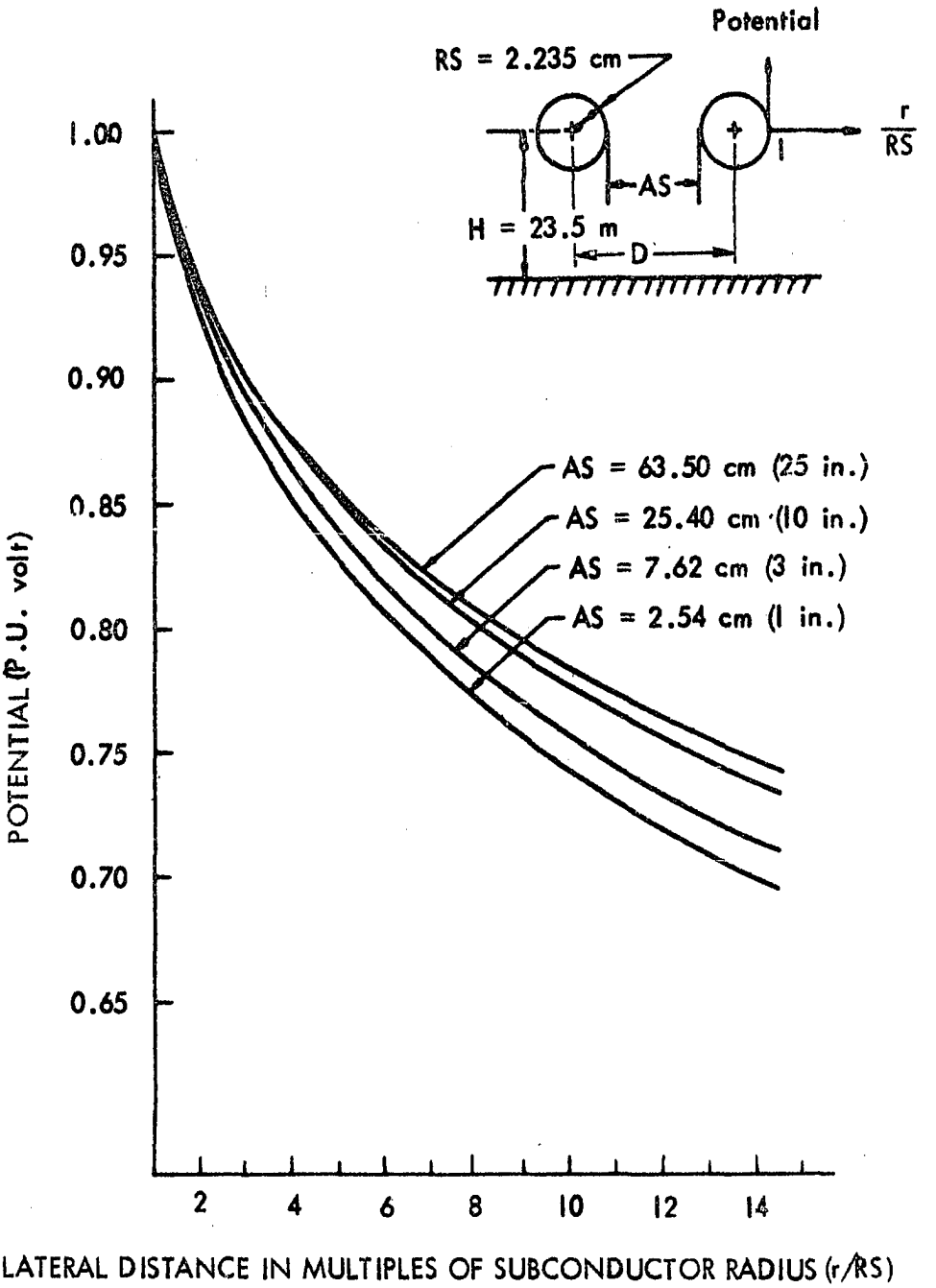
Potential
RS = 2.235 cm
AS
H = 23.5 m
D
r/RS
1.00
0.95
0.90
0.85
0.80
0.75
0.70
0.65
AS = 63.50 cm (25 in.)
AS = 25.40 cm (10 in.)
AS = 7.62 cm (3 in.)
AS = 2.54 cm (1 in.)
POTENTIAL (P.U. volt)
2
4
6
8
10
12
14
LATERAL DISTANCE IN MULTIPLES OF SUBCONDUCTOR RADIUS (r/RS)

Figure 6.8. Electric field distribution along lateral axis of subconductor for different subconductor spacings, unipolar line

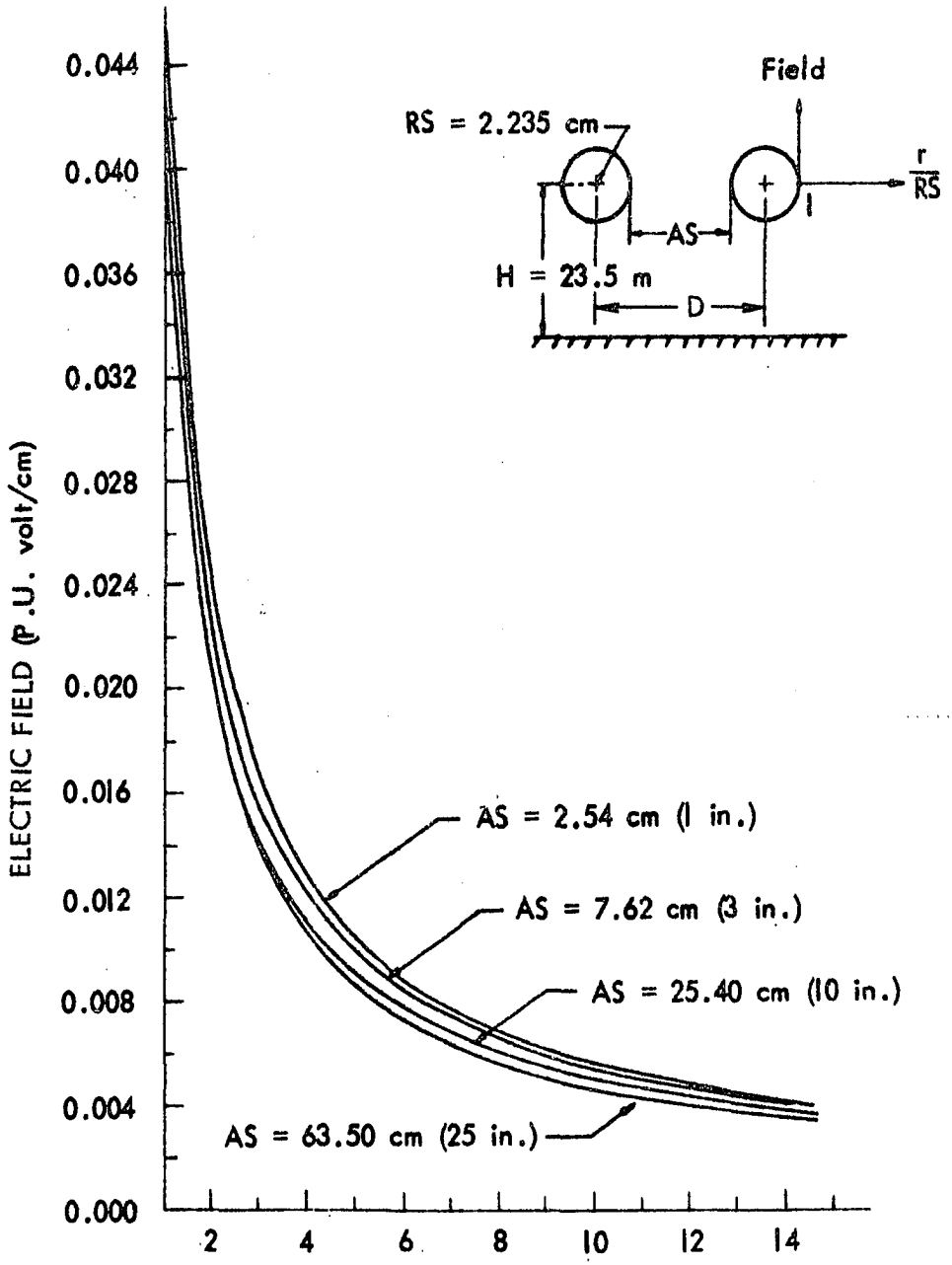
Field
RS = 2.235 cm
r/RS
AS
H = 23.5 m
D
0.044
0.040
0.036
0.032
0.028
0.024
0.020
0.016
0.012
0.008
0.004
0.000
ELECTRIC FIELD (P.U. volt/cm)
AS = 2.54 cm (1 in.)
AS = 7.62 cm (3 in.)
AS = 25.40 cm (10 in.)
AS = 63.50 cm (25 in.)
2
4
6
8
10
12
14
RADIAL DISTANCE IN MULTIPLES OF SUBCONDUCTOR RADIUS (r/RS).

Figure 6.9. Maximum magnitude of electric field on subconductor surface vs subconductor spacing for different subconductor heights above ground, unipolar line

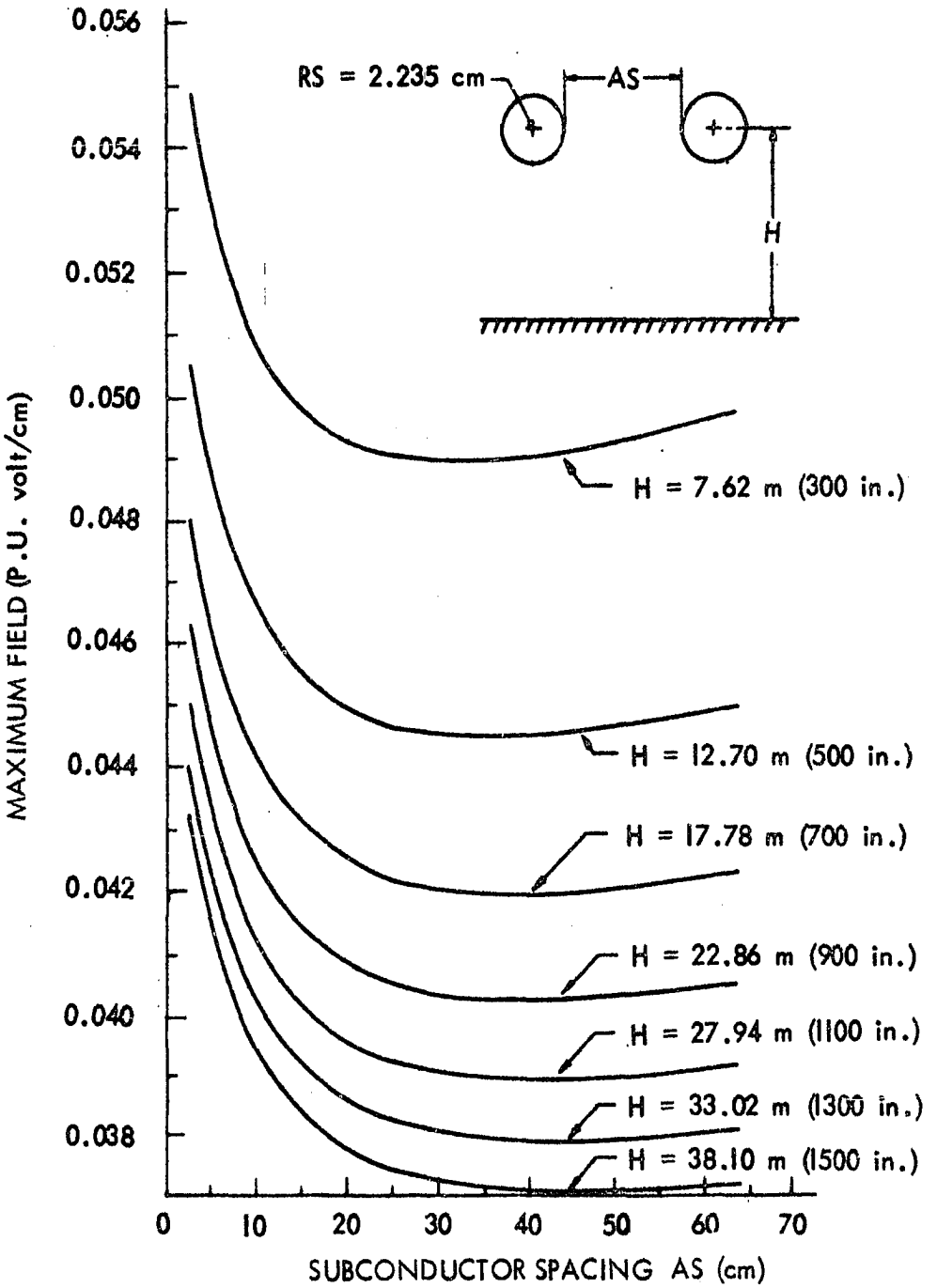
0.056
0.054
0.052
0.050
0.048
0.046
0.044
0.042
0.040
0.038
MAXIMUM FIELD (P.U. volt/cm)
RS = 2.235 cm
AS
H
H = 7.62 m (300 in.)
H = 12.70 m (500 in.)
H = 17.78 m (700 in.)
H = 22.86 m (900 in.)
H = 27.94 m (1100 in.)
H = 33.02 m (1300 in.)
H = 38.10 m (1500 in.)
0
10
20
30
40
50
60
70
SUBCONDUCTOR SPACING AS (cm)

Figure 6.10. Maximum magnitude of electric field on subconductor surface vs subconductor height above ground for different subconductor spacings, unipolar line

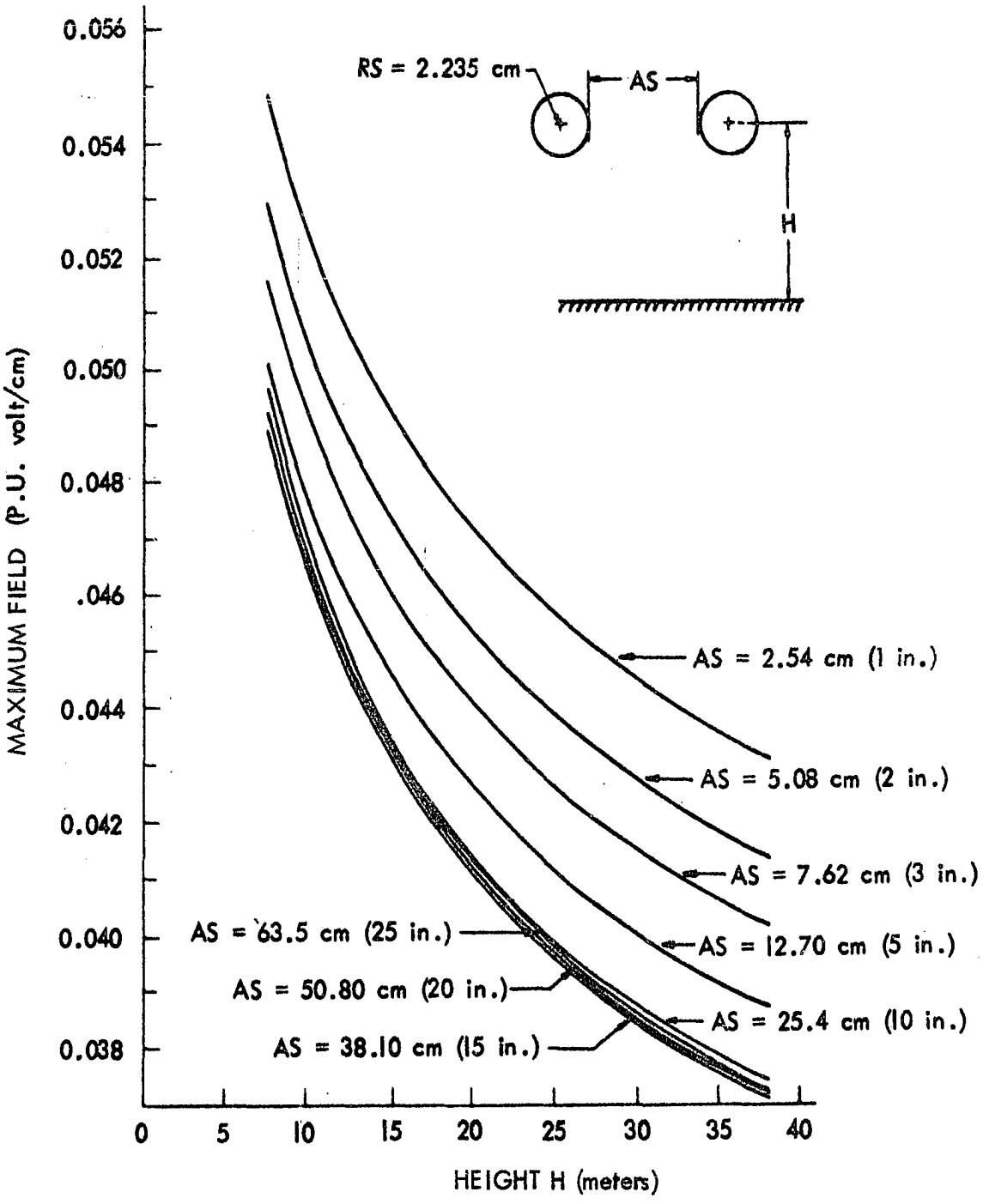
RS = 2.235 cm
AS
H
0.056
0.054
0.052
0.050
0.048
.046
0.044
0.042
0.040
0.038
MAXIMUM FIELD (P.U. volt/cm)
AS = 2.54 cm (1 in.)
AS = 5.08 cm (2 in.)
AS = 7.62 cm (3 in.)
AS = 12.70 cm (5 in.)
AS = 25.4 cm (10 in.)
AS = 38.10 cm (15 in.)
AS = 50.80 cm (20 in.)
AS = 63.5 cm (25 in.)
0
5
10
15
20
25
30
35
40
HEIGHT H (meters)

Figure 6.11. Equipotential lines in the vicinity of subconductors (P.U. volt), unipolar line

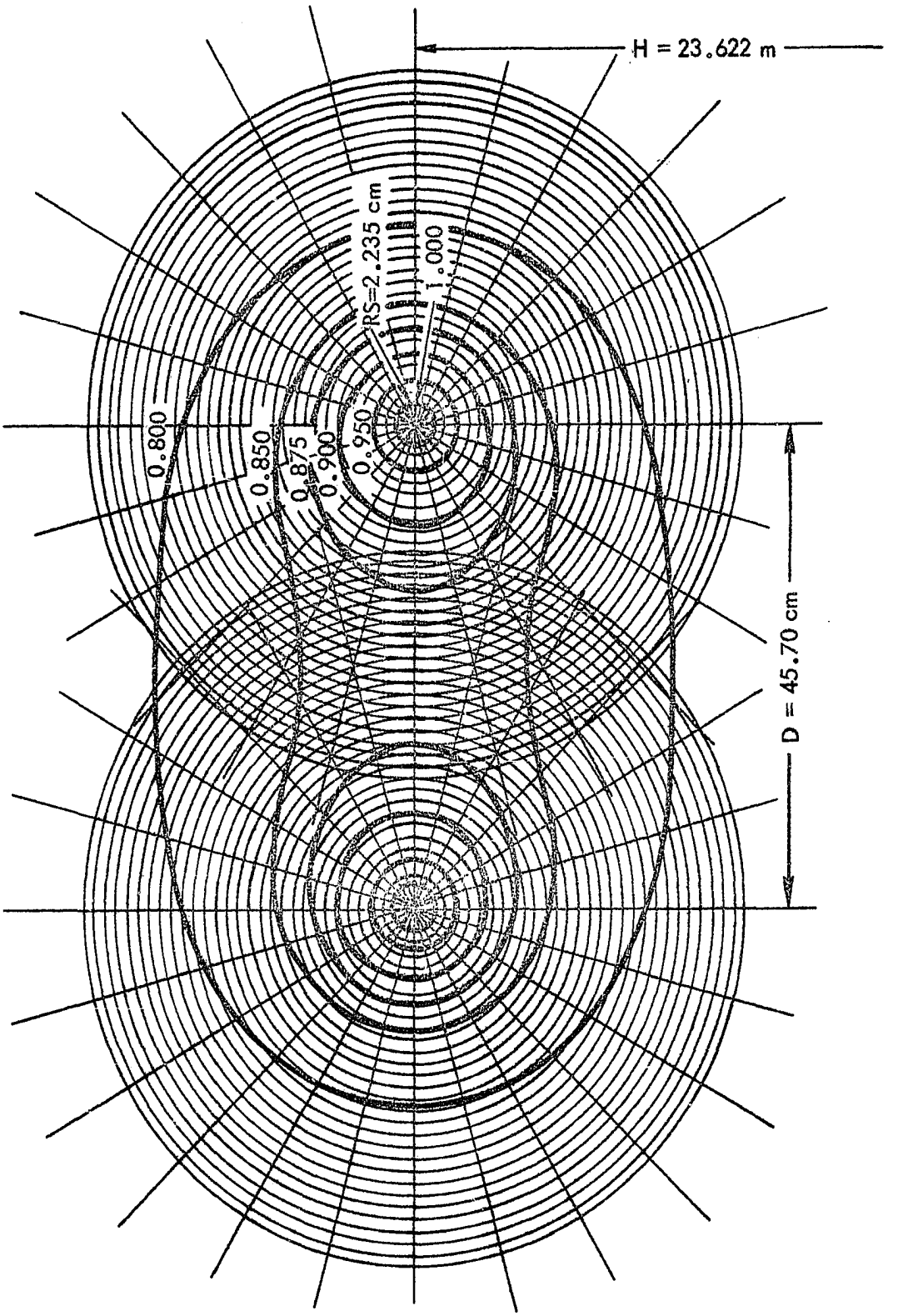
H = 23.622 m
RS=2.235 cm
1.000
0.950
0.900
0.875
0.850
0.800
D = 45.70 cm

Figure 6.12. Equigradient lines in the vicinity of subconductors (P.U. volt/cm), unipolar line

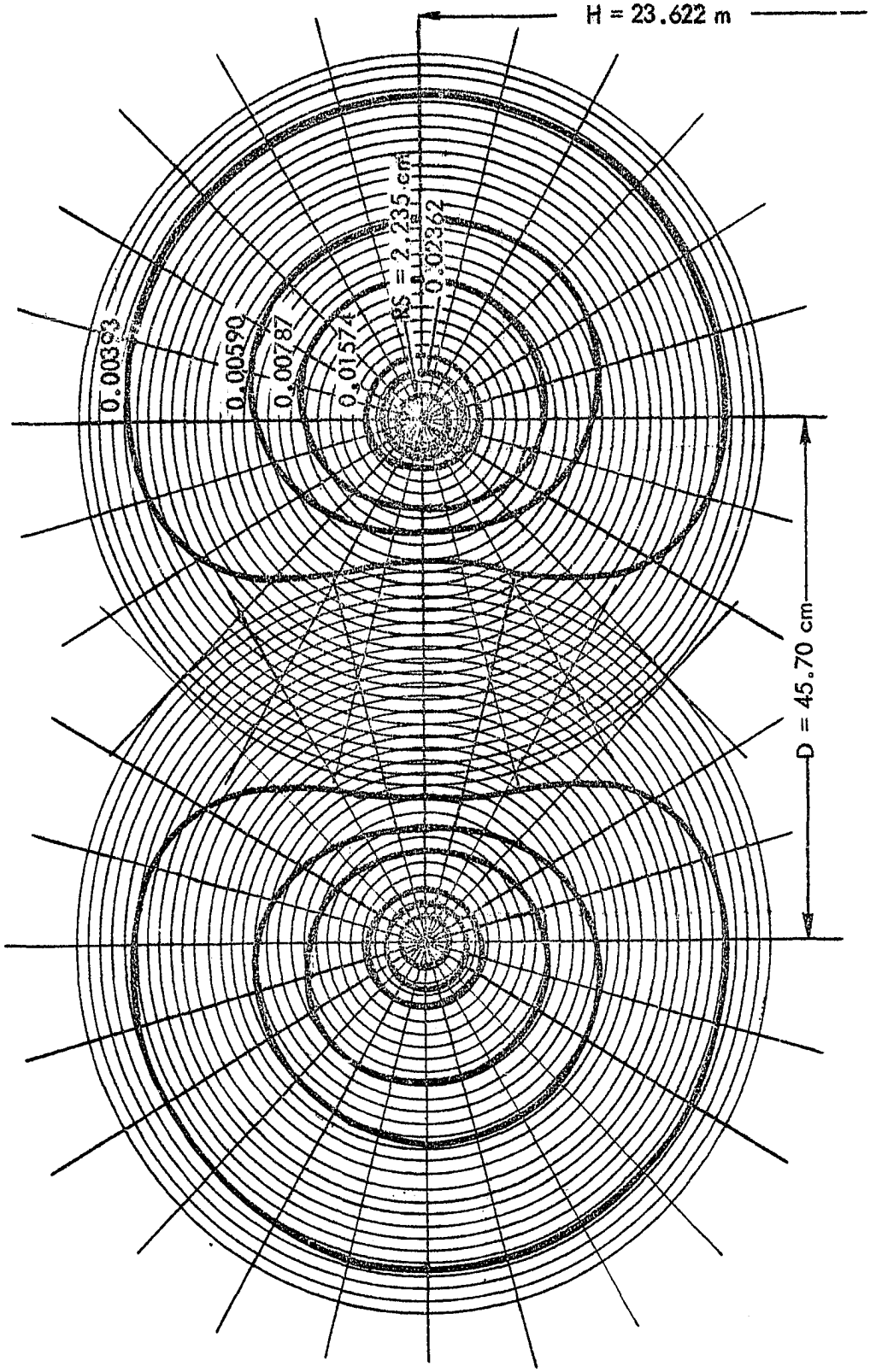
H = 23.622 m
0.00393
0.00590
0.00787
0.01574
RS = 2.235 cm
0.02362
D = 45.70 cm

Figure 6.13. Potential distribution along lateral axis of subconductor I for different subconductor spacings, bipolar line

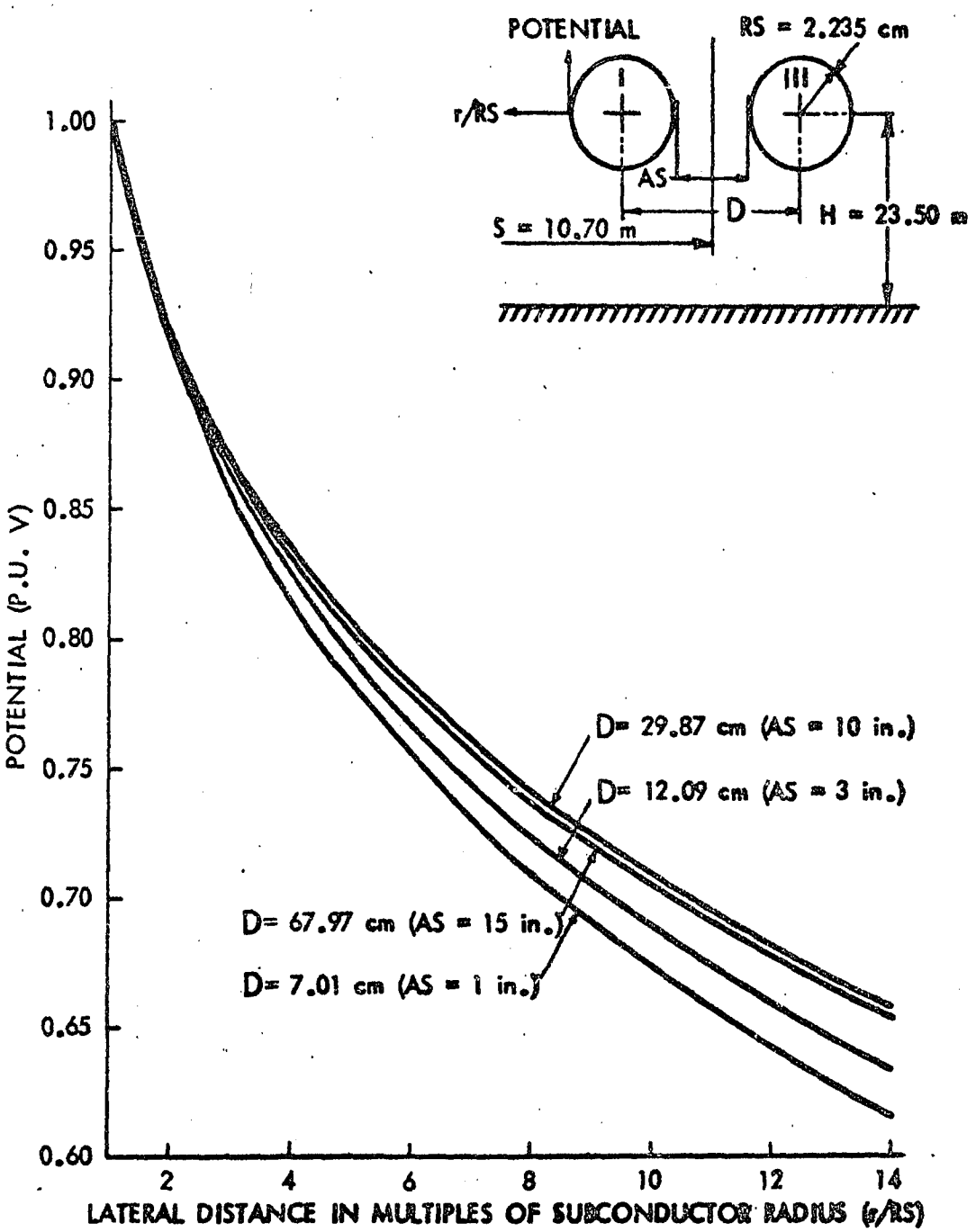
POTENTIAL
RS = 2.235 cm
I
III
r/RS
AS
D
S = 10.70 m
H = 23.50 m
1.00
0.95
0.90
0.85
0.80
0.75
0.70
0.65
0.60
POTENTIAL (P.U. V)
D= 29.87 cm (AS = 10 in.)
D= 12.09 cm (AS = 3 in.)
D= 67.97 cm (AS = 15 in.)
D= 7.01 cm (AS = 1 in.)
2
4
6
8
10
12
14
LATERAL DISTANCE IN MULTIPLES OF SUBCONDUCTOR RADIUS (r/RS)

to 45 cm depending upon the value of H. This value is not very pronounced, however, since the curves (Figure 6.9) remain quite flat over a certain region.

This is also illustrated in Figure 6.10 in which $E_{max}$ is plotted against H with AS as a parameter. The lowest curve obtained was that of AS=38.10 cm. This value is surprisingly close to the one used by the Bonneville Power Administration for its 750 kV dc line which is 41.25 cm (11).

Finally, the equipotential and equigradient curves plotted for this conductor are shown in Figures 6.11 and 6.12, respectively. While these curves are very illustrative, they do not supply the numerical data needed for special investigations. These equigradient curves of Figure 6.12 agree quite closely in shape with the ones published earlier (26, 27). However the later curves were expressed in terms of ratios to the maximum surface gradient and were obtained by neglecting ground. Here, the effect of ground can be clearly recognized. Figures 6.13 through 6.19 are also obtained from several computer outputs representing different geometrical bipolar twin-bundle line parameters.

Figures 6.13, 6.14, 6.15, 6.16, 6.17 and 6.18 correspond to Figures 6.7, 6.8, 6.9, 6.10, 6.11 and 6.12 of the unipolar line, respectively. An interesting observation is that keeping the separation S between the positive and negative conductors constant, the potential at a certain location along

Figure 6.14. Electric field distribution along lateral axis of subconductor I for different subconductor spacings, bipolar line

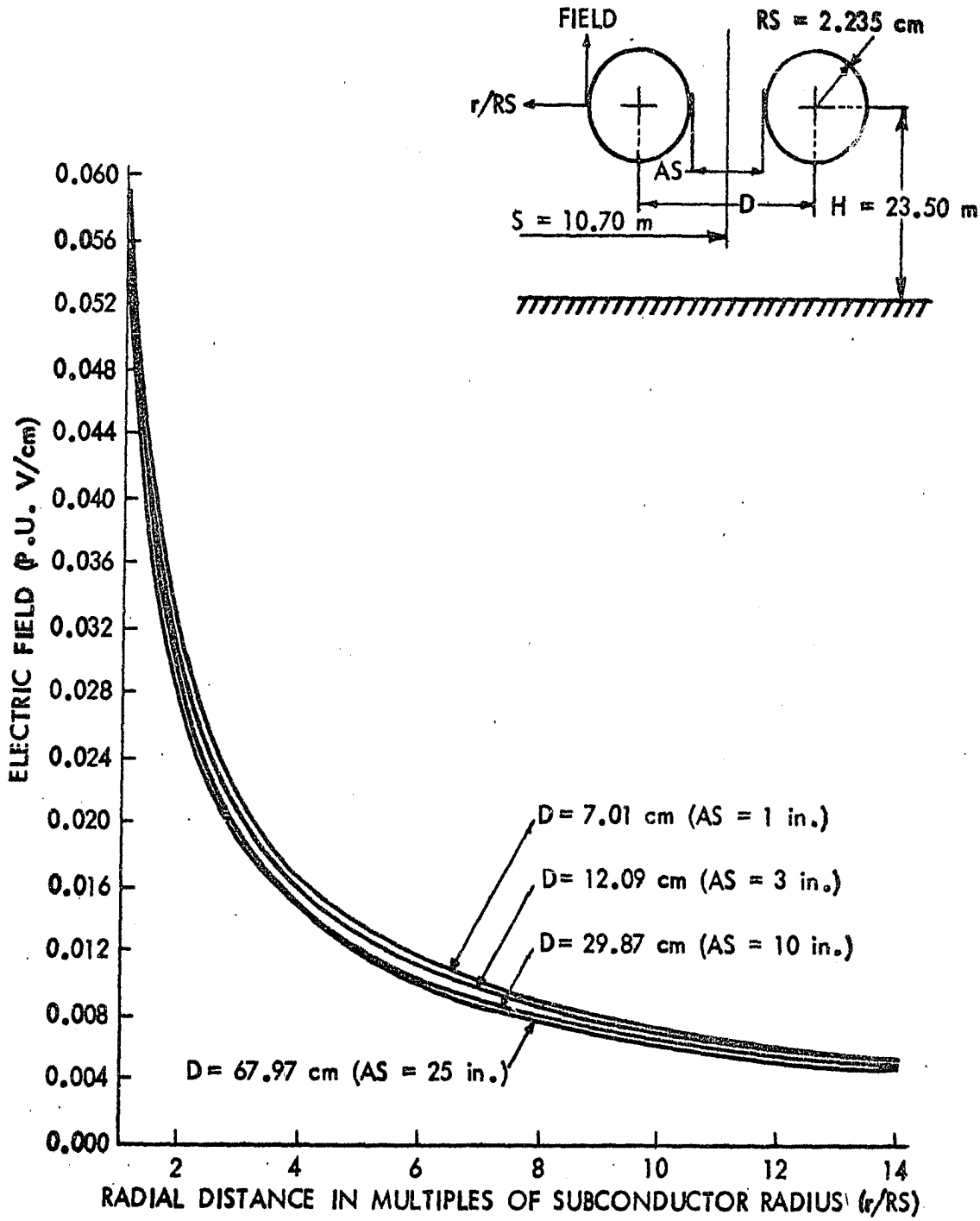
FIELD
RS = 2.235 cm
r/RS
AS
D
H = 23.50 m
S = 10.70 m
0.060
0.056
0.052
0.048
0.044
0.040
0.036
0.032
0.028
0.024
0.020
0.016
0.012
0.008
0.004
0.000
ELECTRIC FIELD (P.U. V/cm)
D = 7.01 cm (AS = 1 in.)
D = 12.09 cm (AS = 3 in.)
D = 29.87 cm (AS = 10 in.)
D = 67.97 cm (AS = 25 in.)
2
4
6
8
10
12
14
RADIAL DISTANCE IN MULTIPLES OF SUBCONDUCTOR RADIUS (r/RS)

Figure 6.15. Maximum magnitude of electric field on subconductor surface vs subconductor spacing for different subconductor heights above ground, bipolar line

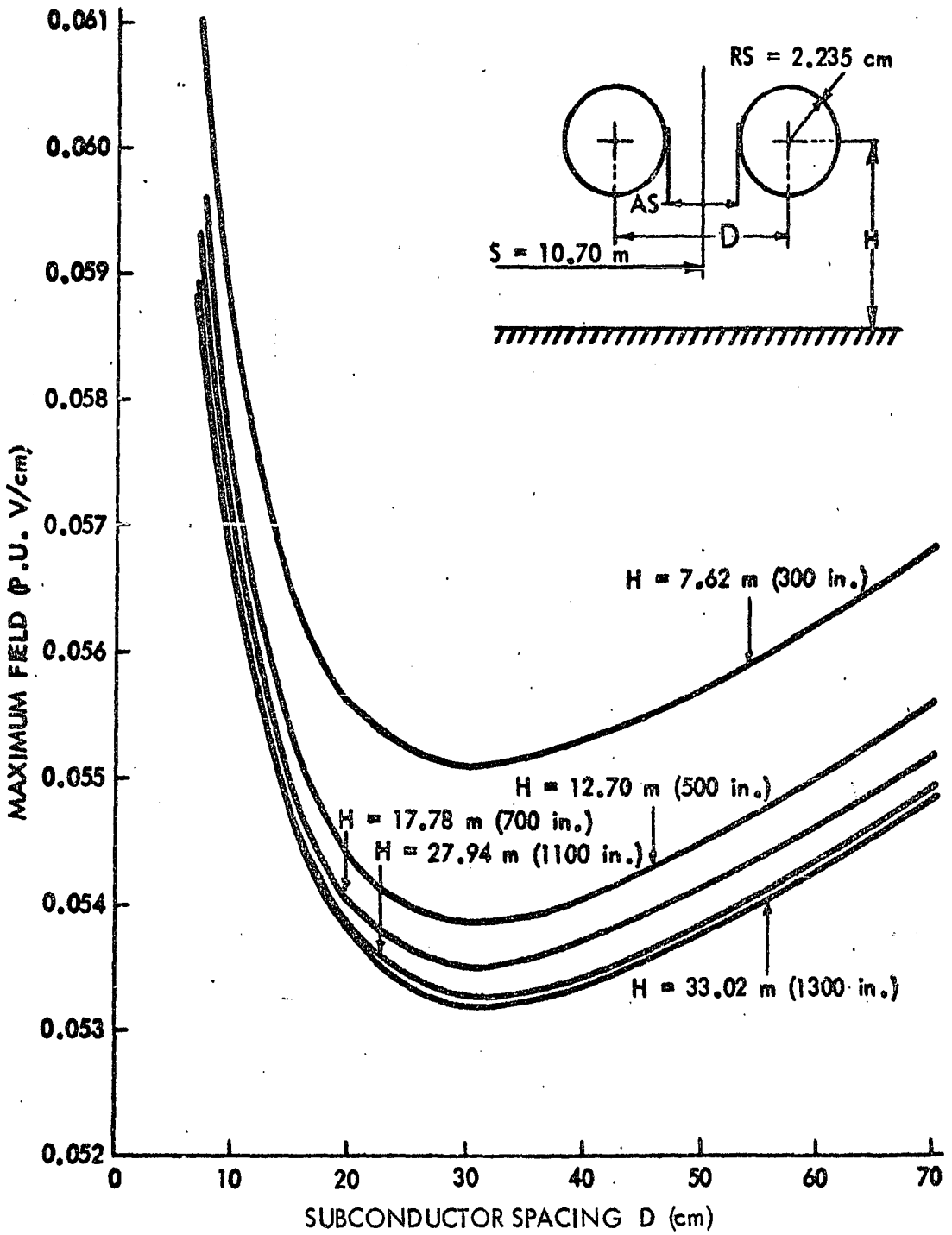
RS = 2.235 cm
AS
D
H
S = 10.70 m
H = 7.62 m (300 in.)
H = 12.70 m (500 in.)
H = 17.78 m (700 in.)
H = 27.94 m (1100 in.)
H = 33.02 m (1300 in.)
MAXIMUM FIELD (P.U. V/cm)
0.061
0.060
0.059
0.058
0.057
0.056
0.055
0.054
0.053
0.052
0
10
20
30
40
50
60
70
SUBCONDUCTOR SPACING D (cm)

Figure 6.16. Maximum magnitude of electric field on subconductor surface vs subconductor height above ground for different subconductor spacings, bipolar line

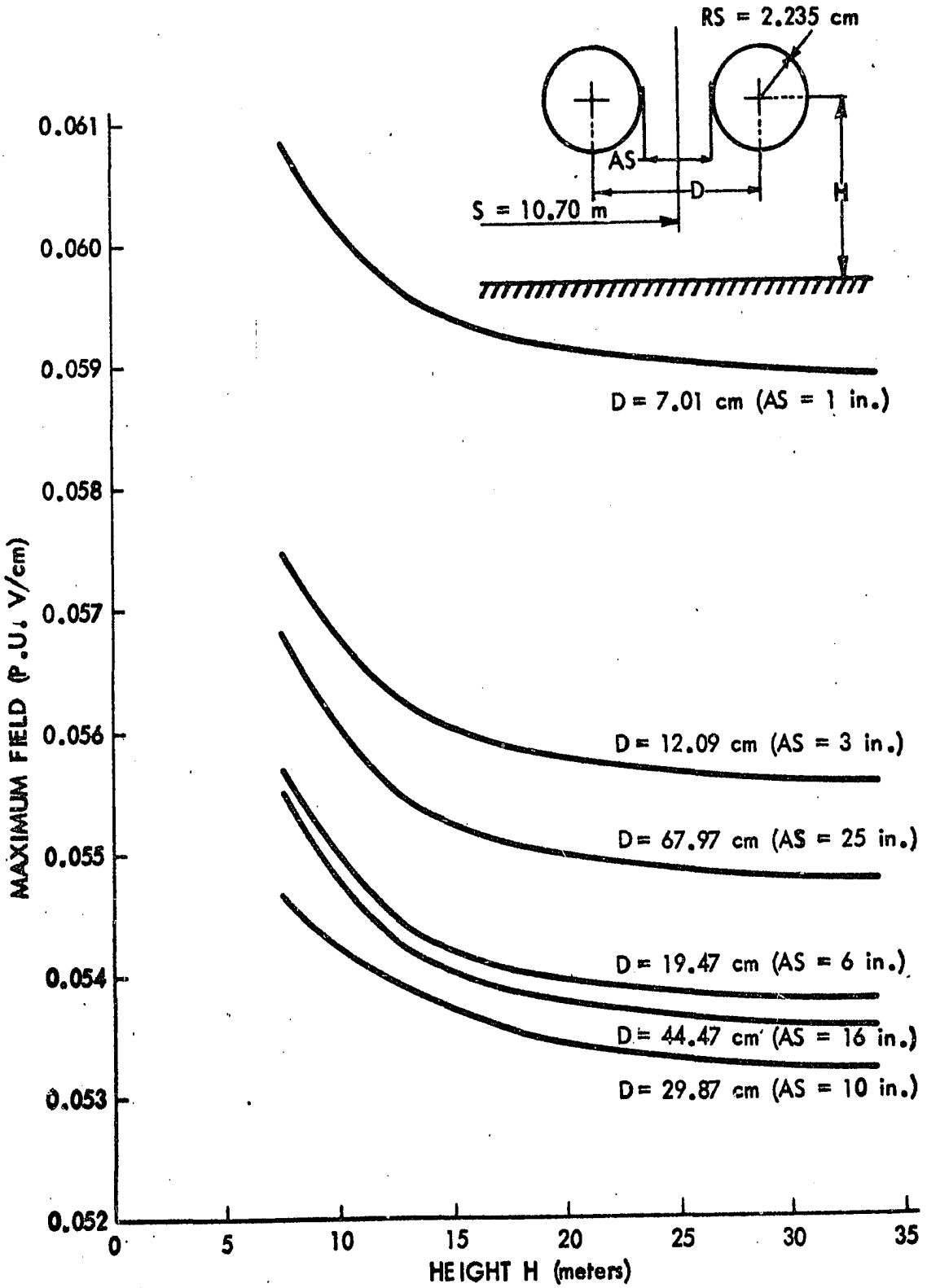
RS = 2.235 cm
AS
D
H
S = 10.70 m
D = 7.01 cm (AS = 1 in.)
D = 12.09 cm (AS = 3 in.)
D = 67.97 cm (AS = 25 in.)
D = 19.47 cm (AS = 6 in.)
D = 44.47 cm (AS = 16 in.)
D = 29.87 cm (AS = 10 in.)
MAXIMUM FIELD (P.U., V/cm)
0.061
0.060
0.059
0.058
0.057
0.056
0.055
0.054
0.053
0.052
0
5
10
15
20
25
30
35
HEIGHT H (meters)

Figure 6.17. Equipotential lines in the vicinity of subconductors (P.U. volt), bipolar line

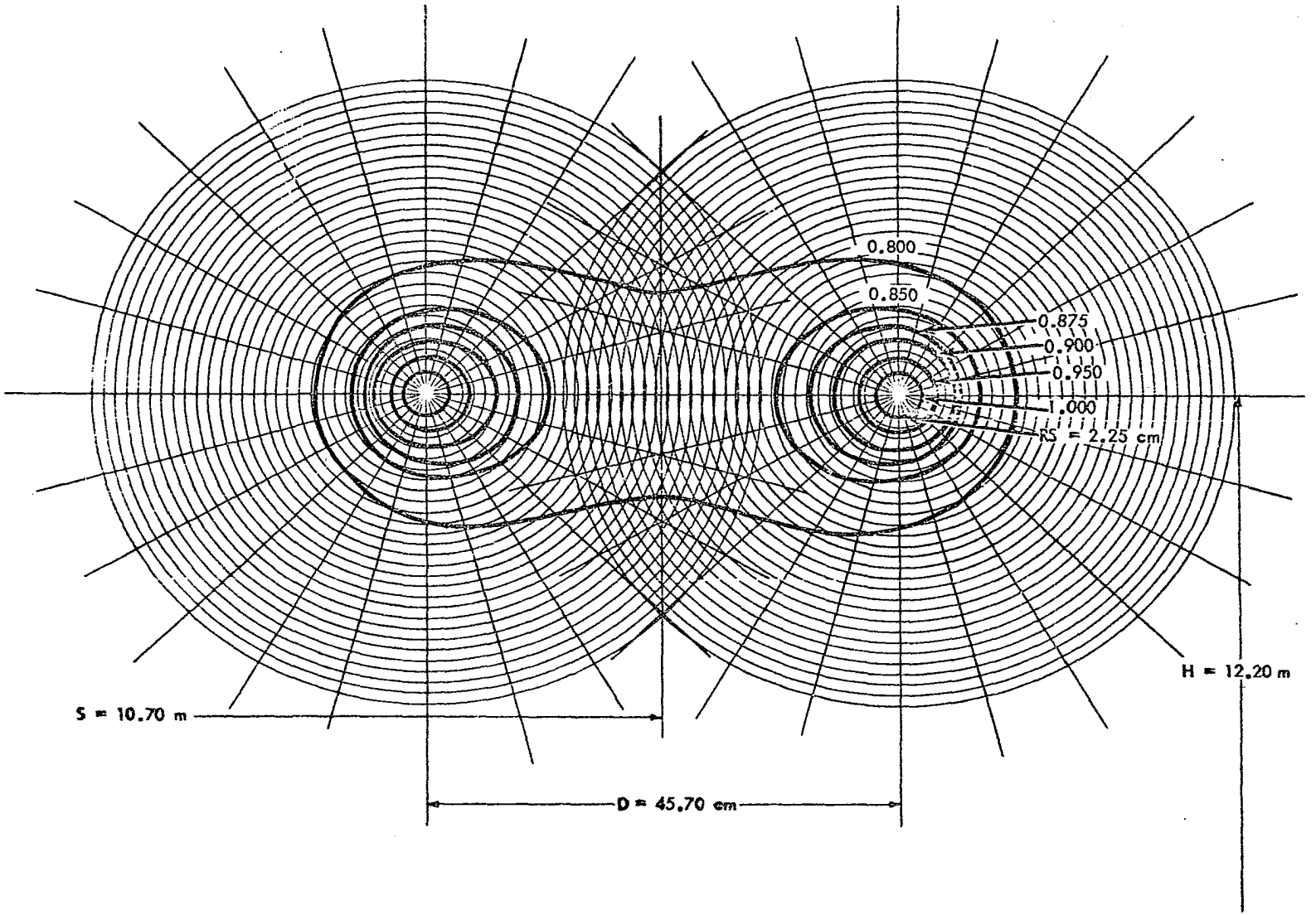
0.800
0.850
0.875
0.900
0.950
1.000
RS = 2.25 cm
H = 12.20 m
S = 10.70 m
D = 45.70 cm

Figure 6.18. Equigradient lines in the vicinity of subconductors (P.U. volt/cm), bipolar line

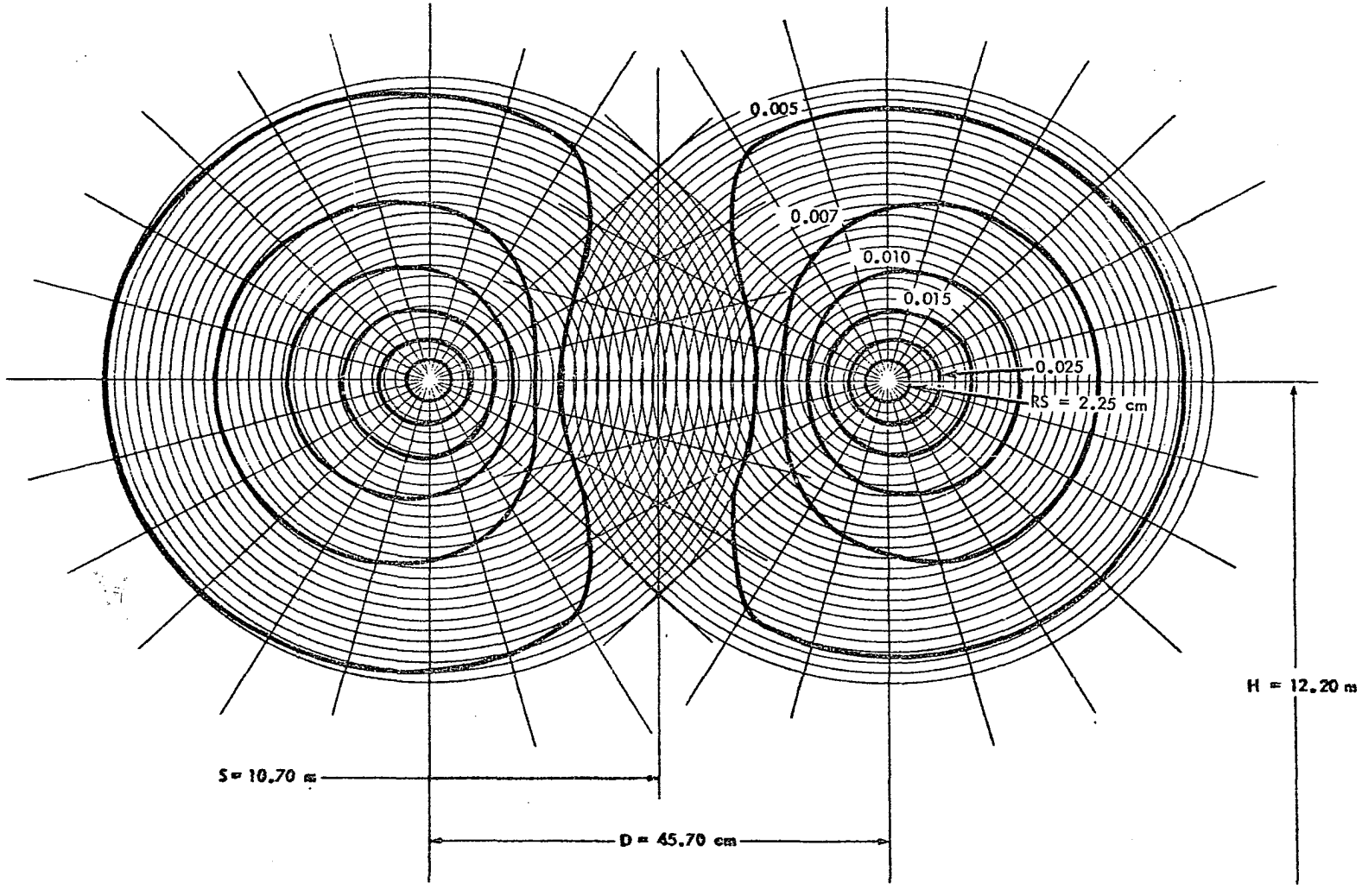
0.005
0.007
0.010
0.015
0.025
RS = 2.25 cm
H = 12.20 m
S = 10.70 m
D = 45.70 cm

the lateral axis increases with increasing the subconductor's spacing (the electric field decreases), up to a value of D=30 cm, and then starts to decrease again with a further increase in D (the electric field increases). This could be attributed to the fact that increasing D beyond a certain value results in getting the positive and negative conductors closer to each other and thus decreasing the potential and increasing the electric field at a given location.

Figures 6.15 and 6.16 show the possibility of neglecting the effect of ground when dealing with bipolar lines, without an appreciable effect on the accuracy. A comparison of Figures 6.9 and 6.16 shows that the electric fields of bipolar lines are higher (by roughly 20 percent) than those of unipolar lines, with the same subconductors radii and spacings. This result is again attributed to the negative conductor of the bipolar line. Also, it is to be noticed that the effect of varying the subconductors spacing and/or height from ground is not appreciable in the bipolar line as compared to the unipolar line.

Figure 6.19 shows that the separation between the positive and negative conductors greatly affects the magnitude of the maximum surface gradient of a bipolar line of a given subconductor radius and spacing. Decreasing the conductor's separation from 8 meters to 4 meters results in increasing

Figure 6.19. Maximum magnitude of electric field on sub-conductor surface vs conductor's separation, bipolar line

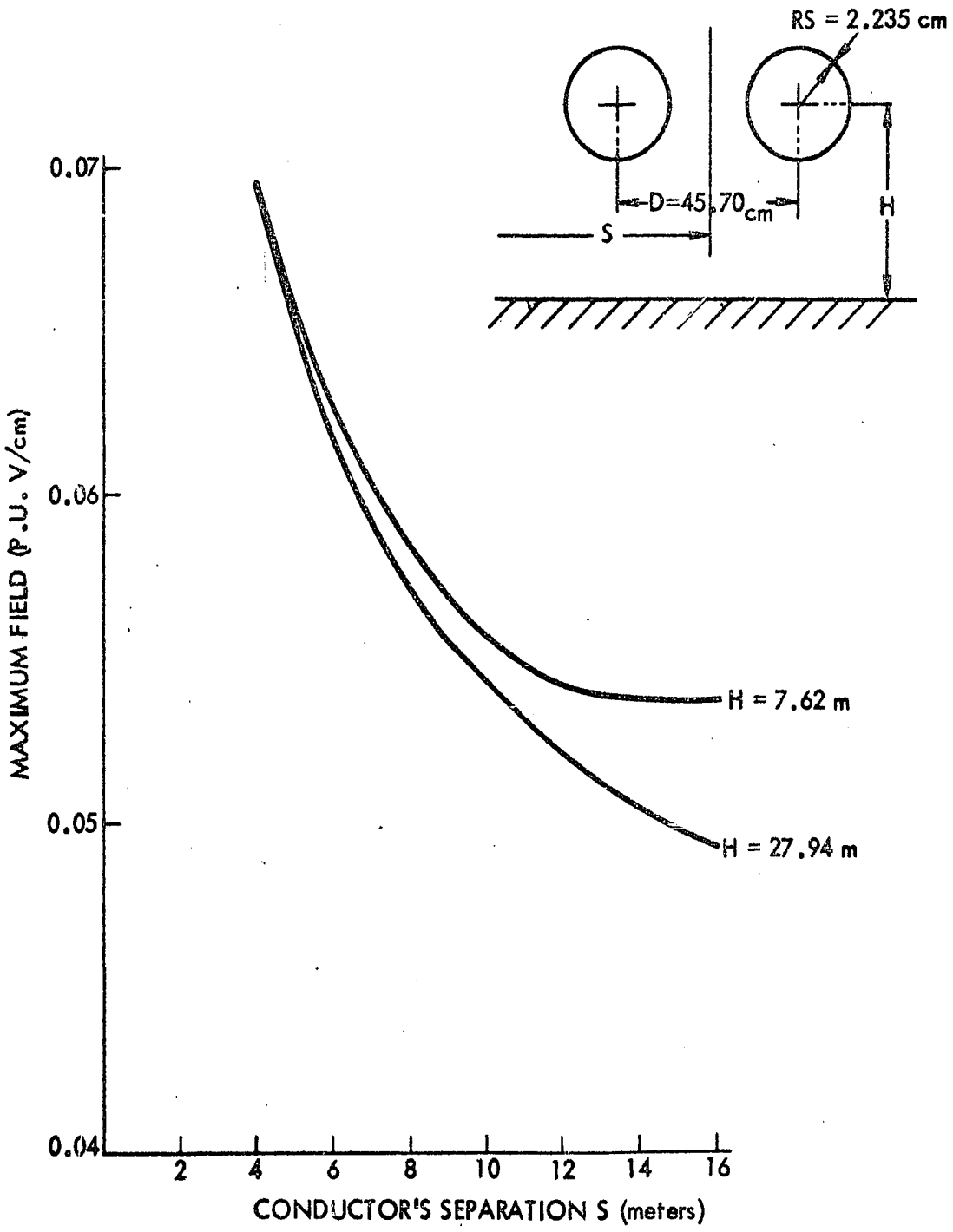
RS = 2.235 cm
D=45.70cm
S
H
0.07
0.06
0.05
0.04
MAXIMUM FIELD (P.U. V/cm)
H = 7.62 m
H = 27.94 m
2
4
6
8
10
12
14
16
CONDUCTOR'S SEPARATION S (meters)

the maximum surface gradient by about 20 percent.

For a unipolar twin-bundle line of subconductor radius RS=2.235 cm, spacing D=45.70 cm, and height H=23.62 m the computed value of maximum surface gradient is 0.0398 p.u. volt/cm. The corresponding value calculated using Equation 2.1 derived by Miller (15) is 0.052 p.u. volt/cm. This shows that the electric field, of a practical size unipolar twin-bundle line, calculated by simulating the conductor charge with one axial line charge is about 25 percent higher than the value obtained using the charge simulation technique and the method of images described in this dissertation.

## B. The Corona Threshold

Different computations of corona thresholds were made for the unipolar and bipolar twin-bundle lines with varying geometrical parameters. In order to check the accuracy of the computed corona thresholds, it is necessary to compare them with corona thresholds that are accurately measured experimentally for the same line configuration and under the same conditions. Experimental measurements of corona voltages were reported by Miller (15) for two unipolar twin-bundle lines of subconductors radii of $\frac{1}{2}$ in. and $\frac{5}{8}$ in. at a height of 12 ft. from ground. His measurements were made for subconductor spacings varying from 8 in. to 20 in. In Figure 6.20 the measured thresholds are compared to those

Figure 6.20. Computed and measured corona thresholds of unipolar twin-bundle conductors (15) vs sub-conductor spacing, for different subconductors radii, H=12 ft.

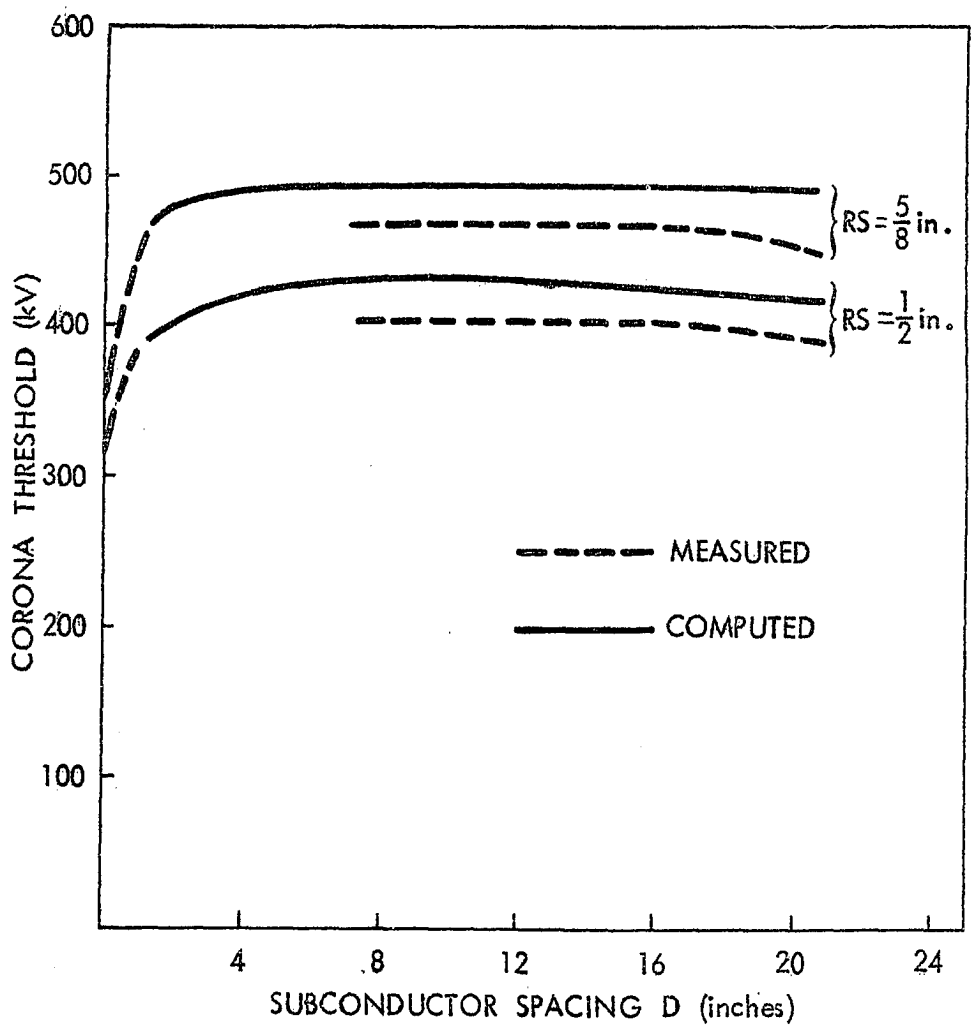
600
500
400
300
200
100
CORONA THRESHOLD (kV)
RS = 5/8 in.
RS = 1/2 in.
MEASURED
COMPUTED
4
8
12
16
20
24
SUBCONDUCTOR SPACING D (inches)

computed for the same unipolar line parameters and under the same physical conditions. This comparison indicates that the computed corona thresholds are very close to the corresponding measured values. However, the observation that the measured thresholds are always below the computed ones, with a deviation of less than 7 percent, is not to be attributed to the accuracy of the computed fields or the mathematical model used, but rather to the fact that the conductors used by Miller could not be made perfectly smooth, resulting in slightly lower measured corona thresholds.

From Figure 6.20 we observe also that using a twin-bundle conductor would result in increasing the corona threshold by roughly 40 percent over its value when using a single conductor (subconductor spacing D=0) of the same diameter.

In Figure 6.21 corona threshold of the bipolar twin-bundle line of subconductor radius RS=2.235 cm and spacing D=45.7 cm are plotted against the subconductor separation S for two different values of conductor height above ground H. Note that the corona thresholds are not considerably increased by increasing the conductor height. However, the effect of the subconductor separation S is rather obvious. Increasing S from 4 meters to 16 meters results in increasing the corona threshold by about 40 percent. This is found to be in complete agreement with the implication of Figure 6.19.

Figure 6.21. Corona thresholds of bipolar twin-bundle conductors vs conductor's separation, RS=2.25 cm, D=45.70 cm

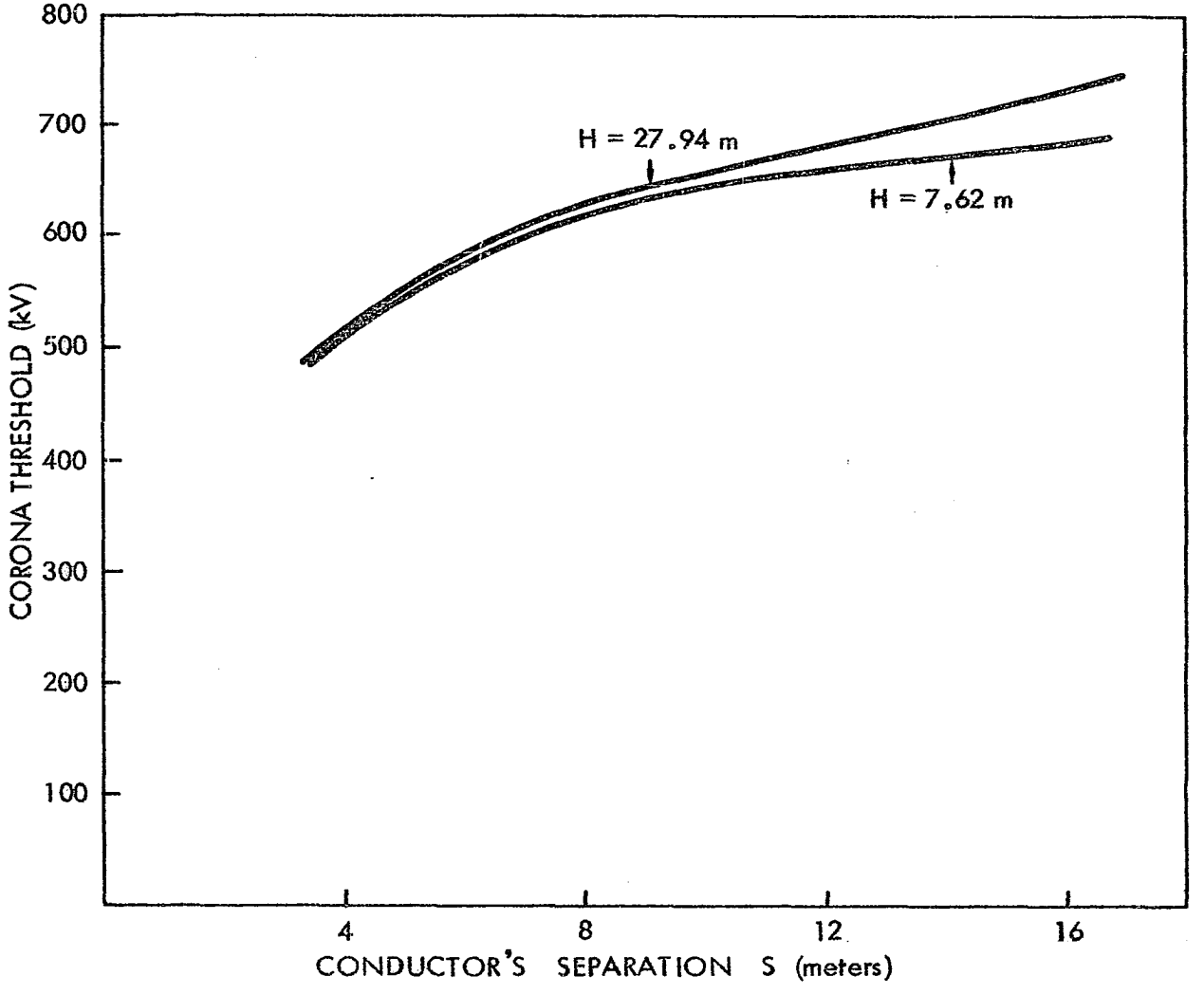
800
700
600
500
400
300
200
100
CORONA THRESHOLD (kV)
H = 27.94 m
H = 7.62 m
4
8
12
16
CONDUCTOR'S SEPARATION S (meters)

In a very recent paper (62) some measurements of corona thresholds for single wires of considerably small radii were reported. Computations are made for a unipolar single conductor (subconductor spacing D=0) of RS=0.23 cm and the measured and computed corona thresholds are plotted in Figure 6.22 for different conductor heights. This figure shows that the computed thresholds are in close agreement with their measured values. The effect of increasing the single conductor radius on the corona threshold is also to be observed by comparing the two curves for RS=0.23 cm and RS=0.5 cm. In Figure 6.23 corona thresholds were computed for different single conductor sizes at a height H=2.5 cm from ground. Again, this figure shows that the corona threshold could be raised by means of increasing the conductor radius.

In Figure 6.24 the maximum surface gradient for corona starting is plotted for different single conductor radii at a constant height H=2.5 cm. This figure indicates that the maximum surface gradient for corona to start is dependent on the conductor size and not a constant.

Figures 6.25, 6.26, and 6.27 are reprints of the computer output for a unipolar twin-bundle line of subconductor radius RS= $\frac{5}{8}$ inch, subconductor spacing D=20 inches at a height of 12 feet above ground at the corona starting potential. Figure 6.25 shows the external field distribution and the corresponding values of Townsend's first ionization

Figure 6.22. Computed and measured corona thresholds of single conductors (62) vs conductor height above ground, for different conductor radii

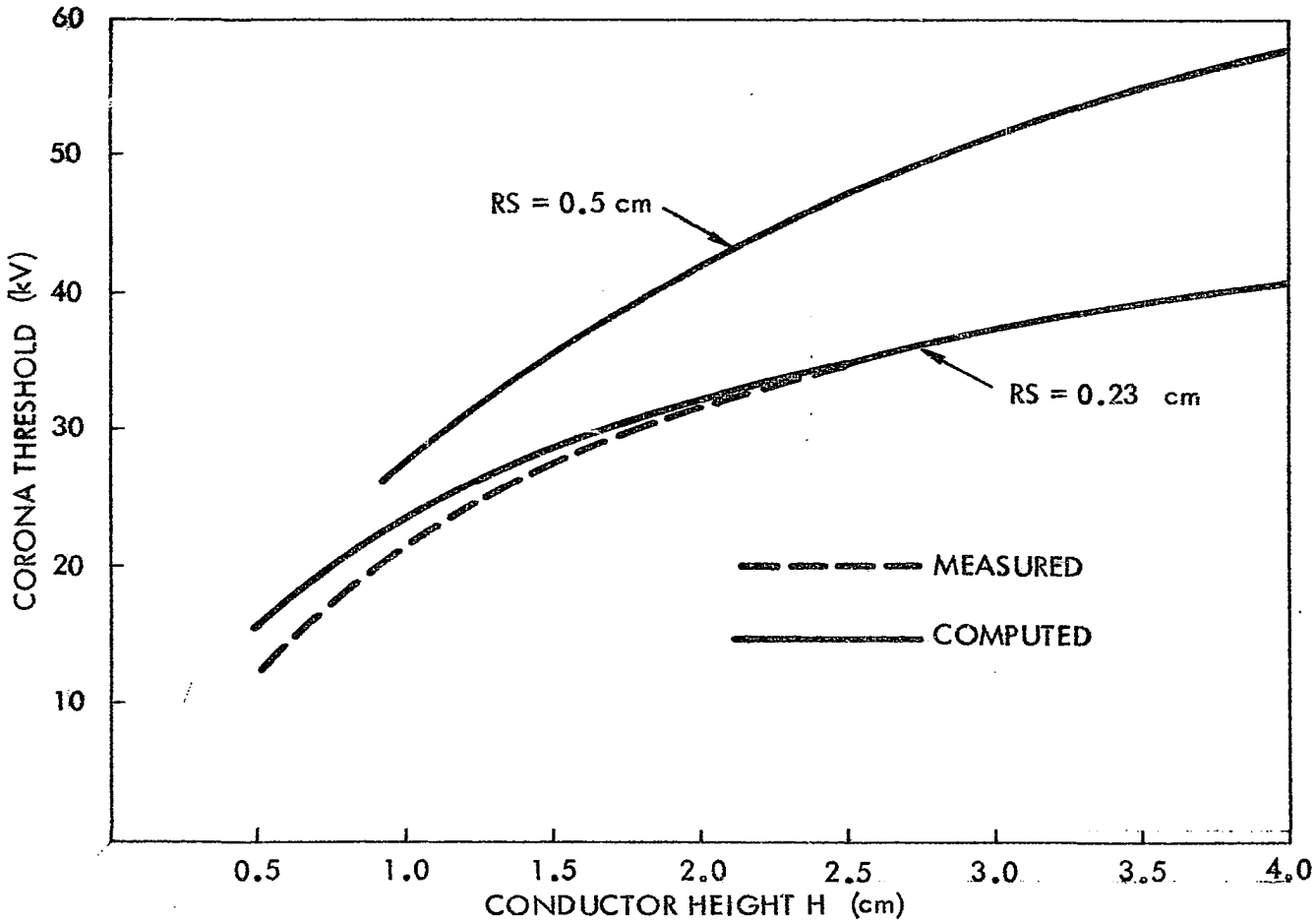
60
50
40
30
20
10
CORONA THRESHOLD (kV)
RS = 0.5 cm
RS = 0.23 cm
MEASURED
COMPUTED
0.5
1.0
1.5
2.0
2.5
3.0
3.5
4.0
CONDUCTOR HEIGHT H (cm)

Figure 6.23. Corona thresholds of single conductors vs conductor radius, H=2.5 cm

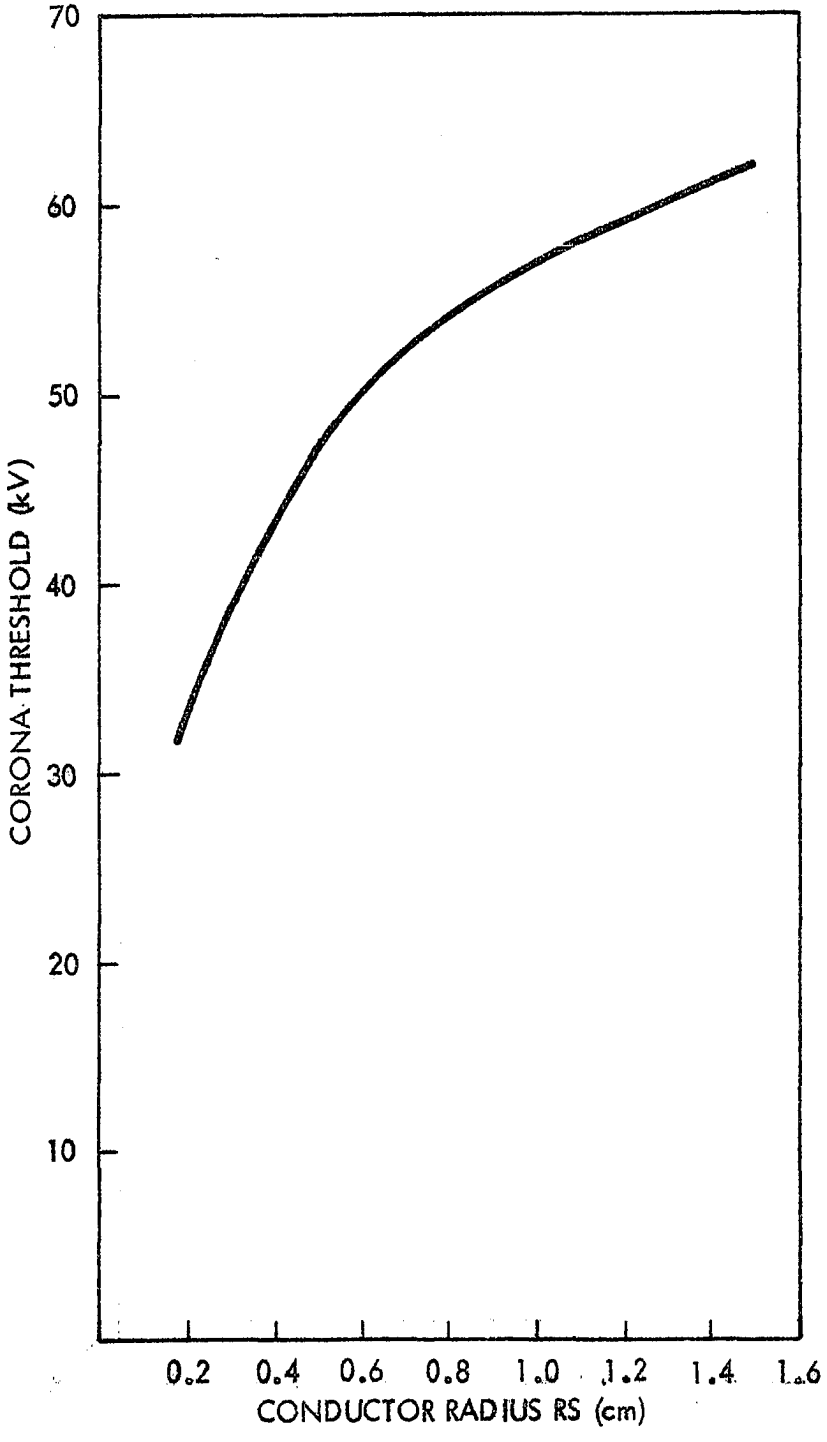
70
60
50
40
30
20
10
CORONA THRESHOLD (kV)
0.2
0.4
0.6
0.8
1.0
1.2
1.4
1.6
CONDUCTOR RADIUS RS (cm)

Figure 6.24. Maximum surface gradient of single conductors at corona threshold for different conductor radii, H=2.5 cm

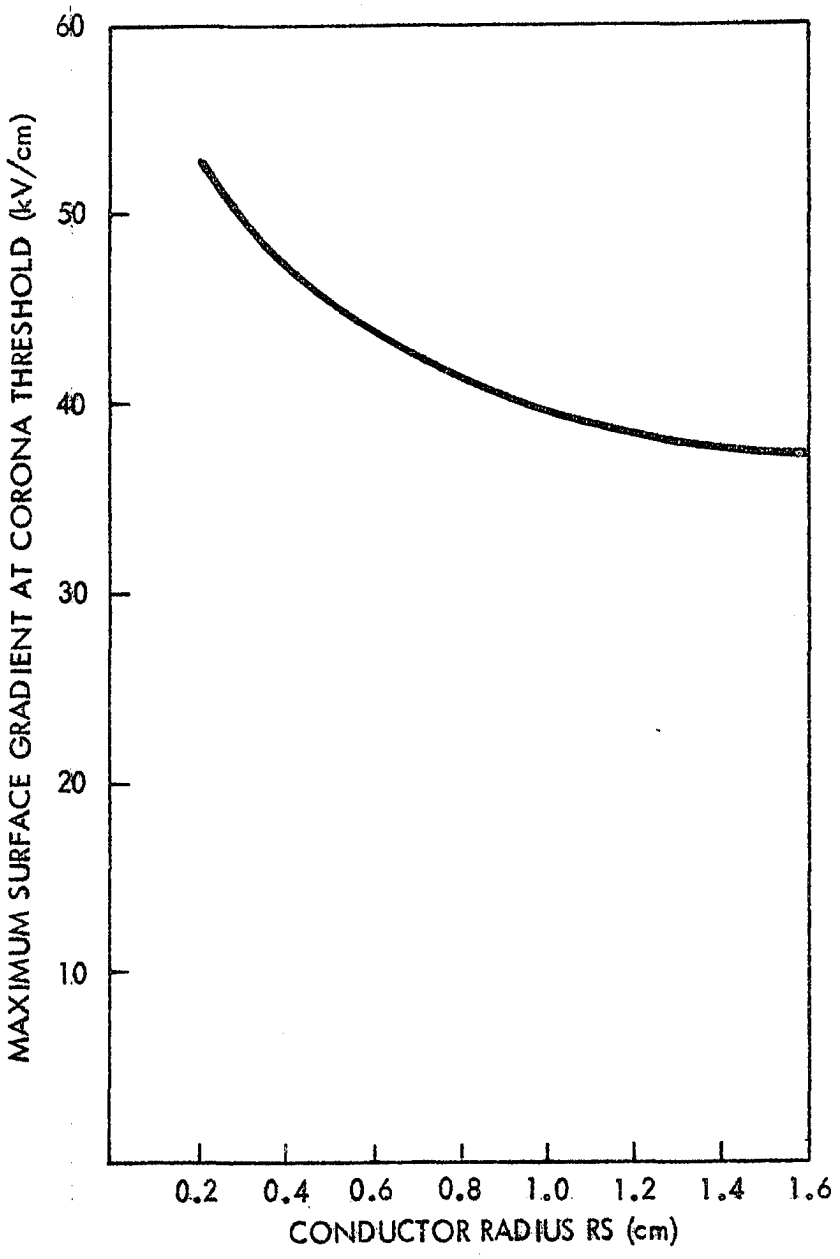
MAXIMUM SURFACE GRADIENT AT CORONA THRESHOLD (kV/cm)
60
50
40
30
20
10
0.2
0.4
0.6
0.8
1.0
1.2
1.4
1.6
CONDUCTOR RADIUS RS (cm)

Figure 6.25. External field and corresponding $\alpha$ and $V_e$ distribution for a unipolar twin-bundle line at the corona threshold, RS= 5/8 in., D=20 in., H=12 ft.

| X (CM) | FIELD (KV/CM) | E/P (VOLT/CM TORR) | ALPHA (CM-1) | EL. DRIFT VEL. (KM/SEC) |
|---|---|---|---|---|
| 1.590000 | 37.495286 | 49.3359 | 38.199040 | 174.280375 |
| 1.599273 | 37.278312 | 49.0504 | 37.443230 | 173.498125 |
| 1.608545 | 37.063900 | 48.7683 | 36.711035 | 172.725112 |
| 1.617818 | 36.852004 | 48.4895 | 36.001502 | 171.961171 |
| 1.627091 | 36.642580 | 48.2139 | 35.313723 | 171.206143 |
| 1.636364 | 36.435585 | 47.9416 | 34.646833 | 170.459873 |
| 1.645636 | 36.230978 | 47.6723 | 34.000012 | 169.722208 |
| 1.654909 | 36.028716 | 47.4062 | 33.372476 | 168.993001 |
| 1.664182 | 35.828759 | 47.1431 | 32.763480 | 168.272106 |
| 1.673455 | 35.631069 | 46.8830 | 32.172311 | 167.559381 |
| 1.682727 | 35.435607 | 46.6258 | 31.598292 | 166.854688 |
| 1.692000 | 35.242335 | 46.3715 | 31.040777 | 166.157893 |
| 1.701273 | 35.051217 | 46.1200 | 30.499148 | 165.468862 |
| 1.710545 | 34.862217 | 45.8713 | 29.972816 | 164.787466 |
| 1.719818 | 34.675300 | 45.6254 | 29.461218 | 164.113580 |
| 1.729091 | 34.490431 | 45.3821 | 28.963817 | 163.447079 |
| 1.738364 | 34.307577 | 45.1415 | 28.480099 | 162.787843 |
| 1.747636 | 34.126705 | 44.9036 | 28.009573 | 162.135754 |
| 1.756909 | 33.947784 | 44.6681 | 27.551769 | 161.490695 |
| 1.766182 | 33.770782 | 44.4352 | 27.106238 | 160.852555 |
| 1.775455 | 33.595667 | 44.2048 | 26.672550 | 160.221221 |
| 1.784727 | 33.422411 | 43.9769 | 26.250292 | 159.596586 |
| 1.794000 | 33.250983 | 43.7513 | 25.839070 | 158.978543 |
| 1.803273 | 33.081355 | 43.5281 | 25.438507 | 158.366990 |
| 1.812545 | 32.913499 | 43.3072 | 25.048241 | 157.761824 |
| 1.821818 | 32.747386 | 43.0887 | 24.667924 | 157.162945 |
| 1.831091 | 32.582991 | 42.8724 | 24.297224 | 156.570256 |
| 1.840364 | 32.420286 | 42.6583 | 23.935822 | 155.983663 |
| 1.849636 | 32.259246 | 42.4464 | 22.504857 | 155.403070 |
| 1.858909 | 32.099845 | 42.2366 | 21.580357 | 154.828388 |
| 1.868182 | 31.942058 | 42.0290 | 20.702629 | 154.259525 |
| 1.877455 | 31.785861 | 41.8235 | 19.868911 | 153.696394 |
| 1.886727 | 31.631230 | 41.6200 | 19.076628 | 153.138909 |
| 1.896000 | 31.478142 | 41.4186 | 18.323375 | 152.586986 |
| 1.905273 | 31.326573 | 41.2192 | 17.606904 | 152.040541 |
| 1.914545 | 31.176502 | 41.0217 | 16.925114 | 151.499494 |
| 1.923818 | 31.027906 | 40.8262 | 16.276043 | 150.963765 |
| 1.933091 | 30.880763 | 40.6326 | 15.657850 | 150.433275 |
| 1.942364 | 30.735052 | 40.4409 | 15.068817 | 149.907950 |
| 1.951636 | 30.590752 | 40.2510 | 14.507329 | 149.387713 |
| 1.960909 | 30.447844 | 40.0630 | 13.971877 | 148.872491 |
| 1.970182 | 30.306307 | 39.8767 | 13.461044 | 148.362212 |
| 1.979455 | 30.166121 | 39.6923 | 12.973501 | 147.856805 |
| 1.988727 | 30.027267 | 39.5096 | 12.508000 | 147.356201 |
| 1.998000 | 29.889727 | 39.3286 | 12.063370 | 146.860332 |
| 2.007273 | 29.753481 | 39.1493 | 11.638511 | 146.369130 |
| 2.016545 | 29.618512 | 38.9717 | 11.232387 | 145.882531 |
| 2.025818 | 29.484802 | 38.7958 | 10.844026 | 145.400470 |

| | | | | |
|---|---|---|---|---|
| 2.035091 | 29.352333 | 38.6215 | 10.472513 | 144.922884 |
| 2.044364 | 29.221087 | 38.4488 | 10.116986 | 144.449710 |
| 2.053636 | 29.091049 | 38.2777 | 9.776634 | 143.980888 |
| 2.062909 | 28.962202 | 38.1082 | 9.450692 | 143.516359 |
| 2.072182 | 28.834528 | 37.9402 | 9.138441 | 143.056063 |
| 2.081455 | 28.708013 | 37.7737 | 8.839200 | 142.599943 |
| 2.090727 | 28.582641 | 37.6087 | 8.552329 | 142.147943 |
| 2.100000 | 28.458396 | 37.4453 | 8.277223 | 141.700007 |
| 2.109273 | 28.335263 | 37.2832 | 8.013311 | 141.256079 |
| 2.118545 | 28.213227 | 37.1227 | 7.760055 | 140.816108 |
| 2.127818 | 28.092274 | 36.9635 | 7.516944 | 140.380040 |
| 2.137091 | 27.972389 | 36.8058 | 7.283496 | 139.947823 |
| 2.146364 | 27.853558 | 36.6494 | 7.059256 | 139.519407 |
| 2.155636 | 27.735768 | 36.4944 | 6.843794 | 139.094742 |
| 2.164909 | 27.619004 | 36.3408 | 6.636701 | 138.673779 |
| 2.174182 | 27.503254 | 36.1885 | 6.437591 | 138.256469 |
| 2.183455 | 27.388504 | 36.0375 | 6.246099 | 137.842765 |
| 2.192727 | 27.274742 | 35.8878 | 6.061878 | 137.432622 |
| 2.202000 | 27.161954 | 35.7394 | 5.884599 | 137.025992 |
| 2.211273 | 27.050128 | 35.5923 | 5.713951 | 136.622831 |
| 2.220545 | 26.939253 | 35.4464 | 5.549639 | 136.223095 |
| 2.229818 | 26.829315 | 35.3017 | 5.391383 | 135.826740 |
| 2.239091 | 26.720303 | 35.1583 | 5.238916 | 135.433724 |
| 2.248364 | 26.612205 | 35.0161 | 5.091986 | 135.044004 |
| 2.257636 | 26.505011 | 34.8750 | 4.950353 | 134.657540 |
| 2.266909 | 26.398708 | 34.7351 | 4.813789 | 134.274290 |
| 2.276182 | 26.293286 | 34.5964 | 4.682077 | 133.894215 |
| 2.285455 | 26.188733 | 34.4589 | 4.555011 | 133.517276 |
| 2.294727 | 26.085040 | 34.3224 | 4.432395 | 133.143433 |
| 2.304000 | 25.982195 | 34.1871 | 4.314044 | 132.772650 |
| 2.313273 | 25.880188 | 34.0529 | 4.199778 | 132.404887 |
| 2.322545 | 25.779009 | 33.9197 | 4.089430 | 132.040110 |
| 2.331818 | 25.678647 | 33.7877 | 3.982838 | 131.678280 |
| 2.341091 | 25.579094 | 33.6567 | 3.879850 | 131.319364 |
| 2.350364 | 25.480338 | 33.5268 | 3.780318 | 130.963325 |
| 2.359636 | 25.382372 | 33.3979 | 3.684104 | 130.610130 |
| 2.368909 | 25.285184 | 33.2700 | 3.591076 | 130.259744 |
| 2.378182 | 25.188767 | 33.1431 | 3.501106 | 129.912133 |
| 2.387455 | 25.093110 | 33.0173 | 3.414073 | 129.567266 |
| 2.396727 | 24.998206 | 32.8924 | 3.329863 | 129.225110 |
| 2.406000 | 24.904044 | 32.7685 | 3.248365 | 128.885633 |
| 2.415273 | 24.810617 | 32.6455 | 3.169474 | 128.548803 |
| 2.424545 | 24.717915 | 32.5236 | 3.093090 | 128.214589 |
| 2.433818 | 24.625931 | 32.4025 | 3.121453 | 127.882962 |
| 2.443091 | 24.534656 | 32.2824 | 2.833802 | 127.553892 |
| 2.452364 | 24.444082 | 32.1633 | 2.574569 | 127.227348 |
| 2.461636 | 24.354201 | 32.0450 | 2.340767 | 126.903302 |
| 2.470909 | 24.265004 | 31.9276 | 2.129742 | 126.581726 |
| 2.480182 | 24.176485 | 31.8112 | 1.939132 | 126.262590 |
| 2.489455 | 24.088635 | 31.6956 | 1.766833 | 125.945868 |
| 2.498727 | 24.001447 | 31.5809 | 1.610973 | 125.631533 |
| 2.508000 | 23.914913 | 31.4670 | 1.469881 | 125.319556 |

Figure 6.25 (Continued)

Figure 6.26. Integral of $\alpha$, avalanche transit time, and radius of positive ion space charge for a unipolar twin-bundle line at the corona threshold, RS= 5/8 in., D=20 in., H=12 ft.

EVALUATION OF THE INTEGRAL OF ALPHA W. R. T. X BETWEEN X = 1.5900AND X = X
USING ROMBERG METHOD

| X | INTEGRAL |
|---|---|
| 2.508000 | 13.108858 |

EXP(INTEGRAL ALPHA DX) = 0.0049 X10E8
**********

EVALUATION OF T : TRANSIT TIME OF ELECTRONS FROM X = 1.5900TO X = X
USING TRAPEZOIDAL RULE (N=99)

| X | T (MIC SEC) |
|---|---|
| 2.508000 | 0.063425 |

RADIUS OF POSITIVE ION SPACE CHARGE = 0.012792 CM

Figure 6.27. External, space charge and resultant field distributions and corresponding $\alpha$-distribution for a unipolar twin-bundle line at the corona threshold, RS= 5/8 in., D=20 in., H=12 ft.

| X (CM) | EXT. FIELD (KV/CM) | SP. CH. FIELD (KV/CM) | RESULTANT FIELD (KV/CM) | E/P (VOLT/CM TORR) | ALPHA (CM-1) |
|---|---|---|---|---|---|
| 0.012792 | 36.897629 | 0.282384 | 37.180013 | 48.921070 | 37.10575536 |
| 0.037792 | 36.321998 | 0.032353 | 36.354351 | 47.834673 | 34.38857053 |
| 0.062792 | 35.764522 | 0.011720 | 35.776242 | 47.074002 | 32.60538127 |
| 0.087792 | 35.224356 | 0.005995 | 35.230351 | 46.355725 | 31.00653330 |
| 0.112792 | 34.700704 | 0.003632 | 34.704336 | 45.663600 | 29.54011511 |
| 0.137792 | 34.192820 | 0.002434 | 34.195254 | 44.993755 | 28.18697553 |
| 0.162792 | 33.700002 | 0.001744 | 33.701746 | 44.344402 | 26.93442823 |
| 0.187792 | 33.221589 | 0.001310 | 33.222900 | 43.714342 | 25.77232098 |
| 0.212792 | 32.756959 | 0.001020 | 32.757980 | 43.102605 | 24.69200482 |
| 0.237792 | 32.305524 | 0.000817 | 32.306341 | 42.508344 | 23.68593038 |
| 0.262792 | 31.866729 | 0.000669 | 31.867398 | 41.930787 | 20.29984885 |
| 0.287792 | 31.440052 | 0.000558 | 31.440610 | 41.369223 | 18.14328580 |
| 0.312792 | 31.024995 | 0.000472 | 31.025468 | 40.822984 | 16.26560441 |
| 0.337792 | 30.621092 | 0.000405 | 30.621497 | 40.291443 | 14.62517933 |
| 0.362792 | 30.227898 | 0.000351 | 30.228249 | 39.774012 | 13.18735340 |
| 0.387792 | 29.844992 | 0.000307 | 29.845299 | 39.270131 | 11.92315220 |
| 0.412792 | 29.471976 | 0.000271 | 29.472247 | 38.779272 | 10.80825726 |
| 0.437792 | 29.108471 | 0.000241 | 29.108712 | 38.300936 | 9.82218124 |
| 0.462792 | 28.754117 | 0.000216 | 28.754333 | 37.834648 | 8.94760230 |
| 0.487792 | 28.408573 | 0.000194 | 28.408767 | 37.379957 | 8.16982422 |
| 0.512792 | 28.071515 | 0.000176 | 28.071691 | 36.936435 | 7.47633685 |
| 0.537792 | 27.742633 | 0.000160 | 27.742792 | 36.503674 | 6.85645662 |
| 0.562792 | 27.421632 | 0.000146 | 27.421778 | 36.081287 | 6.30103154 |
| 0.587792 | 27.108234 | 0.000134 | 27.108367 | 35.668904 | 5.80219810 |
| 0.612791 | 26.802169 | 0.000123 | 26.802292 | 35.266174 | 5.35318024 |
| 0.637791 | 26.503185 | 0.000114 | 26.503299 | 34.872761 | 4.94812260 |
| 0.662791 | 26.211037 | 0.000105 | 26.211142 | 34.488345 | 4.58195165 |
| 0.687791 | 25.925494 | 0.000098 | 25.925592 | 34.112621 | 4.25025977 |
| 0.712791 | 25.646334 | 0.000091 | 25.646425 | 33.745296 | 3.94920804 |
| 0.737791 | 25.373344 | 0.000085 | 25.373429 | 33.386091 | 3.67544465 |
| 0.762791 | 25.106323 | 0.000079 | 25.106402 | 33.034740 | 3.42603605 |
| 0.787791 | 24.845076 | 0.000074 | 24.845150 | 32.690987 | 3.19840882 |
| 0.812791 | 24.589418 | 0.000070 | 24.589488 | 32.354589 | 3.00325769 |
| 0.837791 | 24.339171 | 0.000066 | 24.339237 | 32.025312 | 2.30395940 |
| 0.862791 | 24.094165 | 0.000062 | 24.094227 | 31.702931 | 1.77733003 |
| 0.887791 | 23.854237 | 0.000059 | 23.854296 | 31.387231 | 1.37846990 |
| 0.912791 | 23.619230 | 0.000055 | 23.619285 | 31.078007 | 1.07470795 |
| 0.937791 | 23.388994 | 0.000053 | 23.389047 | 30.775062 | 0.84212883 |
| 0.962791 | 23.163386 | 0.000050 | 23.163435 | 30.478205 | 0.66312473 |
| 0.987791 | 22.942266 | 0.000047 | 22.942313 | 30.187254 | 0.52465871 |

coefficient $\alpha$ and the electron drift velocities. In Figure 6.26 the integral of $\alpha$ is printed together with the avalanche transit time and the radius of the positive ion space charge. Figure 6.27 shows the distribution of external, space charge, and resultant fields and the corresponding values of $\alpha$.

# VII. SUMMARY AND CONCLUSIONS

A method for the calculation of the potential and electric field distribution is proposed based on a charge simulation technique and the method of images. It has been successfully applied to unipolar and bipolar twin-bundle conductor systems, with ground included. The maximum deviation of the calculated potential at any point on the conductor circumference from the actual conductor potential is less than 0.1 percent. For a unipolar twin-bundle line of practical size, the maximum surface gradient calculated using a single axial line charge simulation is about 25 percent higher than the value obtained by this method. Unlike other approximate methods for field computations, this method has no restrictions with regard to the geometrical parameters of the line. There is no limitation on the minimum subconductor spacing. A subconductor spacing of zero is used to obtain the electric field distribution of a single unipolar or bipolar line. The computer time used to calculate and print the potential and electric field distribution, in magnitude and direction, according to study type 1 is less than 40 seconds.

The method of charge simulation, furthermore, provides for a simple way of calculating the line capacitance. With one volt applied to the conductor, the sum of the axial line charges divided by a factor of $18 \times 10^9$ yields the line

capacitance in farads/meter.

A mathematical model representing the actual physical processes that lead to corona in a nonuniform field is described. A computer program is developed that uses the accurately calculated electric fields (as a subroutine) together with the mathematical model and solves for the corona threshold of twin unipolar and bipolar bundle conductors, as well as single conductors. The corona thresholds computed are in close agreement with published values that are measured experimentally. The computation time varies from 40 seconds to 2 minutes depending on how far the initial threshold value used is from the correct value.

The calculation of the corona starting voltage based on the criterion that the maximum surface gradient attains a specified constant value is shown to be inaccurate due to the variation of the maximum gradient with the subconductor radius.

The total number of electrons in the avalanche tip at the corona threshold is in the order of $10^5$-$10^6$ for the unipolar line and $10^6$ for the bipolar line. Its value increases slightly with increasing the subconductor radius. However, taking the value of the total number of electrons for corona starting to be of the order of $10^6$ seems to be a more acceptable criterion and could be used as a simple means of prediction of the corona threshold of practical

sizes of bundle conductor systems, with reasonable accuracy. This number of electrons is lower than the experimental value of $10^8$ reported by Loeb and others (16, 40) and slightly higher than the experimental value of $10^5$ reported by English and others (16).

At the corona threshold the avalanche transit time is in the order of $10^{-8}$ second and the radius of the positive ion space charge is 0.01 to 0.02 cm for the range of conductor sizes and configurations reported in the previous chapter. Their exact values, however, are determined by the electric field distribution for a particular configuration. For a constant height above ground, the values of transit time and positive space charge radius increase slightly with the increase of the conductor radius.

The computer determination of electric fields based on the principle of charge simulation has also been proven to be successful for the point-to-plane gap (55). It could be tried for a system of n-bundle conductors as well as different symmetrical and asymmetrical configurations; examples are multiple point electrodes, a sphere with a recessed shaft, and a hollow cylindrical electrode against infinite plane for the symmetrical gaps; and a sphere against a point electrode for the asymmetrical gaps.

The computer program developed for the calculation of the corona threshold, based on the mathematical model described

in this dissertation, could be applied to any gap configuration of known electric field distribution. Furthermore, it could be used to calculate corona thresholds under various atmospheric conditions, provided that experimental information regarding the physical parameters, namely $\alpha$, u, $V_e$, $D_e$, under those conditions is available.

# VIII. BIBLIOGRAPHY

1. Adamson, C. and Hingorani, N. G. High voltage direct current power transmission. 1st ed. London, England, Garraway Limited. 1960.

2. Konti-Skan 250-KV dc link readied for full load. Electrical World 163: 24-25. 1965.

3. New Zealand inaugurates interisland HVDC. Electrical World 164: 20-21. 1965.

4. Progress on the Sardinia-Italy direct current link. Direct Current 9: 40-41. 1964.

5. Kuwahara, S. New types of frequency converter projects in Japan. American Power conference Proceedings 26: 884-892. 1964.

6. 750-KV dc intertie rescheduled for April 1969. Electrical World 164: 98-101. 1965.

7. DC transmission to boost Vancouver Island supply. Electrical World 163: 44-47. 1965.

8. CIGRE and UNIPEDE: direct current power transmission discussed at international conferences. Direct Current 9: 73-88. 1964.

9. Gehrig, E. H., Peterson, A. C., Clark, C. F., and Rednour, T. C. Bonneville Power Administration's 1100-KV direct current test projects: II-radio interference and corona loss. IEEE Transactions on Power Apparatus and Systems 86: 278-290. 1967.

10. Taylor, E. R., Kalcio, N., and Pakala, W. E. The Apple Grove 750-KV project-775 KV radio influence and corona loss investigations. IEEE Transactions on Power Apparatus and Systems 84: 573-579. 1965.

11. Gens, R. S. and Stevens, R. F. The high-voltage dc test program of the Bonneville Power Administration. Electrical Engineering 82: 246-252. 1963.

12. Cahen, F. and Pelissier, R. The use of bundle conductors for extra-high voltage lines - results of tests at the 500 KV experimental station of Chevilly. Bull., Societé Francaise des Electriciens, Malakoff, France, sixth series, 8: 111-160. 1948.

13. Bartenstein, R. and Lesch, G. Mesures des pertes par effect de couronne et des perturbations radiophoniques a'la station de recherches de Manheim-Rheinan avec étude speciale de conducteurs en faisceaux. CIGRE R. 402. 1956.

14. Vorobeu, A. V. and Tikhodeev, N. N. Influence of geometric parameters on high voltage dc transmission lines on their universal corona characteristics, Part I Unipolar lines, Part II Bipolar lines. Zhurnal Tekhnicheskoi Fiziki 26: 759-771. 1956.

15. Miller, C. J. Mathematical prediction of radio and corona characteristics of smooth, bundled conductors. AIEE Transactions on Power Apparatus and Systems 75, Part III: 1029-1035. 1956.

16. Loeb, L. B. Electrical coronas. Berkeley, California, University of California Press. 1965.

17. Thomas, P. H. Output and regulation in long-distance lines. AIEE Transactions 28, Part I: 615-640. 1909.

18. Thomas, P. H. Calculation of the high-tension lines. AIEE Transactions 28, Part I: 641-686. 1909.

19. Whitehead, J. B. System of electrical transmission. U.S. Patent 1,078,711. 1910.

20. Clarke, E. Three-phase multiple-conductor circuits. AIEE Transactions 51: 820-821. 1932.

21. Reichman, J. Bundled conductor voltage gradient calculations. AIEE Transactions on Power Apparatus and Systems 78, Part III-A: 598-607. 1959.

22. King, S. Y. The electric field near bundle conductors. Institution of Electrical Engineers Proceedings 106, Part C: 200-206. 1959.

23. Sreenivasan, T. V. Potential, potential gradient and evaluation of corona loss in dual conductor transmission lines. Institute of Engineers (India) 40, Part 2: 419-428. 1960.

24. Quilico, G. The electric field of twin-conductors. Elettrotecnica 10: 530-538. 1954.

25. Dareskii, A. E. The electrostatic field of a split phase. Elektrichestvo 9: 16-19. 1958.

26. Timascheff, A. S. Field patterns of bundle conductors and their electrostatic properties. AIEE Transactions on Power Apparatus and Systems 80, Part III: 590-597. 1961.

27. Timascheff, A. S. Equigradient lines in the vicinity of bundle conductors. AIEE Transactions on Power Apparatus and Systems 82, Part II: 104-110. 1963.

28. Tikhodeev, N. N. Some peculiarities of corona discharge on bundle conductors at a constant voltage (Abstract). Journal of Technical Physics 23, No. 10: 1773. 1953.

29. Tikhodeev, N. N. On the calculation of initial voltages of the total corona on dc transmission lines. Elektrichestvo 10: 12-19. 1957.

30. Bewley, L. V. Two-Dimensional Fields in Electrical Engineering. New York, New York, Dover Publications, Inc. 1963.

31. Sarma, P. S. and Janischewskyj, W. Electrostatic field of a system of parallel cylindrical conductors. IEEE Transactions on Power Apparatus and Systems 88: 1069-1079. 1969.

32. Aleksandrov, G. N. Converted method of images in a circle and its application to the solution of plane electrostatic field problems. Elektrichestvo 9: 20-23. 1958.

33. Aleksandrov, G. N. Corona discharge on transmission lines (Russian). Moscow, USSR, Energia. 1964.

34. Roth, A. Hochspannungstechnik. Vienna, Springer-Verlag. 1965.

35. Peek, F. W. Dielectric phenomena in high-voltage engineering. New York, New York. McGraw-Hill. 1929.

36. Meek, J. M. and Craggs, J. D. Electrical breakdown of gases. Oxford, England, Clarendon Press. 1953.

37. Ganger, B. Der elektrische durchschlag von gasen. Berlin, Germany, Springer-Verlag. 1953.

38. Loeb, L. B. and Meek, J. M. The mechanism of the electric spark. Stanford, California, Stanford University Press. 1941.

39. Raether, H. Über den aufbau von gasentladungen. Z. fur Physik 117: 375 and 524. 1941.

40. Raether, H. Electron avalanches and breakdown in gases. London, England, Butterworths. 1964.

41. Llewellyn-Jones, F. Ionization and breakdown in gases. New York, New York, John Wiely and Sons. 1957.

42. Cobine, J. D. Gaseous conductors. New York, New York, Dover. 1958.

43. Nasser, E. Fundamentals of gaseous ionization and Plasma electronics. Unpublished mimeographed notes. Ames, Iowa, Department of Electrical Engineering, Iowa State University of Science and Technology. 1968.

44. Schumann, W. O. Elektrische durchbruchfeldstarke von gasen. Berlin, Germany, Springer-Verlag. 1923.

45. Ver Plank, D. W. Calculation of initial breakdown voltages in air. AIEE Transactions 60: 99-104. 1941.

46. Hutton, J. G. Determination of corona starting voltages for nonuniform fields in air. AIEE Transactions 66: 1674-1680. 1947.

47. Loeb, L. B. Certain aspects of the mechanism of spark discharge. Physical Society, London Proceedings 60: 561-573. 1948.

48. Fisher, L. H. Some aspects of Meek's sparking equation. Physical Review 69: 530. 1946.

49. Fisher, L. H. An attempt to verify the theory of the long spark of Loeb and Meek. Physical Review 72: 423-428. 1947.

50. Fisher, L. H. and Weissler, F. L. The apparent breakdown of Meek's streamer criterion in divergent gaps due to the failure of Townsend's ionization function. Physical Review 66: 95-102. 1944.

51. Hopwood, W. The positive streamer mechanism of spark breakdown. Physical Society, London Proceedings 62, Sec. B: 657-664. 1949.

52. Pedersen, A. Calculation of spark breakdown or corona starting voltages in nonuniform fields. IEEE Transactions on Power Apparatus and Systems 86: 200-206. 1967.

53. Jorgensen, M. O. Elektrische Funkenspannungen. Copenhagen, Denmark, Munksgaard. 1943.

54. Pedersen, A. Calculation of spark breakdown voltages in air at atmospheric pressure. Applied Scientific Research, Holland B1: 299-306. 1949.

55. Abou-Seada, M. S. and Nasser, E. Digital computer calculation of the electric potential and field of a rod gap. IEEE Proceedings 56: 813-820. 1968.

56. Boast, W. B. Vector fields. New York, New York, Harper and Row. 1964.

57. Fulks, W. Advanced calculus. 4th ed. New York, New York, John Wiley and Sons, Inc. 1964.

58. Brown, S. C. Basic data of plasma physics, 1966. 2nd ed. Cambridge, Massachusetts, The M.I.T. Press. 1966.

59. Loeb, L. B. Fundamental processes of electrical discharge in gases. New York, New York, John Wiley and Sons, Inc. 1947.

60. Organick, E. I. A fortran primer. Reading, Massachusetts, Addison-Wesley. 1965.

61. Ralston, A. A first course in numerical analysis. New York, New York, McGraw-Hill, Inc. 1965.

62. Vuhuu, Q. and Comsa, R. P. Influence of gap length on wire-plane corona. IEEE Transactions on Power Apparatus and Systems 88: 1462-1475. 1969.

## IX. ACKNOWLEDGMENTS

The author wishes to express his sincere appreciation to his major professor Dr. Essam Nasser for suggesting the problem and for his considerable and constructive guidance throughout the development of this thesis.

The author also wishes to acknowledge the financial support rendered to him by the Power Affiliates Program at Iowa State University.

It is the author's opinion that a great deal of the credit should go to the government and people of the United Arab Republic for giving him this opportunity.